AD-A181 177 ZONAL MODELS OF TURBULENCE AND THEIR APPLICATION TO FREE SHEAR FLOWS(U) STANFORD UNIV CA THERMOSCIENCES DIV K TZUOO ET AL NOV 86 TF-27 F49620-86-K-0008 1/2

UNCLASSIFIED F/G 20/4 NL

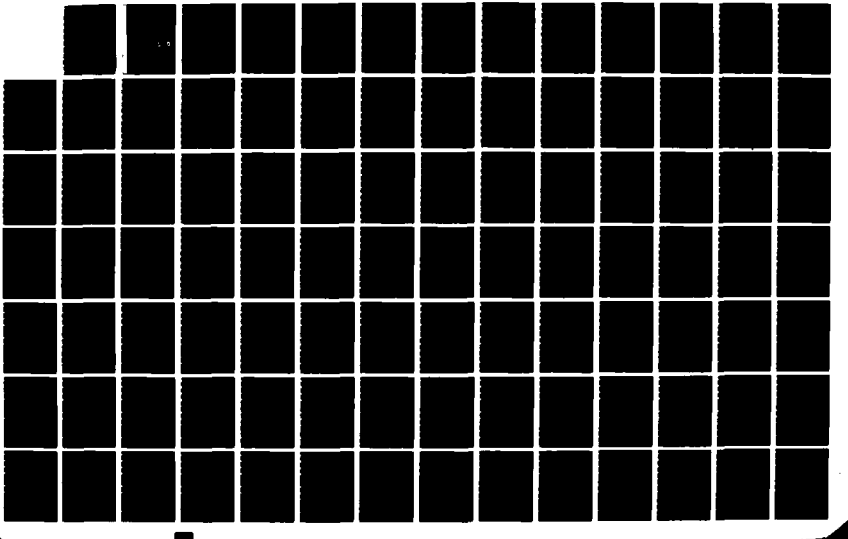

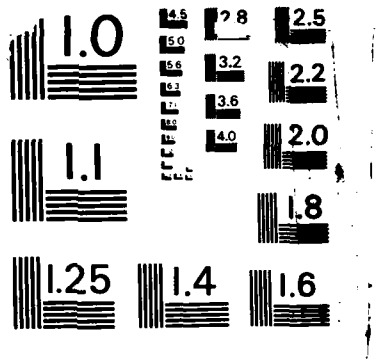

MICROCOPY RESOLUTION TEST CHART

NATIONAL BUREAU OF STANDARDS-1963-A

Need AD #

ZONAL MODELS OF TURBULENCE AND THEIR APPLICATION TO FREE SHEAR FLOWS

B87-0963

by

K.-L. Tzuoo, J. H. Ferziger and S. J. Kline

Prepared from work sponsored by
Air Force Office of Scientific Research
under Contract AF-F49620-86-K-0008

Supported in part by the Allison Gas-Turbine Division
of General Motors through a GM Fellowship

Report No. TF-27

Thermosciences Division
Department of Mechanical Engineering
Stanford University
Stanford, California 94305

November 1986

ZONAL MODELS OF TURBULENCE

AND THEIR APPLICATION TO FREE SHEAR FLOWS

by

K.-L. Tzuoo, J. H. Ferziger, and S. J. Kline

Prepared from work sponsored by the

Air Force Office of Scientific Research

under Contract AF-F49620-86-K-0008

Supported in part by the Allison Gas-Turbine Division

of General Motors through a GM Fellowship

Technical Report TF-27

Thermosciences Division
Department of Mechanical Engineering
Stanford University
Stanford, California 94305

November, 1986

Acknowledgments

The authors thank Professors W. C. Reynolds and M. G. Mungal for their valuable ideas and comments. Special thanks are due to Messrs. S. Bordalo, R. Avva, R. van der Wijngaart, and B. Afshari for their helpful suggestions through numerous discussions.

The present work is sponsored by the AFOSR under Contract AF-F49620-86-K-0008. One of the authors (KLT) gratefully acknowledges the Allison Gas-Turbine Division of General Motors for its financial support through a GM Fellowship.

Ms. Ruth Korb, who has done an excellent job in preparing the final form of this report, is also acknowledged.

ZONAL MODELS OF TURBULENCE AND THEIR APPLICATION TO FREE SHEAR FLOWS

Abstract

The concept of zonal modeling is tested by using three homogeneous flows. Turbulence models are constructed independently for various zones. A parameter that governs the readjustment of the flow from one zone to another is introduced. This readjustment parameter reflects the changes in physics involved in the transition process. The results of the zonal concept are very promising.

The idea is then applied to the development of improved models for free shear flows. A close examination of the experimental data of various free shear flows is first performed. The standard $K-\varepsilon$ model is adopted as a base model since it predicts many flows reasonably well. Zonal models for well-defined zones are constructed independently by systematically modifying the standard $K-\varepsilon$ model to reflect the physics associated with the zones.

It is found that two governing parameters suffice to classify all free shear flows considered, and they are therefore used in the present model. The first parameter represents the ratio of the inertial force to the driving force of the shear layer or, alternatively, the ratio of eddy turn-over time to the characteristic free stream time. It determines the relative importance of the diffusion process in the turbulence transport mechanism. The larger this parameter, is the more important the diffusion process of turbulence becomes. The other parameter is a measure of lateral vortex stretching. Strong vortex stretching reduces the correlation between turbulent shear stress and turbulent kinetic energy and hence reduces the spreading rate of the flow.

There are a total of three zones found in the class of free shear flows; they represent the limiting values of the two governing parameters. The zonal models for these three zones are built separately. They are then blended to allowed readjustments between zones by means of readjustment parameters that are functions of the governing parameters. As a result, a unified zonal model for all free shear flows is produced.

This unified zonal model is used to predict five basic free shear flows. The agreement with data is excellent. Comparisons of model performance are made with the standard $K-\varepsilon$ model.

Table of Contents

List of Tables

List of Figures

Nomenclature

a_1 a_2	Model constants in Eqs. (2.3.23) and (2.3.24).
b_s, b_a, b_p	Constants in readjustment parameters.
C, C_s	Constants in readjustment parameters λ_1 and λ_2.
C_μ	Model constant in model of ν_t.
C_{ε_1}, C_{ε_2}	Model constants in model equation for ε.
D	Diameter.
E	Grid expansion function in Eq. (4.2.2).
f	Nondimensional velocity profile in Eq. (3.2.1).
F	Function defined in Eq. (5.2.3).
F_1, F_2	Functions.
g	Nondimensional shear stress profile in Eq. (5.2.5).
G	Function defined in Eq. (5.2.4).
I_n	Constant defined in Eq. (3.2.11).
I_n'	Constant defined in Eq. (3.3.6).
J	Momentum flux of jets.
K	Turbulent kinetic energy.
L	Width of mixing layers defined by $y_{\sqrt{0.9}} - y_{\sqrt{0.1}}$.
P	Production rate of turbulent kinetic energy.
q	Function of β defined in Eq. (5.2.8).
q'	Function of β defined in Eq. (6.2.5).
r	Coordinate in the radial direction.
R	Free stream velocity ratio of a mixing layer, $U_{\infty_2}/U_{\infty_1}$.
R_T	Eddy Reynolds number defined in Eq. (3.2.14).
$R_{1/2}$	Radius of curvature of the vortex line passing the point of $\delta_{1/2}$.
S	Vortex stretching parameter defined in Eq. (6.3.3).

S_{ij}	Strain tensor.
sp	Spreading parameter defined in Eq. (3.2.17).
t	Time.
U	Mean velocity component in x-direction.
U_1	Velocity excess or velocity deficit.
U_{1m}	Maximum U_1.
U_J	Jet velocity at the nozzle exit.
U_∞	Free stream velocity.
U_{∞_1}	Free stream velocity of high velocity side in a mixing layer.
U_{∞_2}	Free stream velocity of low velocity side in a mixing layer.
$-\overline{u'v'}$, $-\overline{u_1u_2}$	Turbulent shear stress.
$-\overline{u_iu_j}$	Reynolds stress.
$\overline{u'^2}$, $\overline{v'^2}$, $\overline{w'^2}$ or $\overline{u_1^2}$, $\overline{u_2^2}$, $\overline{u_3^2}$	Components of turbulent kinetic energy.
V	Mean velocity component in y-direction.
x	Streamwise coordinate.
x_o	Virtual origin.
$\vec{X}$	Position vector in old reference frame.
$\vec{X}'$	Position vector in new reference frame.
y	Coordinate in direction normal to the flow.
y_x	y-coordinate where $U = U_{\infty_2} + x(U_{\infty_1} - U_{\infty_2})$ in a mixing layer y-coordinate.

Subscripts

j	j^{th} grid in normal direction.
n	n^{th} step in streamwise direction.
CL	Centerline.

Greek Symbols

δ_{ij}	Kronecker delta tensor.
$\delta_{1/2}$	Half-velocity width.
ε	Dissipation rate of turbulent kinetic energy.
Γ_s, Γ_a, Γ_p	Strain rates.
σ_k, σ_ε	Model constants in diffusion terms.
θ	Momentum thickness defined in Eq. (3.2.7).
η	Nonmensional coordinate in normal direction.
ν	Kinematic viscosity.
ν_t	Eddy (turbulent) viscosity.
λ, λ_1, λ_2	Readjustment parameters.
β	Governing parameter in model constants.
κ	Karman constant.
Δx	Step size in streamwise direction.
Δy	Mesh size in normal direction.

Chapter I

INTRODUCTION

1.1 General Introduction to Zonal Modeling

Methods of simulating turbulent flows can be classified according to the following scheme (Kline et al. (1981)):

1. Correlations
2. Integral methods
3. One-point closure methods
4. Two-point closure methods
5. Large-eddy simulation
6. Full simulation

As one moves downwards in the list, each method requires more computational resources but less modeling than those above it; consequently, one might think it should also be more accurate. However, the higher-level simulations also require more complex data inputs which are often not as accurately known. Therefore, a simulation at a given level is not always more accurate than simulations at lower levels. This remark applies primarily to levels 2, 3, and perhaps 4. Also, owing to the tremendous cost of simulating even the simplest flows by means of high level simulations (large-eddy simulation and full simulation) on present computers, such simulations can serve only as research tools and not engineering design tools at the current time.

In the trade-off between accuracy and computation time, one-point closure methods seem to offer the best compromise for high technology applications at the present time. The one-point closure category includes: (i) mixing-length; (ii) one- and two-equation models; and (iii) Reynolds stress and algebraic stress models; these three approximations are sometimes referred to as yesterday's, today's, and tomorrow's models, respectively. The latter remark is based on the idea that this ordering represents a ranking of the quality of the models, i.e., that each succeeding model is more exact than its predecessors; this may not always be the case (see, for example, Kline et al. (1981)).

On balancing all these factors, we believe it is better to adopt the pragmatic view that turbulence models are engineering correlations in a more sophisticated guise and that the only true test of quality is performance. Of the models mentioned, Reynolds stress models are still in the development stage, and two-equation and algebraic stress models are the most popular ones at present (see, for example, Rodi (1980)). Two-equation models also have important advantages in flexibility and range of application compared to one-equation models.

Two-equation models consist of an assumed functional form for the structure of the Reynolds stress tensor (usually the eddy viscosity assumption) and two partial differential equations for turbulent kinetic energy and another turbulence quantity that provides a length scale. The most commonly used two-equation models are K-ε, K-L, and K-ω models (where K = kinetic energy; ε = dissipation of turbulence; L = length scale; and ω = vorticity).

Looking at the results presented in 1980-81 AFOSR-HTTM-Stanford Conference on Complex Turbulent Flows, we find, for many of the flows tested, *two-equation models gave the best predictions.* However, for others, some of the simpler models, including integral and mixing length models, were as good or better. Unfortunately, which method is best varies from case to case. Each of the models in the 1980-81 Conference required modifications or special treatments for particular flows. No single model presented was accurate over the wide range of cases used. Moreover, some computors reported success on some classes of flows followed by degradation of the results when attempts were made to extend the range of flows without change of model or constants.

Although having a universal model is desirable, the preceding paragraph indicates that no such model exists at present. It also appears such a model would need to be very complicated and would probably be difficult to apply. (This opinion is now shared by W. C. Reynolds, who has been a leading proponent of universal models for some years, private comunication.) It is our view that models should be closely tied to the structure of the flow phenomena they are supposed to represent. This view is shared by many others but has rarely been used as the basis for models. Since different parts of flow fields often have quite different

flow structures, it may be impossible to model all flows, or even all of a single complex flow field, with a universal model. Furthermore, if we try to construct a universal model by using one flow to determine one model constant and another flow for another model constant, we may, to some degree, "contaminate" the model and render it invalid for either flow. As a result, the model may not be accurate for either flow. We will show below that this "contamination" is stronger than has been generally recognized for two-equation models.

Since a complex flow field contains several flow zones with different physical structures, and since universal closure models are usually "contaminated", it seems logical to construct models in which each flow zone is modeled independently. Here we define a flow zone as a distinct part of the flow field with definable and distinctive physical characteristics. This point deserves emphasis -- the models are tied to the local characteristics of the flow, not to the flow as a whole and certainly not to a wide variety of flows. Most flows contain more than one zone. For example, a diffuser flow with separation (Fig. 1.1) can be regarded as a composite of six flow zones: (A) the potential core; (B) the attached boundary layer; (C) the detachment zone; (D) the recirculation zone; (E) the free shear layer; (F) the reattachment zone. With zonal models, we can provide a separate model for each zone. It should be much easier to construct accurate models for zones than for the flow field as a whole, and the models can be much simpler than a universal model would need to be. Equally importantly, there is little, if any, danger of contamination. Fortunately, there is a limited number of types of flow zones in flows with engineering application. Therefore, the task of zonal modeling is large but finite. We believe that the zonal modeling approach will probably yield accurate engineering methods more quickly than will a search for a single universal closure model.

In this approach, the definition of a "zone" must be subject to pragmatic testing. At the beginning, we select a region we believe has distinct physics as a candidate zone. We then construct a model for that zone. If the model works within the desired accuracy, the zone definition is accepted. However, the process may not end here. The following possibilities arise:

(a) The region is not adequately modeled. In this case, the zone may need to be broken into two or more regions each with a different model; the zonal definition is then narrowed.

(b) The model works not only for the region intended, but for other regions as well. In this case, the definition of the zone can be broadened.

Thus in each case, we are guided by the success of the model and not by our initial guesses. In the end, what is seen as a zone therefore depends strongly on the model used.

For free shear flows, we began by adopting the classic classification scheme, that is, jets, wakes, and mixing layers were assumed to be distinct zones. Since jets and wakes have both planar and axisymmetric realizations, there are five basic cases. In each case there is a near field and a far field. This suggests that as many as ten zones might be needed. In addition, there are co-flowing jets and mixing layers with variable ratio of the velocities of the two main streams. Given this range of cases, it was not entirely clear what to select as zones. We started by assuming the need for a separate model for each flow. In the end, we found that many cases could be fitted with a single model, so that there are only three zones in the final model; the classification was not obvious a priori.

This process sounds awkward; in practice, however, it not only led to resolution in a reasonable time, but also was instructive in providing information about the basic parameters needed to model free shear flows and hence about the underlying physics. In the end, we were able to unify the models to form a single model with two parameters. This model is more successful than any we are aware of. We were able to use linear first-order equations for all the readjustment processes (to be described later).

If the flow field is decomposed into zones, as suggested above, there exist regions between the zones which can be called "readjustment regions", where the structure adjusts from that of the old zone to that of the new one. Physically, these readjustments are transitions from one type of structure to another. The modeling of these readjustment

regions must reflect this changing physics. Pragmatism requires that, at least at the outset, we adopt the simplest possible model for the readjustment regions. It also means that, to minimize the difficulty of blending, the models for various zones should have the same form; for example, they may all be of the $K-\varepsilon$ type. A linear blending model using a first-order lag equation meets the simplicity criterion; our expectation is that it may be able to represent most readjustment regions with reasonable accuracy. Thus far, our expectation has been fulfilled as will be reported in later chapters. However, we do not rule out the possibility that more sophisticated blending models may be needed in some cases.

To recapitulate, in constructing zonal models, we shall be guided by following criteria:

1. ACCURACY. Each model should represent the zone it is designed for with sufficient accuracy. Acceptable accuracy may vary with application. For the cases of interest to the authors, 5% accuracy in most integral parameters is a reasonable goal. In other applications, for example, environmental flows, much less accuracy may suffice.

2. SIMPLICITY. We want the model for each flow zone to be as simple as possible, consistent with engineering accuracy.

3. UNIFORMITY. We want the zonal models to be uniform in the sense that the variables used in each zone should be as similar as possible in order to simplify the zone readjustments. This will also help to make model development and assessment relatively straightforward. Two-equation models and, particularly, $K-\varepsilon$ models, will be selected as the basis on which to build the zonal models; this will allow maximum advantage to be taken of existing models.

4. INDEPENDENCE. We want the ability to alter the model in one zone without affecting the models in other zones. This will allow tuning for each zone separately. It also avoids the "contamination" problem discussed above.

5. CLOSE CONNECTION TO PHYSICS. As mentioned earlier, turbulence models should reflect the physics of the phenomena they are intended to represent. However, incorporating physics into a model is difficult and

has rarely been done. There is considerable accumulated knowledge on flow structures which should be useful in this effort.

6. NEGLIGIBLE NUMERICAL ERRORS. This is not really a modeling issue, but we need to eliminate uncertainty due to the numerical errors in computation. This is necessary if one is to evaluate the models objectively and requires the construction of accurate and stable numerical methods. At present, adequate numerical methods exist only for some types of flows and more should become available in the next few years.

1.2 An Overview of Modeling for Turbulent Free Shear Flows

1.2.1 Background for Free Shear Flows

Free shear flows are those flows in which there is no direct effect of solid boundaries. This class of flows consists of five basic flows; the mixing layer, and the plane and axisymmetric jets and wakes. As with boundary layers, these flows have a single predominant flow direction and hence the shear stresses and diffusion fluxes are significant only in directions perpendicular to the predominant direction. Furthermore, pressure gradients normal to the predominant flow direction are usually unimportant. Consequently, the equations governing these flows are identical to those of boundary layers. For this reason, the free shear flows and boundary layers are sometimes called thin shear layers. The free shear flows are all inherently unstable and transition from laminar to turbulent occurs at Reynolds numbers between 15 and 30 based on shear-layer width. It is almost impossible to maintain a laminar free shear flow in the laboratory and all free shear flows of practical engineering interest are turbulent.

Free shear flows play significant roles in many engineering applications. Jet engines, jet ejectors, fuel-oxidizer mixing in propulsive devices, and wakes behind airplanes and submarines are a few examples. Also, in flows with separation, free shear flow may represent a zone of the whole flow. Indeed, free shear flow zones are commonly seen in engineering flows (see Kline et al. (1981)).

Turbulent free shear flows are a good starting point for studying turbulence because they are relatively simple and hence offer a better

chance for understanding. Most of the turbulence structures in engineering flows are not well understood at the present time. When extra strains, such as the effects of solid walls and pressure or temperature gradients, are added to the flows, the turbulence evolution becomes more complicated and more difficult to understand.

In classic theory, power laws describe the downstream variation of the layer width and the velocity decay with downstream distance for many free shear flows (see, for example, Schlichting (1979) and Tennekes and Lumley (1972)). These power laws are exact for laminar flows and are based on dimensional arguments and the momentum integral equation for turbulent flows. Although not exact, power laws do provide a guideline of the behavior of the flows and experimentalists often use power laws for fitting data.

With present computers, we cannot solve the full time-dependent Navier-Stokes equations (full turbulence simulation), which are the only truly universal "model" for all the turbulent flows, except for very simple flows. Fortunately, the details of a turbulent flow are rarely needed; time-averaged quantities usually suffice even when the mean flow is unsteady. Time-averaged equations are therefore used for most engineering calculations. In the process of time averaging, however, most of the detailed information contained in the Navier-Stokes equations is lost and, as a result of the nonlinearity, the time-averaged equations do not form a closed set of equations. Closure of the set of time-averaged equations requires a turbulence model describing the Reynolds stresses in terms of quantities that can be calculated.

1.2.2 Eddy Viscosity Model

Boussinesq (1877) initiated the concept of eddy viscosity; it is still widely used in turbulence modeling. He suggested that the effective turbulent shear stress, arising from the cross-correlation of the fluctuating velocities, be replaced by the product of mean velocity gradient and a quantity called the "eddy viscosity" or "turbulent viscosity". This model resembles the stress-strain relationship in laminar flows. Unlike the molecular viscosity, the eddy viscosity is not a property of the fluid. Its value varies from point to point in the

flow, and is largely determined by the characteristics of the turbulence at the point in question. The introduction of the eddy viscosity provides a framework for turbulence modeling, but it does not itself constitute a model; there remains the task of expressing the eddy viscosity in terms of known or calculable quantities.

The mixing length hypothesis, introduced by Prandtl (1925), has been a major success in turbulence modeling. It assumes that the eddy viscosity is proportional to the product of the density, a length scale, and a velocity scale. For two-dimensional flows, it further assumes that the velocity scale can be replaced by the product of the length scale and the mean velocity gradient. This reduces the number of unknowns to one, a length scale known as the mixing length. For flows bounded by walls, the length scale is proportional to the distance from the wall in regions very close to the wall (inner layer) and to the layer thickness where the wall effect is small (outer layer). For turbulent free shear flows, the length scale should be proportional to the width of the layer, but the proportionality constant varies from flow to flow (see, for example, Launder and Spalding (1972)). There is no way of predicting the constant for a flow that has not been measured. This lack of generality is a major drawback of this method.

For free shear flows, the mixing length model assumes constant length scale across the layer at a given downstream location. Another class of models assumes the eddy viscosity constant across the layer. In these models, the velocity scale is taken as the maximum velocity difference in the layer rather than the product of length scale and velocity gradient. Generally, the constant eddy viscosity model performs less satisfactorily than the mixing length model. However, the constant eddy viscosity model allows similarity solutions for which the problem can be reduced to an ordinary differential equation (Schlichting (1979) and White (1974)). This was a major advantage when high-performance computers and accurate numerical methods for solving partial differential equations were not available.

1.2.3 Two-Equation Models

It was not until the late 1960s that differential equations were used to calculate the velocity and length scales that determine the eddy viscosity. In these models, the velocity scale is proportional to the square root of the turbulent kinetic energy which is obtained by solving a differential equation. If the length scale is prescribed, we have the so-called one-equation models. Alternatively, the length scale may be derived from another differential equation; we then have two-equation models. Several length-scale-determining equations have been proposed. The one which describes the turbulent energy dissipation rate has been favored by many researchers. The reason lies in the fact that this quantity appears in the turbulent kinetic energy equation. This model is called the K-ε model and has enjoyed a great deal of success since Jones and Launder (1972) first proposed it. Rodi (1972) has used it extensively in the prediction of free shear flows. Two-equation models do not require flow-specific length scale information and offer the possibility of achieving the generality that the mixing length and constant eddy viscosity models lack. However, the performance of the K-ε model falls short of the desired accuracy. For example, the standard K-ε model over-predicts the spreading rate of an axisymmetric jet by 30-35% and under-predicts the plane wake spreading rate by nearly 40%. The reason for the poor predictions of these flows may be contamination. On the other hand, only slight adjustments are required to improve the model. Details will be given in later chapters.

This provides the motivation for the present study of free shear flows. We will apply the zonal modeling strategy to the development of improved models. We begin with a close examination of the physics of individual zones and then incorporate as much of what we learn as possible into the model. The standard K-ε model is adopted as a base model since it predicts many flows reasonably well. Systematic modification of the model constants for well-defined zones is performed and then the zonal models are blended to allow readjustments between the zones. It is found that one primary and one secondary parameter suffice to classify and predict all free shear flows considered. The primary parameter is the free stream velocity divided by the maximum velocity

difference in the layer; it represents the ratio of the inertial force to the driving force. This parameter is zero for "pure" jets. It varies from a small value to infinity in co-flowing jets or wakes. In mixing layers, this parameter is fixed at some finite value, determined by the velocity ratio of the two streams, and can take on values from one to infinity. As this parameter increases, the driving force becomes smaller compared to the inertial force, it is harder for eddies to penetrate into the free stream, and the flow becomes more parallel. In this limit, the dominant mechanism of the turbulence transport is diffusion. This effect is simulated by changing two model constants.

The secondary parameter is a measure of lateral vortex stretching. This vortex stretching reduces the correlation between the shear stress and the turbulent kinetic energy. For example, the maximum value of $|\overline{u'v'}|/K$ is only about 0.23 in axisymmetric "pure" jet, in which vortex stretching is strongest, while it is about 0.3 in all plane flows. This effect disappears in far-downstream axisymmetric flows. Change of one model constant is required to incorporate this effect.

Experiments are the basis of our understanding of turbulence phenomena and provide the data required to fix the model constants or functions. Therefore, they are crucial in the development of zonal models and readjustments. There are extensive experiments on turbulent free shear flows. They will be carefully reviewed below.

In Chapter II, the standard "universal" model is reviewed and the zonal modeling concept is tested on three homogeneous flows. In Chapter III, a survey of free shear flow experiments is performed. In Chapters IV and V, a zonal modeling approach is used for the development of the model for plane and axisymmetric free shear flows respectively. In Chapter VI, a summary of the new model that brings together the plane and axisymmetric flows is presented.

Chapter II

ZONAL MODELING OF HOMOGENEOUS FLOWS

2.1 Background

Since the introduction of the idea of zonal modeling (Kline et al. (1981)), many researchers have shown interest in the approach. Others have criticized it and raised questions. It was not clear whether this concept would work, although it appeared to have promise. It was therefore decided to make a quick test of the idea before initiating a significant effort.

Homogeneous flows were selected for this task. Homogeneous flows are ones in which statistical turbulence quantities are independent of spatial position and, therefore, functions of time only; they may contain a mean flow with a constant rate of strain. Since nearly all engineering flows are inhomogeneous, homogeneous flows have little direct engineering application. Nevertheless, they are simple turbulent flows and, consequently, it is easier to construct models for them than for inhomogeneous ones. We shall use these homogeneous flows, because they provide an easy test of the zonal modeling concept and will lay a foundation for later development of zonal modeling for more complex flows.

In this chapter, zonal models for three homogeneous turbulent flows are developed. These are: homogeneous shear; plane strain; and axisymmetric strain flows. All of these flows start with isotropic turbulence as the initial condition. When shear or strain is applied to the flow, the turbulence begins to depart from isotropy and undergoes a transition or readjustment to a state which depends on the nature of the applied strain. After a long enough time, the turbulence reaches an asymptotic state. These flows can be regarded as consisting of two zones separated by a readjustment stage; the two zones are the initial isotropic flow zone and the fully-developed zone. Since homogeneous flows are time-developing flows, these flow zones occur in time rather than in space. Although the dimension of variation is different from the flow zones described in Chapter I, the concept is much the same.

2.2 The Standard K-ε Model

Before developing the new zonal models for homogeneous flows, it is worthwhile to examine the existing "universal" K-ε model (see, for example, Rodi, 1980). In this model, the Reynolds stress tensor is modeled using the eddy viscosity concept:

$$-\overline{u_i u_j} = \nu_t \left(\frac{\partial U_i}{\partial x_j} + \frac{\partial U_j}{\partial x_i} \right) - \frac{2}{3} \delta_{ij} K \qquad (2.2.1)$$

The eddy viscosity is given by:

$$\nu_t = C_\mu \frac{K^2}{\varepsilon} \qquad (2.2.2)$$

The turbulent kinetic energy, K, and rate of dissipation of the turbulent kinetic energy, ε, are governed by the differential equations:

$$\frac{DK}{Dt} = \nu_t \left(\frac{\partial U_i}{\partial x_j} + \frac{\partial U_j}{\partial x_i} \right) \frac{\partial U_i}{\partial x_j} - \varepsilon + \frac{\partial}{\partial x_i} \left(\frac{\nu_t}{\sigma_k} \frac{\partial K}{\partial x_i} \right) \qquad (2.2.3)$$

$$\frac{D\varepsilon}{Dt} = C_{\varepsilon_1} \frac{\varepsilon}{K} \nu_t \left(\frac{\partial U_i}{\partial x_j} + \frac{\partial U_j}{\partial x_i} \right) \frac{\partial U_i}{\partial x_j} - C_{\varepsilon_2} \frac{\varepsilon^2}{K} + \frac{\partial}{\partial x_i} \left(\frac{\nu_t}{\sigma_\varepsilon} \frac{\partial \varepsilon}{\partial x_i} \right) \qquad (2.2.4)$$

where U_i is the mean velocity in the i-direction. C_μ, C_{ε_1}, C_{ε_2}, σ_k, and σ_ε are model constants. The first two terms on the right hand side of each model equation represent production and destruction of the quantity whose evolution the equation describes. The last terms of these two equations represent diffusion, which plays no role in homogeneous flows.

Values of $C_\mu = 0.09$, $C_{\varepsilon_1} = 1.44$, $C_{\varepsilon_2} = 1.92$, $\sigma_k = 1.0$, and and $\sigma_\varepsilon = 1.3$ are widely used for the model constants. For reference, we shall call these the "standard values" and the model equations with these values the "standard K-ε model".

The five standard values of model constants were determined as follows:

1. C_{ε_2}: In homogeneous grid turbulence, diffusion and production are zero so C_{ε_2} is the only constant that plays a role in Eqs. (2.2.3) and (2.2.4). From the measured rate of decay of turbulent kinetic

energy, C_{ε_2} can be determined and is found to lie in the range 1.8 to 2.0; as noted above, 1.92 is the most commonly used value.

2. C_μ: In local-equilibrium shear layers, production and dissipation are essentially equal, and Eqs. (2.2.1) and (2.2.2) can be combined to yield $C_\mu = \left(\overline{u_1 u_2}/K\right)^2$. Measurements show that $-\overline{u_1 u_2}/K \approx 0.3$ in these flows, so that $C_\mu = 0.09$.

3. C_{ε_1}: In near-wall regions of boundary layers, the velocity profile is nearly logarithmic, production is approximately equal to dissipation, and the convection of dissipation is negligible. In this situation, Eq. (2.2.4) reduces to

$$C_{\varepsilon_1} = C_{\varepsilon_2} - \frac{\kappa^2}{\sigma_\varepsilon \sqrt{C_\mu}}$$

where $\kappa = 0.41$.

4. Finally, the diffusion constants σ_k and σ_ε were assumed to be close to unity and they were tuned by computer optimization. C_{ε_2} is then obtained from the eequation above.

Note that at least three different types of flows (homogeneous grid turbulence, equilibrium free shear layer, and boundary layer) were used to determine the model constants. This use of different flows causes the type of contamination described in the introduction. The standard K-ε model probably predicts boundary-layer flows better than other flows because two of the model constants were set using data from boundary-layer flows. However, the standard model, although widely used, cannot be expected to work well "universally". We shall assess how well (or badly) it does for a number of flows and several variables in this work.

Applied to homogeneous flows, Eqs. (2.2.3) and (2.2.4) reduce to

$$\frac{dK}{dt} = \nu_t \left(\frac{\partial U_i}{\partial x_j} + \frac{\partial U_j}{\partial x_i} \right) \frac{\partial U_i}{\partial x_j} - \varepsilon \qquad (2.2.5)$$

$$\frac{d\varepsilon}{dt} = C_{\varepsilon_1} \frac{\varepsilon}{k} \nu_t \left(\frac{\partial U_i}{\partial x_j} + \frac{\partial U_j}{\partial x_i} \right) \frac{\partial U_i}{\partial x_j} - C_{\varepsilon_2} \frac{\varepsilon^2}{k} \qquad (2.2.6)$$

and only three model constants, C_μ, C_{ε_1}, and C_{ε_2}, remain in the equations. Note that the physics from which C_μ and C_{ε_1} were determined are not appropriate to homogeneous flows. Therefore it is questionable whether the standard K-ε model is acccurate for such flows. In fact, its performance for the homogeneous flow cases in the 1980-81 Stanford Conference was not good. Some examples of the performance of this model for homogeneous flows will be given later.

In the present study, zonal models for homogeneous shear flow, homogeneous axisymmetric strain flow, and homogeneous plane strain flow are constructed as described below. The inputs used to build the models came from the full turbulence simulations by Rogallo (1981) and Lee and Reynolds (1985). These zonal models perform considerably better than the standard K-ε model in predictions of these flows, since they have been tuned for these flows.

2.3 Zonal Models for Homogeneous Flows

2.3.1 Homogeneous Shear Flow

Homogeneous sheared turbulence is a flow in which initially isotropic turbulence is subjected to a mean shear flow. After application of the shear, the structure of the turbulence becomes anisotropic. The flow gradually adjusts to the shear and, after a long enough time, appears to reach a fully-developed or asymptotic state in which the physics no longer changes. This flow can be regarded as consisting of two flow zones connected by a readjustment stage. The two zones are the isotropic initial flow zone and the fully-developed shear flow zone. These two flow zones occur in the time domain. Between these two time periods is the readjustment stage where the change of physics takes place. The readjustment is the most interesting part of this flow and the part to which most of our attention will be devoted.

In shear flows, the strain tensor is

$$S_{ij} = \begin{pmatrix} 0 & \Gamma_s/2 & 0 \\ \Gamma_s/2 & 0 & 0 \\ 0 & 0 & 0 \end{pmatrix} \qquad (2.3.1)$$

where $\Gamma_s = dU/dy$ is the shear rate. The most important Reynolds stress component is $\overline{u_1 u_2}$. Initially, in the isotropic state,

$$\overline{u_i u_j} = \frac{2}{3} \delta_{ij} K \tag{2.3.2}$$

i.e., $\overline{u_1 u_2} = 0$, and in the fully-developed state,

$$\overline{u_1 u_2} = -0.32K \tag{2.3.3}$$

where $K = (\overline{u_1^2} + \overline{u_2^2} + \overline{u_3^2})/2$ is the turbulent kinetic energy. Equation (2.3.3) correlates the experimental data extremely well. No modeling is needed for the other components of the Reynolds stress. We shall therefore adopt this as our model for the fully-developed state.

In the readjustment region, we shall assume that $\overline{u_1 u_2}$ can be represented by a simple blend of the initial and final states:

$$\overline{u_1 u_2} = -0.32 \lambda K \tag{2.3.4}$$

where λ is the readjustment parameter utilized to model the change of physics. It is defined to have the range $0 \geq \lambda \geq 1$.

In line with the philosophy of simplicity expounded in the introduction, we shall assume the readjustment parameter obeys a first-order lag equation, specifically, λ is determined by the first-order ordinary differential equation:

$$\frac{d\lambda}{dt} = b_s \Gamma_s (1 - \lambda) \tag{2.3.5}$$

where b_s is a dimensionless constant. This choice of lag equation makes the rate of change of the physics greatest for small λ. This behavior accords with observation. The solution to Eq. (2.3.5) is

$$\lambda = 1 - e^{-b_s \Gamma_s t} \tag{2.3.6}$$

By fitting the experimental data from Case 376A of the 1980-81 conference, it is found that

$$b_s = 1.5 \tag{2.3.7}$$

The model equation for K can be written, with the help of Eq. (2.3.4), as

$$\frac{dK}{dt} = 0.32\ \lambda\Gamma_s K - \epsilon \qquad (2.3.8)$$

The first term on the right hand side is the rate of production of kinetic energy. When $\lambda = 0$, the production term vanishes and Eq. (2.3.8) reduces to a form appropriate to isotropic flows. When $\lambda = 1$, Eq. (2.3.8) models fully-developed shear flows.

Following the form used in the standard K-ϵ model, the ϵ model equation can be written as

$$\frac{d\epsilon}{dt} = C_{\epsilon_1} 0.32\ \lambda\Gamma_s \epsilon - C_{\epsilon_2} \frac{\epsilon^2}{K} \qquad (2.3.9)$$

Fitting Rogallo's (1981) full simulation, we find

$$C_{\epsilon_1} = 1.406 \qquad (2.3.10)$$

and

$$C_{\epsilon_2} = \frac{11}{6} \qquad (2.3.11)$$

This value of C_{ϵ_2} has some analytical underpinning and is favored by Reynolds (1976). When $\lambda = 0$, Eq. (2.3.9) reduces to the model for the decay of isotropic turbulence (see Reynolds (1976)), and as λ is increased from zero, the production of dissipation term (the first term) increases.

The Reynolds stress model, Eq. (2.3.4) and the K and ϵ equations (2.3.8) and (2.3.9), together with the equation for the readjustment parameter, Eq. (2.3.6) constitute the zonal model for homogeneous shear flows with isotropic initial fields. When $\lambda = 0$, the system reduces to the model for isotropic flow and, when $\lambda = 1$, to the fully-developed shear flow model. As λ moves between zero and unity, the system undergoes a transition from one form to the other and allows an adequate readjustment from one zone to the other. Results obtained with this model will be given below.

2.3.2 Homogeneous Axisymmetric Strain Flow

Again, in this flow the initial velocity field is isotropic turbulence. At time $t = 0$, it begins to be stretched in one direction and compressed equally in the other two directions. This axisymmetric strain causes anisotropy; turbulence fluctuations in the stretching direction are reduced while those in the compression directions are increased. This is a result of the vortex filaments aligning with the stretching direction. After the strain is applied for a sufficiently long time, the Reynolds stress reaches a fully-developed structure. Between the initial and asymptotic states, the Reynolds stress undergoes a transition from one type of structure to the other. Again the time history can be decomposed into two zones separated by a readjustment stage.

The strain tensor for axisymmetric strain is

$$S_{ij} = \begin{pmatrix} \Gamma_a & 0 & 0 \\ 0 & -\Gamma_a/2 & 0 \\ 0 & 0 & -\Gamma_a/2 \end{pmatrix} \qquad (2.3.12)$$

where $\Gamma_a = dU/dx$ is the strain rate. The Reynolds stress in the isotropic state is given by Eq. (2.3.2). After the turbulence undergoes axisymmetric strain for a long period, the Reynolds stress tensor reaches an asymptotic state in which

$$\overline{u_i u_j} = \left(\frac{2}{3}\delta_{ij} - \frac{2}{3\Gamma_a} S_{ij} \right) K \qquad (2.3.13)$$

which shows that the component energy approaches zero in the stretching direction and K in each of the compression directions. Again assuming a monotonic variation from the initial state described by Eq. (2.3.2) and the state defined by Eq. (2.3.13), we have

$$\overline{u_i u_j} = \left(\frac{2}{3}\delta_{ij} - \lambda \frac{2}{3\Gamma_a} S_{ij} \right) K \qquad (2.3.14)$$

where $0 \le \lambda \le 1$, with $\lambda = 0$ corresponding to the initial state and $\lambda = 1$ to the fully-developed state.

The behavior of A, the readjustment parameter, is again assumed to be described by a first-order lag equation

$$\frac{dA}{dt} = b_a \tau_a (1 - A) \tag{2.3.15}$$

where b_a is a constant which need not be the same as b_s of Eq. (2.3.5). The solution to Eq. (2.3.15) is

$$A = 1 - e^{-b_a \tau_a t} \tag{2.3.16}$$

Fitting Rogallo's (1981) full simulation, we find that

$$b_a = 1.15 \tag{2.3.17}$$

With Eq. (2.3.14), the K model equation is

$$\frac{dK}{dt} = A \tau_a P - \varepsilon \tag{2.3.18}$$

Again we use the standard form of the ε model equation for this flow and arrive at

$$\frac{d\varepsilon}{dt} = C_{\varepsilon 1} A \tau_a P - C_{\varepsilon 2} \frac{\varepsilon^2}{K} \tag{2.3.19}$$

However, within the philosophy of zonal modeling, there is no reason why the constants need be the same as those in the previous case. In fact, $C_{\varepsilon 1}$ and $C_{\varepsilon 2}$ were determined by fitting data from Rogallo (1981) and found to be

$$C_{\varepsilon 1} = 2.0 \tag{2.3.20}$$

and

$$C_{\varepsilon 2} = \frac{11}{6} \tag{2.3.21}$$

Thus, Eqs. (2.3.14), (2.3.18), and (2.3.19), along with Eq. (2.3.16) form the zonal model for axisymmetric strain flows. Again, when $A = 0$, the model reduces to that for isotropic turbulence, while for $A = 1$, it becomes a model appropriate for turbulence which has undergone strong axisymmetric strain.

2.3.3 Homogeneous Plane Strain Flow

In this flow, the initially isotropic flow field is stretched in one direction and compressed in a second direction, with the third direction being neither stretched nor compressed. The fluctuations diminish in the stretching direction and increase in the compression direction while remaining close to $2K/3$ in the neutral direction. Eventually, the Reynolds stress approaches a fully-developed structure. Thus, the two-zone concept in the time domain applies to this flow.

The strain tensor for plane strain is

$$S_{ij} = \begin{pmatrix} 0 & 0 & 0 \\ 0 & -\Gamma_p & 0 \\ 0 & 0 & \Gamma_p \end{pmatrix} \qquad (2.3.22)$$

where $\Gamma_p = dW/dz = -dV/dy$ is the strain rate. We can model the normal Reynolds stresses (or the component energies) by

$$\frac{\overline{u_1^2}}{K} = \frac{2}{3} + \lambda \frac{\Gamma_p \frac{K}{\epsilon}}{a_1 + a_2 \Gamma_p \frac{K}{\epsilon}} \qquad (2.3.23)$$

$$\frac{\overline{u_2^2}}{K} = \frac{2}{3} + \lambda \left(\frac{2}{3} - \frac{\Gamma_p \frac{K}{\epsilon}}{a_1 + a_2 \Gamma_p \frac{K}{\epsilon}} \right) \qquad (2.3.24)$$

$$\frac{\overline{u_3^2}}{K} = \frac{2}{3} - \lambda \frac{2}{3} \qquad (2.3.25)$$

where a_1 and a_2 are constants, and $0 \leq \lambda \leq 1$ is the readjustment parameter. As in the above two flows, λ is found from a first-order linear ordinary differential equation:

$$\frac{d\lambda}{dt} = b_p \Gamma_p (1 - \lambda) \qquad (2.3.26)$$

with the solution

$$\lambda = 1 - e^{-b_p \Gamma_p t} \tag{2.3.27}$$

The constant b_p may be different than in the other flows. Note that, in this case, unlike the previous ones, for fixed total strain $\Gamma_p t$, $\overline{u_1^2}$ and $\overline{u_2^2}$ vary with the dimensionless strain rate $\Gamma_p K/\varepsilon$ while $\overline{u_3^2}$ is independent of the strain rate.

To determine the three constants, a_1, a_2, and b_p in the model, we used the following procedure:

1. By fitting the data of $\overline{u_3^2}/K$ from Lee and Reynolds' (1985) full simulation, it is found that

$$b_p = 1.1 \tag{2.3.28}$$

2. From rapid distortion theory for plane strain, Batchelor and Proudman (1954), both $\overline{u_1^2}$ and $\overline{u_2^2}$ tend to approach K for large values of $\Gamma_p t$ when Γ_p is large. This is because, under these conditions, the vortex filaments align with the stretching direction so rapidly that the component energies in the other two directions each share half of the total energy $2K$. This yields:

$$a_2 = 3 \tag{2.3.29}$$

3. Finally, by fitting Lee and Reynolds' (1985) data for $\overline{u_2^2}/K$, the component energy in the compression direction, it is found that

$$a_1 = 26.3 \tag{2.3.30}$$

With the developed normal stress functions, Eqs. (2.3.23), (2.3.24), and (2.3.25), the two model equations for K and ε can be written as

$$\frac{dK}{dt} = \lambda \Gamma_p \left(\frac{4}{3} - \frac{\Gamma_p \frac{K}{\varepsilon}}{a_1 + a_2 \Gamma_p \frac{K}{\varepsilon}} \right) K - \varepsilon \tag{2.3.31}$$

and

$$\frac{d\varepsilon}{dt} = C_{\varepsilon_1} \lambda \Gamma_p \left(\frac{4}{3} - \frac{\Gamma_p \frac{K}{\varepsilon}}{a_1 + a_2 \Gamma_p \frac{K}{\varepsilon}} \right) \varepsilon - C_{\varepsilon_2} \frac{\varepsilon^2}{K} \tag{2.3.32}$$

Fitting the full simulation data of Lee and Reynolds (1985), we obtain

$$C_{\varepsilon_1} = 1.75 \tag{2.3.33}$$

and

$$C_{\varepsilon_2} = \frac{11}{6} \tag{2.3.34}$$

Therefore, the zonal model for the plane strain consists of the model equations (2.3.31) and (2.3.32) the Reynolds normal stress functions, Eqs. (2.3.23), (2.3.24), and (2.3.25), and the readjustment parameter, Eq. (2.3.27).

2.3.4 Summary

In summary, the modal constants b, C_{ε_1}, and C_{ε_2} for the three zonal models developed here are tabulated as below. The constants C_{ε_1} and C_{ε_2} in the standard K-ε model are also included for comparison. Note that the ε-model equations (2.2.6), (2.3.9), (2.3.19) and (2.3.32) are all written in a consistent form:

$$\frac{d\varepsilon}{dt} = C_{\varepsilon_1}\frac{P\varepsilon}{K} - C_{\varepsilon_2}\frac{\varepsilon^2}{K}$$

where $P = -\overline{u_i u_j} S_{ij}$ is the production rate of turbulent kinetic energy.

Table 2.1

Comparison of Model Constants (Homogeneous Flows)

	Standard k-ε Model	Zonal Model		
		Homogeneous Shear Flow	Homogeneous Axisymmetric Strain	Homogeneous Plane Strain
Lag constant b		1.5	1.14	1.1
C_{ε_1}	1.44	1.406	1.7	1.75
C_{ε_2}	1.92	1.833	1.833	1.833

Note that, although our models are simple, they apply strictly only to cases in which one fixed type of strain is applied to initially isotropic turbulence. More complex cases, such as those with initially anisotropic states or strains which vary with time may not be amenable to treatment by these models. However, as our purpose is to demonstrate the inadequacy of the standard $K-\varepsilon$ model and the validity of the zonal concept and not to develop a general model of homogeneous flows, these are not serious deficiencies for our purposes. Certainly, a universal model would be valuable but, as noted earlier, it would also need to be much more complicated. This is the trade-off we intended to make; we give up hope of universality for simplicity while maintaining accuracy.

2.4 Results and Comparisons

Due to the nature of homogeneous flows, there is no convection or diffusion of turbulence. This fact allows reduction of the model equations from their normal partial differential equation form to a much simpler ordinary differential equation form. These model equations can be easily solved by numerical integration.

The Runge-Kutta fourth-order integration scheme seems ideal for this integration, and is used in the present study. This scheme is of high accuracy so that numerical errors are eliminated and the true performance of the model can be evaluated. The three zonal models for homogeneous flows described above are tested. The results obtained are compared with those predicted by the standard $K-\varepsilon$ model. Test cases are provided by Rogallo's (1981) and Lee and Reynolds' (1985) full simulations, and the experiments accepted for the 1980-81 Stanford Conference (Kline et al. (1981)).

2.4.1 Homogeneous Shear Flows

1. Rogallo's Full Simulation

Rogallo's (1981) full simulation of homogeneous shear flows were used to test both the zonal model and the standard $K-\varepsilon$ model. The results are shown in Figs. 2.1-2.4 for various shear rates and viscosities. The initial turbulence of the full simulation is unrealistic (undeveloped isotropic field, square spectrum), and it takes time for

the simulation to develop a realization of real turbulence. Therefore, the prediction of these flows by both models was begun at the third time-step of Rogallo's data. Also, the last data points of the full simulations are unreliable. This is because the eddy sizes grow with time, and when they approach the dimension of the box used in the simulation, the periodic boundary conditions used by Rogallo become invalid. For each case, twice the kinetic energy (i.e., 2K) and Reynolds stress $-\overline{u_1 u_2}$ vs. time are plotted in Fig. (a) and dissipation level ε vs. time in Fig. (b). For all cases, the zonal model predictions agree satisfactorily with the full simulation data. On the other hand, the standard K-ε model predictions of the three quantities all grow too fast. The assumed functional form of the Reynolds stress for the K-ε model, i.e.,

$$-\overline{u_1 u_2} = C_\mu \frac{K^2}{\varepsilon} \frac{dU}{dy}$$

is responsible for the overprediction of the growth by the K-ε model, because, at the given levels of K, ε, and dU/dy, this Reynolds stress function gives

$$-\overline{u_1 u_2} > 0.32\ K$$

which makes the production rate too high and hence overpredicts all the three quantities.

2. 1980-81 Conference Cases 376A and 376B

The zonal model and the standard K-ε model were both employed to predict the two homogeneous shear flow cases (376A, 376B) from the 1980-81 Stanford Conference. The results are shown in Figs. 2.5 and 2.6, respectively. The zonal model agrees quite well with the experimental data for both cases. The standard K-ε model underestimates K and $-\overline{u_1 u_2}$ for case 376A and overestimates them for case 376B. The Reynolds stress function again seems to be the source of the under/over predictions by the K-ε model; the predicted values of $-\overline{u_1 u_2}$ are considerably smaller and greater than 0.32K for cases 376A and 376B, respectively. This violates the established result that $-\overline{u_1 u_2} \approx$

0.32K. In the zonal model for the shear flows, however, $-\overline{u_1 u_2} = 0.32K$ is explicitly built into the Reynolds stress function.

2.4.2 Homogeneous Axisymmetric Strain Flows

Eight cases of Rogallo's (1981) full simulations of homogeneous axisymmetric strain flows with various strain rates and two different viscosities were used for testing the zonal model and the standard K-ε model. Figures 2.7-2.14 compare the predictions of both models with the full simulation. For each case, Fig. (a) shows the total and component energies of the turbulence vs. time and (b) the dissipation rate. The zonal model performs quite well for the whole range of strain rates. For the low-strain-rate cases, the standard K-ε model accurately predicts K but not the component energies. The dissipation level is also incorrect since it must compensate for the erroneous production rate. When the strain rate is high, the K-ε model can no longer provide accurate prediction of K. It is obvious that the assumed Reynolds stress function in the K-ε model is incorrect for these flows.

No appropriate experiment for this type of flows is available from the 1980-81 Stanford Conference to test the zonal and K-ε models.

2.4.3 Homogeneous Plane Strain Flows

1. Lee and Reynolds' Full Simulation

Lee and Reynolds' (1985) simulation provides six cases of plane strain flows with the strain rate varying from 0.65 sec^{-1} to 100 sec^{-1}. The zonal and standard K-ε models are tested against these data. The results of total and component energies and dissipation vs. time are presented in Figs. 2.15-2.20. The zonal model predicts the flows accurately over the entire range of strain rates simulated. The K-ε model, however, does not perform well in any case, especially for high strain rates; the component energies are all seriously in error. When strain rate is high, the smallest component energy (in the stretching direction) even becomes negative, which is physically impossible. This again suggests that the K-ε model Reynolds stress function is not suitable for plane straining flows and further reinforces the remark on "contamination" in the introduction.

2. 1980-81 Conference Cases 374A and 374B

Two plane strain flows, cases 374A and 374B, in 1980-81 Stanford Conference were used to further test the zonal and K-ε models. The results of the total and component energies vs. time are shown in Figs. 2.21 and 2.22 for these two cases. Contrary to the previous flows, the K-ε model performs slightly better than the zonal model for case 374A and about equally well as the zonal model for case 374B. One possible explanation is that the initial conditions of experiments are anisotropic which makes the initial production rate not equal to zero while the zonal model starts with isotropic flow field and zero initial production rate. Furthermore, a more careful study of the experimental data indicates that the Reynolds stress structure in the experiments is much different from that in Lee and Reynolds' simulation.

No model can simulate discrepant results for a single physical situation. The problem in this case is that the experimental data and the full simulation are in disagreement. It is hard to explain this difference. This clearly needs more attention. Until this problem is resolved, these data *cannot* provide a reliable check on model performance. We used the full simulations to set the model and are therefore unable to predict the experimental data. The reverse could have been the case, i.e., if we used the experimental data to set the model, we would fail to predict the full simulation results.

2.5 Conclusions of the Test

The study of zonal models for homogeneous flows, which was meant to test the zonal modeling concept and to lay the ground-work for models of more complex flows, has proven a success. The results presented above show that zonal models perform far better than the standard K-ε model in all usable cases. The improvement is largely due to zonal models being able to avoid "contamination" of the flow physics; of course, the extra degrees of freedom which the zonal concept offers make it much easier to obtain accurate fits to the data. A good model should reflect the physics; the Reynolds stress representation is the tool for accomplishing this. The physics is not universal. This is reflected by the inability of the Reynolds stress function in the standard K-ε model to

fit the range of flows considered. This is the major drawback of the standard K-ε model, at least for these flows. With the zonal approach, on the other hand, we can incorporate more physics of each zone into the model by constructing a Reynolds stress function which represents much of the physics of that zone. Although this requires more work and a careful study of each flow zone, it can be done once and for all. The gains obtained by whis work are obvious. As can be seen in this chapter, the Reynolds stress functions are different for the three homogeneous flows and the ability to incorporate this is the strength of the zonal approach.

Furthermore, the zonal model has the ability to adjust from one zone to another via a blending parameter governed by a lag equation. The addition of a lag equation provides one more degree of freedom. Physically, the lag equation allows adjustment of the physics as the flow changes its structure. This is one of the most attractive features of zonal models. In this connection, it is worth note that the various K-ε models, including the standard model, as presented in the 1980-81 Stanford Conference, all use constants set for equilibrium situations in homogeneous flows, boundary layers, and free shear layers. As a result, all these methods perform badly for situations where flows are far from equilibrium and in the readjusting regions that carry the flows back toward equilibrium. An example is the boundary layer downstream of a reattaching free shear layer, as occurs in the backward-facing step. Some additional degree of freedom in the models is therefore apparently necessary for K-ε type models if they are to provide good prediction for nonequilibrium and readjusting flows. The zonal approach as used in this study supplies the necessary degrees of freedom; thus the use of a "readjustment model" is not merely an artifice that allows fitting, but is rather a necessary step in modeling the physics accurately.

In summary, the three zonal models in this chapter were constructed systematically. They all consist of a specific Reynolds stress function, a first-order lag equation, and two model equations which have the format of the K-ε model equations. The results suggest a promising future for the zonal modeling concept.

Chapter III

A REVIEW OF FREE SHEAR FLOW EXPERIMENTS

3.1 Preliminary Remarks

In this chapter, turbulent free shear flow measurements are reviewed. Numerous free shear flow experiments have been performed. However, the agreement among experiments on the same flow is rather poor in some cases, particularly with respect to the turbulence data. Since these data are to be used in constructing models and tuning model constants, it is essential to justify the available data and to identify which are reliable.

There are some reviews of free-shear-flow experiments available -- for example, Newman (1966) and Harsha (1971). However, they are limited to earlier data whose accuracy is not known. Moreover, they deal mostly with mean-flow quantities; very few turbulence quantities were examined. Rodi (1972) made a more thorough study of free-shear-flow experiments for his modeling work. He reviewed both mean and turbulence quantities for a wide range of flows. In a later publication, Rodi (1975) provided another detailed but similar survey. However, it has been more than a decade since Rodi's last review. Many more data have recently become available. Furthermore, Rodi's reviews contain no experiment that covers both the near and far fields or a wide range of the ratio of velocity difference to free-stream velocity. The details of turbulence evolution in this whole range are not clear. Such information, however, is very important in turbulence modeling; this provides the motivation of the present review.

Experiments on five basic free shear flows are reviewed in this chapter. These flows are plane jets, plane wakes and mixing layers, axisymmetric jets, and axisymmetric wakes. "Pure" jets (jets issuing into stagnant surroundings) and co-flowing jets are considered separately.

In addition to global parameters, such as the spreading rate and the centerline velocity decay rate, we shall consider the profiles of the streamwise mean velocity, turbulent kinetic energy, and turbulent

shear stress in this chapter. Since the turbulent shear stress is the most important Reynolds stress for thin shear layers, it will receive particular attention. (Recall that it determines the model constant C_μ in the K-ε model.)

In this survey, power laws serve to correlate the data. The momentum integral equation provides a relationship between the characteristic velocity and the width of the layer and is used as an internal consistency check. Moreover, given the streamwise velocity profile, the transverse velocity and turbulent shear stress can be found from the continuity and momentum equations. This provides a check on the shear stress measurements. There is no easy way, however, to validate the turbulent kinetic energy data except by comparing the profiles from different experiments. The rate of dissipation of turbulent kinetic energy is rarely measured. Even if measured and reported, the uncertainties are large and difficult to estimate. Therefore, the dissipation rate is not examined here.

3.2 Plane Free Shear Flows

3.2.1 Jets

Many experiments have been performed on plane jets. We shall consider some of the well-recognized ones. Heskestad (1965) and Gutmark and Wygnanski (1976) measured jets issuing into stagnant surroundings ("pure" jets). Bradbury (1965), in order to reduce the measurement errors near the edge of the jet, had the jet exhaust into a slow-moving airstream. Although this co-flowing jet departs only slightly from the self-preserving "pure" jet, its spreading rate is considerably lower than that of a "pure" jet. Bradbury and Riley (1967) carried out co-flowing jet experiments with various ratios of free stream velocity to jet exhaust velocity.

An empirical formula for the streamwise velocity profile (Bradbury, 1965) fits the data for all velocity ratios quite well:

$$\frac{U_1}{U_{1m}} = f(\eta) = \exp\left[-0.6749\eta^2\left(1 + 0.0269\eta^4\right)\right] \qquad (3.2.1)$$

where

$$U_1 = U - U_\infty \tag{3.2.2}$$

is the velocity excess, and

$$\eta = \frac{y}{\delta_{1/2}} \tag{3.2.3}$$

U_∞ is the free stream velocity, U_{1m} is the maximum value of U_1 (which occurs at the centerline), y is the distance from the centerline, and $\delta_{1/2}$ is the half-velocity width (the y value at which $U_1 = U_{1m}/2$). In their "pure" jet experiments, Heskestad and Gutmark and Wygnanski reported profiles that have a slightly less rapid approach to the free stream velocity. However, the differences are too small to be significant. Furthermore, Eq. (3.2.1) also represents the self-preserving profiles of axisymmetric jets (Bradbury, 1967), and wakes (Townsend, 1956) with only small discrepancies. We shall therefore use this formula for all the jet velocity profiles.

Co-flowing jets have significantly different characteristics than "pure" jets although the "pure" jet is a limiting case of the co-flowing jet. We shall examine co-flowing jets separately.

Pure Jets

Jets issuing into still surroundings become self-similar after the potential core disappears. The mean velocity reaches self-similarity much earlier than the turbulence quantities. How fast this takes place depends on the nozzle condition. In the self-similar region, the jet width and the centerline velocity obey power laws. The virtual origin differs from experiment to experiment. Heskestad and Gutmark and Wygnanski suggested that

$$\frac{d\delta_{1/2}}{dx} = 0.108 \pm 0.003 \tag{3.2.4}$$

and

$$\frac{d(J/U_{1m}^2)}{dx} \approx 0.16 \tag{3.2.5}$$

where

$$J = \int_{-\infty}^{\infty} U^2 dy \qquad (3.2.6)$$

J is the momentum flux and is the invariant for a pure jet by virtue of the momentum theorem. Equations (3.2.4) and (3.2.5) are also in excellent agreement with the review of experiments by Rodi (1972).

The turbulent kinetic energy and shear stress profiles of various experiments are compared in Figs. 3.1 and 3.2 respectively. The agreement is within the uncertainty of the data. Among them, Bradbury's (1965) data are particularly favored by Rodi (1972). The shear stress can be obtained by solving continuity and momentum equations assuming the correctness of Eqs. (3.2.1) and (3.2.4); the result is also shown in Fig. 3.2. It agrees well with Bradbury's and Gutmark and Wygnanski's data. Heskestad's data, on the other hand, show a 15% lower peak value of the shear stress profile; these data are not consistent with the values calculated using his own velocity profile (see Fig. 29 in Heskestad, 1965). We conclude that Heskestad's data are less reliable than those of Bradbury or Gutmark and Wygnanski.

Co-Flowing Jets

A jet issuing into a uniformly moving stream cannot be self-similar because U_∞/U_{1m} varies with x (Townsend, 1956); therefore we are interested in the streamwise flow development. To our knowledge, only Bradbury and Riley (1967) reported co-flowing jet measurements covering a wide range of velocity ratios. They showed, using dimensional arguments, that the co-flowing jet approaches the behavior of a self-preserving "pure" jet as $(x-x_o)/\theta \to 0$ and a self-preserving wake as $(x-x_o)/\theta \to \infty$. They verified these results experimentally. Here, x_o is the apparent origin of the flow and is the only influence the nozzle conditions have on the flow and θ is the momentum thickness of the jet defined as

$$\theta = \int_{-\infty}^{\infty} \frac{U}{U_\infty}\left(\frac{U}{U_\infty} - 1\right) dy \qquad (3.2.7)$$

The limiting behaviors were also suggested by Townsend (1956).

Bradbury and Riley reported that the data can be correlated in two limiting cases as follows. In the limit $(x-x_o)/\theta \to 0$,

$$\frac{\delta_{1/2}}{\theta} = 0.109 \frac{x - x_o}{\theta} \tag{3.2.8a}$$

and

$$\left(\frac{U_\infty}{U_{1m}}\right)^2 = 0.16 \frac{x - x_o}{\theta} \tag{3.2.8b}$$

In the limit $(x-x_o)/\theta \to \infty$,

$$\left(\frac{\delta_{1/2}}{\theta}\right)^2 = 0.1 \frac{x - x_o}{\theta} \tag{3.2.9a}$$

and

$$\left(\frac{U_\infty}{U_{1m}}\right)^2 = 0.41 \frac{x - x_o}{\theta} \tag{3.2.9b}$$

Note that Eqs. (3.2.8a) and (3.2.8b) reduce to Eqs. (3.2.4) and (3.2.5) as $U_\infty \to 0$; this shows that, in the early stage, a co-flowing jet behaves similarly to a "pure" jet. In addition, Bradbury and Riley provided the width and centerline velocity excess versus downstream distance in a dimensionless form that collapses all the co-flowing jet data except for the initial developing stage, cf., Figs. 3.3 and 3.4.

With the mean velocity profile represented by Eq. (3.2.1), the momentum integral equation, Eq. (3.2.7), becomes

$$\frac{\delta_{1/2}}{\theta}\left(\frac{U_{1m}}{U_\infty}\right)^2 I_2 + \frac{\delta_{1/2}}{\theta}\frac{U_{1m}}{U_\infty} I_1 = 0.5 \tag{3.2.10}$$

where

$$I_n = \int_o^\infty f^n d\eta \tag{3.2.11}$$

Equations (3.2.10) and (3.2.11) provide a relationship between the jet width and the centerline velocity excess. In the limit $(x-x_o)/\theta \to 0$ (self-preserving "pure" jet), the first term on the left-hand-side of Eq. (3.2.10) dominates. On the other hand, in the limit $(x-x_o)/\theta \to \infty$ (self-preserving wake), the second term dominates. Therefore, Eq. (3.2.10) becomes

$$\frac{\delta_{1/2}}{\theta}\left(\frac{U_{1m}}{U_\infty}\right)^2 I_2 = 0.5 \qquad (3.2.12)$$

and

$$\frac{\delta_{1/2}}{\theta}\frac{U_{1m}}{U_\infty} I_1 = 0.5 \qquad (3.2.13)$$

respectively, in the two limits.

Equations (3.2.8) and (3.2.9) satisfy Eqs. (3.2.12) and (3.2.13), respectively, within 2%, providing a consistency check. Furthermore, co-flowing jet data given by Bradbury and Riley also agree with Eq. (3.2.10) within 2%.

Neither turbulent kinetic energy nor shear stress profiles were reported by Bradbury and Riley. However, the eddy Reynolds number defined by

$$R_T = \delta_{1/2} U_{1m} \frac{\int_o^\infty \left(\frac{\partial U}{\partial y}\right)^2 dy}{\int_o^\infty \left(-\overline{u'v'}\right) \frac{\partial U}{\partial y}\, dy} \qquad (3.2.14)$$

was tabulated. The only conclusion that can be drawn from the eddy Reynolds number data is that, when going downstream in a co-flowing jet, the shear stress level (normalized by U_{1m}^2) increases to an asymptotic upper limit equivalent to far-field wake flows. This indicates that a far-field co-flowing jet behaves similarly to a far-field wake. These results will help us clarify the controlling physical parameters in free shear flows.

3.2.2 Wakes

Plane wake experiments include those behind flat plates, those behind circular cylinders, and some intermediate cases. Although the near fields of wake flows depend heavily on the initial conditions, i.e., the shape of the body that generates the wake and whether or not there is vortex shedding, the far fields display a universal asymptotic self-similar state. Townsend (1949) measured a wake behind a circular

cylinder and claimed that self-similarity is achieved 500 diameters downstream of the cylinder. The centerline velocity deficit at the last station was about 3% of the free stream velocity. A complete set of turbulence measurements was reported. However, Townsend's data were taken only in the far-field asymptotic self-similar region. They do not, therefore, provide any information on the evolution of the flow into the asymptotic state. Chevray and Kovasznay (1969), Andreopoulos and Bradshaw (1980), and Ramaprian, Patel and Sastry (1982) investigated the wake of a flat plate. Their measurements were made in the near field; the centerline velocity deficit at the last measurement station is at least 20% of the free stream velocity. An analysis of the momentum integral equation similar to Eq. (3.2.10) and examining the size of the terms show that these flows are not near the far wake asymptote.

More recently, Pot (1979) studied the flat plate wake flow from the trailing edge of the plate to a location sufficiently far downstream that the far wake asymptote is clearly reached. He reported all the turbulence data necessary for the present study. Pot's data set and that of Townsend will be examined here.

The far-field velocity profiles of Townsend and Pot are well approximated by Eq. (3.2.1) when U_1 is taken to be the velocity deficit $U_\infty - U$. Velocity profiles at the last few stations of Chevray and Kovasznay, Andreopoulos and Bradshaw, and Ramaprian, Patel and Sastry all agree with this empirical formula although their experiments were not carried far enough downstream to fully reach the asymptotic state. This indicates that the mean flow quantities settle down to a self-similar stage much earlier than the turbulence quantities, as has been found in a wide variety of other flows.

Pot's far-field data suggest

$$\left(\frac{\delta_{1/2}}{\theta}\right)^2 = 0.1\,\frac{x - x_o}{\theta} \qquad (3.2.15)$$

and

$$\left(\frac{U_\infty}{U_{1m}}\right)^2 = 0.43\,\frac{x - x_o}{\theta} \qquad (3.2.16)$$

These equations agree with (3.2.9a) and (3.2.9b) which describe the behavior of the far-field co-flowing jet. This again confirms that far-field wakes and far-field co-flowing jets have common characteristics. A spreading parameter defined by

$$sp = \frac{U_\infty}{U_{1m}} \frac{d\delta_{1/2}}{dx} \tag{3.2.17}$$

is 0.103 according to Eqs. (3.2.15) and (3.2.16), compared to a value of 0.098 reported by Rodi (1972) from Townsend's data. The 5% difference is within the uncertainty of the data.

The counterpart of Eq. (3.2.10) for wake flow is

$$-\frac{\delta_{1/2}}{\theta}\left(\frac{U_{1m}}{U_\infty}\right)^2 I_2 + \frac{\delta_{1/2}}{\theta}\frac{U_{1m}}{U_\infty} I_1 = 0.5 \tag{3.2.18}$$

Pot's wake width and centerline velocity deficit data were checked against Eq. (3.2.18). The agreement is excellent (within 3%) except at the first two stations where the velocity profiles are not close to the self-similar form.

It is clear from Pot's data that both the turbulent kinetic energy and shear stress (both normalized by U_{1m}^2) increase with downstream distance to the asymptotic far wake values. Figure 3.5 shows the maximum shear stress and maximum kinetic energy in the layer as functions of downstream distance. The far-field shear stress level is between 0.05 and 0.053, which agrees well with Townsend's value (0.051). Moreover, using 0.103 for the spreading parameter defined by Eq. (3.2.17) and the velocity profile, Eq. (3.2.1), the shear stress can be derived from the momentum equation. The resulting maximum shear stress is about 0.053 which agrees with the data from both sources. The far-field kinetic energy level is about 0.18 in Pot's data and less than 0.14 in Townsend's data. It is hard to justify the discrepancy between these two data sets. However, we tend to believe Pot's data, for the following reasons. Firstly, Pot's experiment is much more recent, and his equipment is more modern. Since much has been learned about hot-wire error control during the intervening period, he should get more reliable results. Secondly, all known plane shear flows have $|\overline{u'v'}|/k \approx 0.3$ in

the equilibrium region. In Townsend's data this ratio become 0.5, while for Pot's data it remains at about 0.3. Thirdly, similar experiments performed by Uberoi and Freymuth (1969) and Thomas (1973) suggested that Townsend's values of $\overline{u'^2}$ are too small.

3.2.3 Mixing Layers

The turbulent plane mixing layer is one of the simplest shear flows. However, complete understanding of the structure of this flow is still far from complete although the general features of the flow were established by Liepmann and Laufer (1947). They made hot wire measurements in a zero-velocity-ratio mixing layer. Their mean velocity and turbulence measurements indicated a very rapid approach to self-similarity. This was regarded as the most reliable and extensive source of mixing layer data for more than two decades. Wygnanski and Fiedler (1970), Patel (1973), and Champagne, Pao and Wygnanski (1976) studied the same flow to obtain higher-order statistical characteristics of the turbulence. The agreement among these experiments is rather poor as will be noted later.

Two-stream mixing layers with finite velocity ratios have not received as much attention. Sabin (1965) measured mean velocity profiles and correlated the spreading parameter for various velocity ratios with a simple function. Miles and Shih (1968) investigated the flow with a wide range of velocity ratios. However, only the spreading parameter as a function of velocity ratio was presented. Spencer and Jones (1971) and Yule (1971) each measured the layers at two different velocity ratios. Both reported detailed velocity profiles and turbulence quantities. The agreement is again poor.

Mixing layers are known to be very sensitive to the initial conditions. For example, placing a trip wire upstream on the splitter plate can alter the spreading rate by more than 20% (Liepmann and Laufer, 1947 and Wygnanski and Fiedler, 1970). They are also sensitive to the boundary conditions imposed. In most cases, mixing layer experiments are conducted in wind tunnels with walls both above and below the flow. This affects the secondary flow speed, the entrainment into the mixing layer and, consequently, the turbulence structure and the spreading

rate. Variations in initial and boundary conditions are probably responsible for the disagreement among experimental data.

Figures 3.6 compares velocity profiles for mixing layers with zero and nonzero velocity ratios. In this figure, y is normalized by a characteristic flow width $\delta = y_{0.9} - y_{0.1}$. Here, y_x is defined as the location where $U = U_{\infty_2} + x(U_{\infty_1} - U_{\infty_2})$. There is considerable scatter of the data near the edges, especially at the zero velocity edge in Fig. 3.6. According to Rodi (1975), however, this is the best way to correlate the data. If the data are plotted versus y/x, as is often done in the literature, the agreement is worse because the spreading rate $d\delta/dx$ varies considerably. The scatter indicates the dificulties in measuring accurately in these regions and perhaps reflects the sensitivity of the layer to the nearness of the boundary walls.

Figure 3.7 shows spreading rates, dL/dx, as a function of the velocity ratio $(R = U_{\infty_2}/U_{\infty_1})$. Note that the layer width L in this figure is defined as

$$L = y_{\sqrt{0.9}} - y_{\sqrt{0.1}}$$

Some of the data were taken from Rodi (1975). The line in the figure represents the spreading rate given by the Evaluation Committee of 1980-81 Stanford Conference. When the extreme values are discarded, the line seems a reasonable average representation for the spreading rate, although it is slightly lower than the average at high velocity ratios.

The profiles of turbulent kinetic energy measured in various experiments are shown in Fig. 3.8(a) and (b) for zero and two finite velocity ratios $(R = 0.3$ and $0.61)$. The agreement is poor except for the shape of the profiles.

The turbulent shear stress profiles are shown in Fig. 3.9(a) and (b) for zero and two finite velocity ratios $(R = 0.3$ and $0.61)$, respectively. Although the agreement is not good, it appears that the nondimensional shear stress increases as the velocity ratio is increased.

There is no way to justify the disagreement because of the different experimental setups in different experiments and the nature of

sensitivity of the flow as explained above. Until this issue is completely resolved, the only quantity that can be used as a guide for modeling seems to be the average spreading rate given by 1980-81 Stanford Conference.

3.2.4 Shear Stress-Kinetic Energy Relationship

The value of $|\overline{u'v'}|/K$ was examined for all plane shear flows. For jets and wakes, this quantity increases linearly from zero at the centerline to a maximum of about 0.3 and then drops back to zero. Townsend's (1949) wake flow is an exception; it shows a maximum value much higher than 0.3. However, it is believed that his measurements of kinetic energy are too low as explained above. For mixing layers, all the available data show that $|\overline{u'v'}|/K$ has a value of about 0.3 in the center and decreases to zero at both edges.

3.3 Axisymmetric Free Shear Flows

3.3.1 Jets

The mean flow field of axisymmetric jets have been studied by numerous researchers (for example, Hinze, 1959), but the turbulence field by only a few. Most of the literature on this flow appeared more than three decades ago when measuring techniques were not very advanced. More recent measurements were made by Wygnanski and Fiedler (1969) and Rodi (1972) for self-preserving pure jets and by Maczynski (1962), Reichardt (1965), and Antonia and Bilger (1973) for co-flowing jets. It is again easier to discuss them separately.

Pure Jets

It was suggested by Bradbury (1967) that Eq. (3.2.1) can also approximate the velocity profiles of axisymmetric jets. However, the pure jet velocity profiles of both Wygnanski and Fiedler (1969) and Rodi (1972) approach zero more slowly than the formula suggests. A similar trend was found in plane jet cases. However, the uncertainty of the measurements is large near the edge (especially when the edge has zero velocity). Consequently, this empirical formula suffices as a first order approximation.

The spreading rates of the pure jets from both Wygnanski and Fiedler (1969) and Rodi (1972) are

$$\frac{d\delta_{1/2}}{dx} = 0.087 \pm 0.002 \qquad (3.3.1)$$

This value agrees with the spreading rate reported by Newman (1967), $d\delta_{1/2}/dx = 0.086$, an average over earlier experiments.

The centerline velocity decay rate, according to Wygnanski and Fiedler, is

$$\frac{d(U_J/U_{1m})}{d(x/D)} \approx 0.2$$

in self-preserving region, where U_J is the jet nozzle exhaust velocity. This converts into

$$\frac{d(J^{1/2}/U_{1m})}{dx} \approx 0.131 \qquad (3.3.2)$$

where

$$J = 2\pi \int_0^\infty U^2 r dr \qquad (3.3.3)$$

J is the momentum flux; it is the invariant for the jet.

The turbulent kinetic energy and shear stress profiles of Wygnanski and Fiedler and Rodi are presented in Figs. 3.10 and 3.11, respectively. The agreement is reasonable. The maximum non-dimensional shear stress of Wygnanski and Fiedler is about 10% less than Rodi's value. The latter is closer to the value (0.0184) calculated from the continuity and momentum equations.

Figure 3.12 shows the ratio $|\overline{u'v'}|/K$ versus the transverse distance for axisymmetric and plane pure jets. The maximum value of $|\overline{u'v'}|/K$ for the axisymmetric cases is about 0.23 vs. 0.3 for the plane cases. We speculate that this is due to lateral vortex stretching which appears only in axisymmetric flows.

Co-Flowing Jets

The velocity profiles measured by Antonia and Bilger (1973) agree with Eq. (3.2.1) satisfactorily, as reported by Bradbury (1967). Rodi (1975) also claims that the shape of velocity profile is approximately the same for both plane and axisymmetric jets, and that it does not vary significantly with either velocity ratio or downstream distance.

Before discussing the spreading and centerline velocity, it is wise to examine the constraint connecting them. With the momentum thickness for axisymmetric jets defined by

$$\theta = \left[2\pi \int_0^\infty \frac{U}{U_\infty} \left(\frac{U}{U_\infty} - 1 \right) r dr \right]^{1/2} \tag{3.3.4}$$

and the help of Eq. (3.2.1), we can write

$$\left(\frac{\delta_{1/2}}{\theta} \right)^2 \left(\frac{U_{lm}}{U_\infty} \right)^2 I_2' + \left(\frac{\delta_{1/2}}{\theta} \right)^2 \frac{U_{lm}}{U_\infty} I_1' = \frac{1}{2\pi} \tag{3.3.5}$$

where

$$I_n' = \int_0^\infty f^n \eta d\eta \tag{3.3.6}$$

In the case of a pure jet, Eq. (3.3.5) reduces to

$$\delta_{1/2}^2 \frac{U_{lm}^2}{J} I_2' = \frac{1}{2\pi} \tag{3.3.7}$$

The pure jet described by Eqs. (3.3.1) and (3.3.2) satisfies Eq. (3.3.7) within 4%.

The spreading and velocity decay rates in Antonia and Bilger's experiment show large uncertainty and scatter. Furthermore, the data do not display internal consistency. Rodi (1975) managed to collapse the jet width, Fig. 3.13, and centerline velocity data, Fig. 3.14, of three experiments for a wide range of velocity ratios. At larger values of x/θ, however, the measured jet widths and centerline velocities do not satisfy Eq. (3.3.5). Since the measurements of centerline velocity are probably more accurate than those of the jet width, a jet width computed from Eq. (3.3.5) with the measured centerline velocity given is also shown in Fig. 3.13.

No measurements of turbulent kinetic energy or shear stress were taken by Maczynski (1962) or Reichardt (1965). Antonia and Bilger's (1973) data show that both the scaled kinetic energy and shear stress increase with downstream distance in their measuring range. The largest value of $|\overline{u'v'}|/U_{1m}^2$ they recorded is about three times that found in pure jets. Although their data must be considered unreliable because of the scatter, the increasing trend of both the non-dimensional kinetic energy and shear stress in co-flowing jets seems to be established. This trend was also found in the plane cases. Indeed, the shear stress obtained from the continuity and momentum equations and the assumed velocity profile confirms this.

With the assumption that the velocity fluctuations in the radial direction are about the same in magnitude as those in the streamwise direction, Antonia and Bilger's turbulence data show a maximum value of $|\overline{u'v'}|/K$ about 0.3. Since their data were taken some distance from the nozzle, where the spreading rate is considerably lower than the pure jet spreading rate, this leads us to believe that the effect of vortex stretching is significant only when the jet spreads rapidly. We shall use this fact in generalizing our parameterization of free shear flows.

3.3.2 Wakes

Axisymmetric wakes are known to be very sensitive to the shape of the wake-generating body (Rodi, 1975). Unless the body is very slender it usually creates vortices in its wake. Different body shapes generate vortices of different strengths. This in turn provides different initial conditions for the various wakes and it takes a very long distance for the flow to "forget" the effects of the initial conditions. Although asymptotic far-field behavior exists, it usually occurs very far downstream from the body.

Many axisymmetric wakes have been studied (e.g., Carmody, 1964; Chevray, 1968; and Uberoi and Freymuth, 1970). Most of them are generated by blunt bodies, e.g., cones, spheres or disks. Unfortunately, they were not studied for a long downstream distance because the researchers were interested mainly in the vortex shedding phenomenon. Only Chevray (1968) measured a wake flow that was extended close to the

self-preserving asymptote. His wake-generating body was a relatively slender 6:1 spheroid and the effect of vortex shedding was reduced. A complete set of mean flow and turbulence quantities was reported.

Chavray's self-similar velocity profiles are well approximated by Eq. (3.2.1). The centerline velocity deficit and the wake width both approach asymptotic power laws. Moreover, the mean flow quantities satisfy (to within 3%) the constraint

$$-\left(\frac{\delta_{1/2}}{\theta}\right)^2\left(\frac{U_{1m}}{U_\infty}\right)^2 I_2' + \left(\frac{\delta_{1/2}}{\theta}\right)^2 \frac{U_{1m}}{U_\infty} I_1' = \frac{1}{2\pi} \qquad (3.3.8)$$

which can be derived in manner of Eq. (3.3.5). According to Rodi (1975), the far-wake spreading parameter defined by Eq. (3.2.17) for this flow is about 0.105, the same as that of Reichardt's (1965) asymptotic co-flowing jet. This confirms that, as in plane cases, an axisymmetric co-flowing jet behaves similarly to an axisymmetric wake in the far field.

The turbulence field of Chevray's wake exhibits a trend similar to that seen in co-flowing jets. The nondimensional kinetic energy and shear stress increase to asymptotic values as the flow develops. Fig. 3.15 shows the maximum values of kinetic energy and shear stress in the layer as functions of downstream distance.

3.4 Conclusions

Experiments on five basic free shear flows were reviewed in this chapter, including both near and far fields, the approach to asymptotic behavior, and co-flowing cases. Whenever possible, the data were checked by analytical relationships for consistency. Good data were identified for each flow. For those cases where scatter and uncertainty were large, trends were established; this will help us, at least qualitatively, to understand the physics. It appears that the measurements become difficult when the velocity or velocity difference is small, for example, near the edges of shear layers. This is probably due to the fact that the uncertainty of the data is larger than the measured values.

In later chapters, we shall use the data reviewed in this chpater to construct models and tune the model constants. The conclusions about limiting forms and their relations to each other through nondimensional correlations established in this chapter will allow us to create a single model for free shear flows containing two nondimensional parameters and a simple, uniform method for treating readjustment regions.

Chapter IV

NUMERICAL METHOD

4.1 Introduction

As a result of the thin shear-layer approximation, the governing equations for both the mean and turbulence fields for free shear flows are parabolic. They are:

$$\frac{\partial U}{\partial x} + \frac{1}{y^i}\frac{\partial}{\partial y}(y^i V) = 0 \tag{4.1.1}$$

$$U\frac{\partial U}{\partial x} + V\frac{\partial U}{\partial y} = \frac{1}{y^i}\frac{\partial}{\partial y}\left[y^i(\nu + \nu_t)\frac{\partial U}{\partial y}\right] \tag{4.1.2}$$

$$U\frac{\partial K}{\partial x} + V\frac{\partial K}{\partial y} = \nu_t\left(\frac{\partial U}{\partial y}\right)^2 - \varepsilon + \frac{1}{y^i}\frac{\partial}{\partial y}\left(y^i\frac{\nu_t}{\sigma_k}\frac{\partial K}{\partial y}\right) \tag{4.1.3}$$

and

$$U\frac{\partial \varepsilon}{\partial x} + V\frac{\partial \varepsilon}{\partial y} = C_{\varepsilon_1}\frac{\varepsilon}{K}\nu_t\left(\frac{\partial U}{\partial y}\right)^2 - C_{\varepsilon_2}\frac{\varepsilon^2}{K} + \frac{1}{y^i}\frac{\partial}{\partial y}\left(y^i\frac{\nu_t}{\sigma_\varepsilon}\frac{\partial \varepsilon}{\partial y}\right) \tag{4.1.4}$$

where $\nu_t = C_\mu K^2/\varepsilon$ is the eddy viscosity. In these equations, $i = 0$ is for plane flows and $i = 1$ for axisymmetric flows. Note that the K-ε model equations are used in Eqs. (4.1.3) and (4.1.4) for the turbulence field. The standard method of solving parabolic equations is to march the solution downstream in the predominant flow direction. This is because information propagates in the flow direction and what happens at any location has no effect upstream. This behavior is a consequence of the characteristics of these equations. In the flow direction, the domain is open and only an initial upstream condition is needed. Two boundary conditions are required in the transverse direction.

The Keller Box method (see, for example, Cebeci and Bradshaw, 1977) is a popular method for solving parabolic equations. This method approximates all variables by their values at points on a rectangular grid and replaces the differential equations by finite difference equations that are averaged over each cell (or box). Figure 4.1(a) shows a typical grid box used in this method. However, experience shows

that this method tends to give oscillatory solutions in the marching direction if the initial condition is not perfect. If the initial condition is too high, the solution at the first step tends to be low so that the average at the center is correct; similarly, the solution at the second step is high. The oscillation continues downstream although its magnitude reduces. Another drawback of this method is its requirement of a V velocity component initial condition. This component is rarely measured in experiments and has to be estimated from the continuity equation.

This provides the motivation for the development of a better numerical scheme for solving the governing equations for free shear flows. In this chapter, a modified Keller Box method that uses a staggered grid system is developed. A transformation of the governing equations equivalent to using a grid expanding with the growth of the layer is first performed. An averaging technique at the first step of the solution procedure eliminates oscillations. Variable step sizes determined by the growth of the layer are used. Finally, the method is tested for some standard cases. The method of generation of initial conditions is described.

4.2 Description of the Numerical Scheme

4.2.1 Transformation of the Governing Equations

To account for the growth of the layer, the governing equations are transformed from the (x,y) physical coordinates to (ξ,η) variables where

$$\xi = x \tag{4.2.1}$$

and

$$\eta = \frac{y}{E(x)} \tag{4.2.2}$$

Here, $E(x)$ is a constant proportional to the thickness of the shear layer. Thus, in the transformed coordinates, the layer thickness is constant and the same number of grid points can be used at each downstream location.

After transformation, the governing equations, Eqs. (4.1.1) to (4.1.4) become

$$\frac{\partial U}{\partial \xi} - \frac{\eta}{E}\frac{dE}{dx}\frac{\partial U}{\partial \eta} + \frac{1}{(E\eta)^i}\frac{1}{E}\frac{\partial}{\partial \eta}\left[(E\eta)^i V\right] = 0 \tag{4.2.3}$$

$$U\frac{\partial U}{\partial \xi} - U\frac{\eta}{E}\frac{dE}{dx}\frac{\partial U}{\partial \eta} + \frac{V}{E}\frac{\partial U}{\partial \eta} = \frac{1}{(E\eta)^i}\frac{1}{E}\frac{\partial}{\partial \eta}\left[(E\eta)^i\,(\nu + \nu_t)\,\frac{1}{E}\frac{\partial U}{\partial \eta}\right] \tag{4.2.4}$$

$$U\frac{\partial K}{\partial \xi} - U\frac{\eta}{E}\frac{dE}{dx}\frac{\partial K}{\partial \eta} + \frac{V}{E}\frac{\partial K}{\partial \eta} = \nu_t\left(\frac{1}{E}\frac{\partial U}{\partial \eta}\right)^2 - \varepsilon + \frac{1}{(E\eta)^i}\frac{1}{E}\frac{\partial}{\partial \eta}\left[(E\eta)^i\,\frac{\nu_t}{\sigma_K}\,\frac{1}{E}\frac{\partial K}{\partial \eta}\right] \tag{4.2.5}$$

and

$$U\frac{\partial \varepsilon}{\partial \xi} - U\frac{\eta}{E}\frac{dE}{dx}\frac{\partial \varepsilon}{\partial \eta} + \frac{V}{E}\frac{\partial \varepsilon}{\partial \eta} = C_{\varepsilon_1}\frac{\varepsilon}{K}\nu_t\left(\frac{1}{E}\frac{\partial U}{\partial \eta}\right)^2 - C_{\varepsilon_2}\frac{\varepsilon^2}{K} + \frac{1}{(E\eta)^i}\frac{1}{E}\frac{\partial}{\partial \eta}\left[(E\eta)^i\,\frac{\nu_t}{\sigma_\varepsilon}\,\frac{1}{E}\frac{\partial \varepsilon}{\partial \eta}\right] \tag{4.2.6}$$

Before solving Eqs. (4.2.3) to (4.2.6), E and dE/dx must be specified. They are determined, in a discrete manner, as follows:

$$E_o = E_1 = 1.0 \tag{4.2.7}$$

and

$$E_{n+1} = E_n\,\frac{(\delta_{1/2})_n}{(\delta_{1/2})_{n-1}}, \qquad n \geq 1 \tag{4.2.8}$$

where the subscript represents the step number in the streamwise direction. dE/dx can be calculated once E is determined. The half-velocity width $(\delta_{1/2})_n$ is easily determined from the converged solution at step x_n.

4.2.2 Grid System

To derive the finite difference equations for a box, it is first necessary to define the locations at which the variables are defined. As shown in Fig. 4.1(b), U, K, and ε are given at the centers of left and right boundaries and V at the centers of top and bottom boundaries of a box. This arrangement makes the streamwise derivatives of U, K and ε, and normal derivative of V much easier to deal with. Furthermore, no V velocity component need be provided at the initial station.

The outermost location of U, K and ε is outside the last box. Therefore the zero boundary conditions of both K and ε on the edge do not cause any difficulty in the calculation of quantities such as K^2/ε or ε^2/K in the last box.

The spacing between grid points in the normal direction can be either constant or variable. The choice is made by the selection of the initial grid. Details will be given in next section. The spacing in the streamwise direction is variable, and the increase in step size is determined by the rate at which the layer grows:

$$\Delta x_n = \Delta x_{n-1} \frac{(\delta_{1/2})_n}{(\delta_{1/2})_{n-1}} \qquad (4.2.9)$$

where $\Delta x_n = x_{n+1} - x_n$.

4.2.3 Formulation of the Finite Difference Equations

Central differencing is used everywhere except where the streamwise velocity is small relative to the normal velocity. This occurs near the edge of pure jets. For those cases, the flow is principally in the normal direction near the edge and central differencing causes oscillation when the cell Reynolds number (based on V and Δy) is larger than two (see Patankar, 1980). To remedy this, upwind differences must be used for the convection terms in the normal direction in this region (Patankar, 1980). A second-order upwind scheme is used near the edge.

The fomulation of the finite difference equations is similar to that of the Keller Box method and can be found in Cebeci and Bradshaw (1977). The details are presented in Appendix A.

4.2.4 Averaging at the First Step

To avoid oscillation of the solution in the streamwise direction, an averaging technique is used at the first step. The initial conditions are generally not correct. The finite difference equations represent an average of the governing equations and tend to produce oscillations with an amplitude equal to the initial error. Averaging of the solutions at the initial and first stations eliminates most of the error and provides an improved initial condition. The solution procedure is then restarted from the center location and a half step is taken so that an improved solution is obtained at the first station. This averaging process is repeated three times. Each time the location of averaged solution is moved forward by half the reduced step size.

After this averaging, the effect of "bad" initial conditions on the solution is greatly reduced. From the second step on, the normal solution procedure is used.

4.2.5 Calculation of Eddy Viscosity

The eddy viscosity is required before the system of equations can be solved. In order to calculate the eddy viscosity, K and ε are needed. Since the solution procedure is iterative, K and ε are lagged by one iteration in the calculation of eddy viscosity. No other variables are lagged in the computation; mean and turbulence quantities are computed simultaneously.

Near the edge of the layer, the profile of eddy viscosity is smoothed when necessary. Bad profiles are sometimes caused by small negative values of K or ε. Because these quantities are very small in this region, they may produce large errors in the eddy viscosity. However, eddy viscosity should approach zero near the edge of the layer. Therefore, whenever a bad value of the eddy viscosity occurs, a value linearly interpolated between the previous good point and zero at the edge replaces the bad value. This smoothing process prevents the bad solution from penetrating into the layer. It is never necessary to use this procedure for more than three or four points near the edge except for far wake flows.

4.2.6 Convergence Criteria

The solution method is iterative. The convergence criterion demands that the increments of U, K, and ε at the point nearest the centerline between iterations be less than 10^{-4} times the values of the quantities at the previous iteration. Typically, the solution converges within five iterations.

4.2.7 Solution Procedures

Provided the solutions at step n have been obtained, the solution procedure can be outlined as follows:

1. In physical coordinates, calculate $\delta_{1/2}$ at step n. Calculate E_{n+1} by Eq. (4.2.8). Calculate dE/dx.
2. Use the solutions at step n as initial guesses for all variables at step n+1.
3. Solve a block tridiagonal system of linear equations that results from the Newton-Raphson linearization of the finite difference equations.
4. Update all variables by adding the increments obtained from step 3 to the old values.
5. Update the eddy viscosity.
6. If the increments satisfy the convergence criteria, stop the iteration and go to the next station. If not, repeat steps 3 to 5.

4.3 Input Data

4.3.1 Initial Conditions

Initial profiles of U, K and ε are required to start the computation. They have to be generated from experimental data. The streamwise velocity is measured in all experiments. For turbulent kinetic energy components, $\overline{u'^2}$ and $\overline{v'^2}$ are measured in most experiments. $\overline{w'^2}$, on the other hand, is not often measured and is usually approximated by the average of $\overline{u'^2}$ and $\overline{v'^2}$. The dissipation rate of turbulent kinetic energy is rarely measured; if it is, the uncertainty is very high. The turbulent shear stress is always recorded. One way

to calculate the dissipation rate is via the relationship for the shear stress used in the K-ε model:

$$\varepsilon = C_\mu \frac{K^2}{(-\overline{u'v'})} \frac{\partial U}{\partial y} \qquad (4.3.1)$$

The dissipation profile obtained by this method is designed to give the right shear stress. All the profile data mentioned above are interpolated with spline fits.

Although there is no need for an initial V profile, the program requires initial guesses for V at the first step. Guessed values of V should be provided but do not need to be accurate. Since V is small, the initial guesses were all taken as zero.

4.3.2 Grid Setup

The grid in the normal direction at the initial station has to be provided. Experience shows forty to fifty grid points should be used. The points should cover the region from $y = 0$ to approximately $y = 2.5\ \delta_{1/2}$. Equal or variable spacing can be used. We found the best choice to be a compound interest grid:

$$\Delta y_{j+1} = k \Delta y_j$$

where $1.03 < k < 1.1$. This makes the grid finer near the centerline and coarser near the edge. In all the computations reported herein, 45 points were used and $k = 1.03$ was used for the first 36 grids from the centerline and $k = 1.08$ for the rest of the domain.

The initial step size has to be specified. A step size of about twice $\delta_{1/2}$ appears to be reasonable. From the second step, the step size will be determined by the rate the layer spreads as described earlier.

4.4 Validation of the Numerical Method

Some validation tests were performed to assess the accuracy of the present numerical method. First a laminar plane jet was computed with a similarity initial condition. The results were checked against the analytical similarity solution. With the 45-point compound interest grid

described above and an initial step size of about 2 $\delta_{1/2}$, the error is 0.003% in the centerline streamwise velocity and 0.16% in the normal velocity at the edge after 30 initial $\delta_{1/2}$. Similar results were obtained for a laminar axisymmetric jet.

A turbulent plane jet calculation was made to test the method when all four equations (the continuity, momentum, K and ε equations) are coupled and have to be solved simultaneously. The results were compared with the similarity solution solved by Paullay et al. (1985). The errors in thickness growth and centerline velocity decay rates are both within 0.1% of the exact solution, while the error in the centerline value of K is about 0.9%. When the number of grid points is increased to 60, almost identical results were obtained. This indicates that grid independence was achieved at about 45 grid points across the layer. A number of streamwise step sizes were tested in the computation; there is no noticeable difference when the step size is $2\delta_{1/2}$ or less. However, the difference becomes large when the step size is $3\delta_{1/2}$ or larger. Therefore, it was determined that a step size of about $2\delta_{1/2}$ is the optimal choice.

4.5 Conclusions

In this chapter, an improved Keller Box method for solving equations of turbulent free shear flows has been described. Several improvements are incorporated in the present method, including a staggered grid, an initial averaging process, and upwind differencing near the edge of the layer. A grid that expands with the layer is used. A variable step size is determined by the growth of the layer. A validation process was performed to verify the accuracy of the method and the programming.

Initial conditions for U, K, and ε, an initial guess for V and the grid at the initial station are required, and their construction was described.

Chapter V

ZONAL MODELING FOR PLANE FREE SHEAR FLOWS

5.1 Introduction

In Chapter III, we examined experimental data on the flows to be studied and identified useful data. In this chapter, with these data as a guide, we shall try to better understand the physics of free shear flows and to construct improved models for these flows within the zonal modeling framework. Our goal is to build a consistent zonal model which can be used for all free shear flows. However, since axisymmetric flows differ so much from plane flows, we shall focus our attention on plane flows in this chapter. After the axisymmetric flows are considered in next chapter, we shall bring these two cases together.

When there is only one important component of the velocity-gradient tensor and the turbulent kinetic energy production and dissipation rates are approximately in balance, the standard K-ε model usually gives acceptable predictions (Launder et al., 1972). The plane pure jet is one example. However, when the shear is weak, the standard K-ε model predicts too slow a spreading rate of free shear flows. To remedy this, in his "extended" K-ε model, Rodi (1972) made the model constant C_μ a function of the ratio of rates of turbulence production and dissipation. This improves the predictions of the global parameters of weak shear flows considerably. However, the predicted profiles do not agree with the experiments. Patel and Scheuerer (1982), in their prediction of a far wake, used a corrected eddy viscosity with an intermittency factor. This model improves the velocity profile but underpredicts the shear stress and hence the spreading rate. Another difficulty with this model is that the intermittency factor has to be obtained from experiments and is different from flow to flow. Others selected the model constants C_{ε_1} or C_{ε_2} as targets for modification in various flows. If done on a flow-by-flow basis, this process removes the possibility of obtaining a model valid for all flows.

It seems, at the present time, that there is no single model that can predict all the plane free shear flows equally well. This provides motivation for the present study.

5.2 Analysis and Physics

Consider a steady symmetric plane jet in a uniform stream. With the thin shear-layer approximation, the governing equations for the flow are identical to those for boundary layers. Beyond the potential core, the development of the flow is independent of the initial conditions, and the profile of the jet becomes self-similar, i.e.,

$$U = U_\infty + U_{1m} f(\eta) \tag{5.2.1}$$

where

$$\eta = \frac{y}{\delta_{1/2}} \tag{5.2.2}$$

In this flow, the effect of the initial conditions persists only a relatively short distance and can be accounted for by use of an effective origin of the flow x_o. Assuming self-similarity, Eqs. (5.2.1) and (5.2.2), we can write from dimensional analysis (see Bilger, 1968):

$$\frac{dU_{1m}}{dx} = F_1(U_{1m}, U_\infty, J)$$

where

$$J = \int_{-\infty}^{\infty} U(U - U_\infty)\, dy$$

J is the excess momentum flux in the jet. This result can also be derived from the momentum integral equation. In nondimensional form, it becomes

$$\frac{d(U_\infty/U_{1m})}{d(x/\theta)} = F_2(U_\infty/U_{1m})$$

or

$$\beta \equiv \frac{U_\infty}{U_{1m}} = F\left(\frac{x - x_o}{\theta}\right) \tag{5.2.3}$$

where θ is defined in Eq. (3.2.7) and is constant throughout the flow.

By similar reasoning, we also obtain

$$\frac{\delta_{1/2}}{\theta} = G\left(\frac{x - x_o}{\theta}\right) \tag{5.2.4}$$

Here, F and G are universal functions for all jet flows. This result is confirmed by the experiment of Bradbury and Riley (1967).

If the jet self-preserving, the velocity can be expressed by Eq. (5.2.1) and shear stress distribution must have the form:

$$-\overline{u'v'} = U_{1m}^2 \, g(\eta) \tag{5.2.5}$$

Substitution of these similarity expressions into continuity and momentum equations and elimination of the transverse velocity V result in:

$$\frac{\delta_{1/2}}{U_{1m}} \frac{dU_{1m}}{dx} f(\beta+f) - \frac{d\delta_{1/2}}{dx} \beta\eta f' - \left(\frac{\delta_{1/2}}{U_{1m}} \frac{dU_{1m}}{dx} + \frac{d\delta_{1/2}}{dx}\right) f' \int_o^\eta f d\eta = g' \tag{5.2.6}$$

where g is defined by Eq. (5.2.5) and f by Eq. (5.2.1). From the momentum integral equation, we have the constraint:

$$\frac{\delta_{1/2}}{U_{1m}} \frac{dU_{1m}}{dx} = q \frac{d\delta_{1/2}}{dx} \tag{5.2.7}$$

where q is a function of β:

$$q = -\frac{I_2 + I_1\beta}{2I_2 + I_1\beta} \tag{5.2.8}$$

Here, I_1 and I_2 are defined by Eq. (3.2.11). Equation (5.2.6) can then be written as

$$\frac{d\delta_{1/2}}{dx}\left[q\beta f + qf^2 - \beta\eta f' - (q+1) f' \int_o^\eta f d\eta\right] = g' \tag{5.2.9}$$

Since $\delta_{1/2}$ and β are functions of x, the only conditions under which self-similarity is obtained, i.e., f and g are independent of x, are (see Townsend, 1956, and Hill, 1965):

$$\beta = 0 \quad \text{and} \quad \beta \to \infty \, ,$$

which correspond to a "pure" jet and a far wake, respectively. For values of β other than these limits, g changes as β varies. On the other hand, f seems to be very insensitive to β, as shown by experiments. Moreover, since F and G in Eqs. (5.2.3) and (5.2.4) are universal functions, β and $\delta_{1/2}$ are related; i.e., for a given β there is only one corresponding $\delta_{1/2}$ and vice versa. Therefore, the shear stress level, g, is only a function of β.

As β increases, the experimental data show that g increases and the η-value corresponding to maximum g moves outwards. This indicates that the turbulence decays more slowly than the centerline velocity. It also suggests that diffusion is increased as β increases; this is required to allow the maximum shear stress location to move outwards faster than the jet or wake spreads. It will be helpful to consider the physical reasons why increasing β has these effects.

Physically, β represents the ratio of the global inertial force to the global driving force for creating shear of the free shear flow. Thus, when β increases, the large eddies become relatively less energetic compared to the inertia of the free stream, and it is harder for them to penetrate into the free stream. As a result, the entrainment rate is reduced and the flow becomes more parallel. In the limit $\beta \to \infty$, the small eddies are more responsible for the turbulence transport, i.e., diffusion is more important. Alternatively, β can be regarded as a ratio of eddy turn-over time to the characteristic free stream time. As this ratio increases, the mixing process is slower relative to the free stream motion, and the flow spreads less rapidly. The slow mixing at high values of β also makes the flow more intermittent. It is well known that intermittent flow exists only near the edge of a "pure" jet, whereas it penetrates almost to the centerline of a far wake (Townsend, 1956). Intermittency increases the gradient of the average turbulence intensity, and therefore the average diffusion rate is increased.

As pointed out in Chapter III, it has been observed by many researchers, including Townsend (1956) and Bradbury and Riley (1967), that in the far field, a co-flowing jet behaves essentially the same as a wake. This means that the turbulence transport is independent of the

sign of the mean velocity gradient. Intuitively, we say that the turbulence rides on the mean flow and only "sees" a local velocity difference without "realizing" its direction. Although the eddies turn in opposite directions, the turbulence transport mechanism appears to be the same for both cases.

From these arguments, we conclude that the turbulence of free shear flows is characterized not by whether the flow is a jet or a wake, but rather by the value of β. Sabin (1965) also found a strong effect of β on mixing rate over a wide range of values of β for the mixing layer. Using similarity arguments, he provided a general relation between spreading rate and β. The same relation was found by Abramovich (1963), apparently independently. This Sabin-Abramovich relation was found to be one of the few universally valid correlations in both the 1972 NASA-Langley Conference on Evaluation of Computation in free shear layers and the 1980-81 AFOSR-Stanford Conference evaluating complex flow fields. Thus the importance of β (or some wholly equivalent parameter of different mathematic form) is fully validated and very widely accepted for the mixing layer case.

All these considerations suggest that a turbulence model designed to simulate these flows in a consistent way should depend on β and not the mean flow type.

In summary, we note the following:

1. The turbulence model should reflect the relative importance of the diffusion process as indicated by the value of β.

2. It appears that we can consider regions with the limits of $\beta \to 0$ and $\beta \to \infty$ as two zones of free shear flows and intermediate values of β as a readjustment zone.

3. A co-flowing jet or a wake starts with a small value of β and develops a larger β downstream. In terms of our model, it starts in the first zone and readjusts toward the second. A "pure" jet, on the other hand, stays in the first zone permanently. A given mixing layer has a constant value of β, but mixing layers as a class have values of β running from 1 to ∞. To apply the zonal modeling approach, we shall model the

two limiting cases first and then patch them together by a blending technique which describes the readjustment.

5.3 Construction of Zonal Models

As noted in Chapter I, the standard K-ε model will be used as a base for the development of zonal models. Therefore, in constructing zonal models we shall first test the standard K-ε model in each case. If it works for a given case, no modifications will be made, since it is then a satisfactory zonal model.

5.3.1 Zonal Model for the Limiting Case $\beta \to 0$

A "pure" jet represents the paradigmatic flow for this zone. After the disappearance of the potential core, a pure jet quickly becomes self-preserving. Therefore, we can use pure jet data at any downstream location to tune the zonal model for this zone.

The standard K-ε model was tested for this flow and gives surprisingly good results. The spreading rate and centerline velocity decay rate are

$$\frac{d\delta_{1/2}}{dx} = 0.108$$

$$\frac{d(J/U_{1m}^2)}{dx} = 0.16$$

which are in excellent agreement with Eqs. (3.2.4) and (3.2.5). The mean velocity, turbulent kinetic energy, and shear stress profiles also agree quite well with experimental data. Figures 5.1 to 5.3 illustrate the agreement.

The standard K-ε model is known to work well for flows with just one significant velocity gradient in which the turbulent kinetic energy production rate approximately equals the dissipation rate. The plane pure jet satisfies these two conditions. Another part of the reason that the standard K-ε model predicts pure jet flows so well is that some of the model constants were based on pure jet data. There is no need to modify the standard model for this zone.

5.3.2 Zonal Model for the Limiting Case $\beta \to \infty$

A far-field wake or co-flowing jet both are instances of this zone. However, U_{1m} is finite at the last measuring station in all experiments. Fortunately, when U_{1m} is less than 10% of U_∞, the flow behaves self-similarly and the asymptotic far-field state is closely approximated. Therefore, measurements which satisfy this criterion can be used. In the co-flowing jet of Bradbury and Riley (1967), U_{1m} is never less than 20% of U_∞; this is not small enough to qualify. Pot's (1979) wake data, on the other hand, reach $U_{1m}/U_\infty = 5\%$. Therefore, the measurements at the last few stations in Pot's experiment will be used to tune the model for this zone. In this range, the global parameters of Pot's data behave as described by Eqs. (3.2.15) and (3.2.16).

The standard K-ε model was first tested. The results are:

$$\frac{d\left(\delta_{1/2}/\theta\right)^2}{d(x/\theta)} = 0.065$$

$$\frac{d\left(U_\infty/U_{1m}\right)^2}{d(x/\theta)} = 0.248$$

These quantities are significantly lower than those of Eqs. (3.2.15) and (3.2.16), respectively. The spreading parameter, as defined in Eq. (3.2.17),

$$sp = 0.0635$$

is more than 35% lower than Pot's and Townsend's values. In addition, the predicted mean velocity, turbulent kinetic energy and shear stress profiles do not agree with the data. Figures 5.4 to 5.6 show the comparisons. Not only are the magnitudes in serious error, the shapes are also not correct, especially near the edge of the layer. These various profiles all go to zero too fast.

From the discrepancies between the K-ε predictions and the experiments, it appears that the diffusion predicted by the standard K-ε model is not sufficiently strong for this zone. To remedy this, we decided to decrease two model constants: C_{ε_1} and σ_k. These changes increase the shear stress as well as diffusion. Although this choice of

model constants may not be unique, it seems the simplest way to achieve the necessary effect. This satisfies our guideline that we want to make the changes as simple as possible when modification is necessary.

After a series of tests against the last few stations of Pot's far wake data, we set the two model constants at:

$$C_{\varepsilon_1} = 1.04 \tag{5.3.1}$$

and

$$\sigma_k = 0.65 \tag{5.3.2}$$

Using these values, all predicted profiles agree reasonably well with the experimental data as shown in Figs. 5.4 to 5.6. Moreover, the global parameters match those described by Eqs. (3.2.15) and (3.2.16) within 3%. They are:

$$\frac{d(\delta_{1/2}/\theta)^2}{d(x/\theta)} = 0.103$$

$$\frac{d(U_\infty/U_{1m})^2}{d(x/\theta)} = 0.437$$

Thus, we have constructed a model for the zone $\beta \to \infty$ by changing two model constants.

5.3.3 Model for the Readjustment Region

We have now zonal models for the limiting cases $\beta \to 0$ and $\beta \to \infty$. Next, we need to combine these to form a complete model. Any flow with β between zero and infinity can be regarded as being in a transitional stage between the two zones. This transition is called a "readjustment" in zonal modeling. To reflect the continuous change of physics in readjustment, we shall patch the two zonal models such that the model constants vary smoothly between the limiting values. The experience with homogeneous flows suggests that the two constants can be expressed as:

$$C_{\varepsilon_1} = 1.44 - 0.4\ \lambda_1 \tag{5.3.3}$$

$$\sigma_k = 1.0 - 0.35\ \lambda_1 \tag{5.3.4}$$

where $0 \leq \lambda_1 \leq 1$ is the readjustment parameter. λ_1 is a function of β and, again in line with earlier experience, we chose it to be the solution of a first-order differential equation:

$$\frac{d\lambda_1}{d\beta} = C(1 - \lambda_1) \tag{5.3.5}$$

where C is a constant to be determined. The solution to Eq. (5.3.5) is

$$\lambda_1 = 1 - e^{-C\beta} \tag{5.3.6}$$

Note that the model constants, Eqs. (5.3.3) and (5.3.4), reduce to the appropriate values for each of the two zones as β approaches the limiting values.

The exponential form of Eq. (5.3.6) makes the constants leave the first zone ($\beta \to 0$) values rather rapidly and reach the second zone values asymptotically. This seems to agree with the data. It is verified by the rapid growth of the maximum turbulent kinetic energy and shear stress in the near field, as shown in Figs. 5.9 and 5.10.

The data at intermediate β values ($\beta < 10$ or $U_{1m}/U_\infty > 0.1$) in Pot's wake experiment are excellent for tuning the readjustment constant C. With the use of these data, it was found that

$$C = 0.18 \tag{5.3.7}$$

This value of C gives good agreement with the data and completes the model for planar free shear flows.

Predictions of the zonal model are compared with Pot's wake data, for the spreading rate, centerline-velocity-deficit decay rate, the maximum kinetic energy, and the maximum shear stress in the layer, respectively, in Figs. 5.7 and 5.10. The agreement is excellent. Also presented in these figures are the results predicted by the standard K-ε model. The disagreement between the data and the standard K-ε model is significant, especially in the far field.

5.4 Tests of the Zonal Model

We have constructed a complete model by patching two zonal models for the extreme cases. This model was tuned using only Pot's wake data. This model gives very good agreement with that data set as seen in the preceding section. However, the purpose of modeling is to enable us not only to utilize the model for flows to which it is tuned, but also to other flows. We use co-flowing jets and mixing layers for this check in this section.

5.4.1 Co-flowing Jets

It was emphasized in Chapter III that behavior of co-flowing jets may vary from "pure" jet flow to self-preserving wake flow. This flow provides a good test for the present model. The data set recorded by Bradbury and Riley (1967) was reviewed in Chapter III and seen to be consistent and of high quality. Also, the data were nondimensionalized to collapse all co-flowing jet data with different ratios of nozzle exhaust to free stream velocity. We shall use this data set in the test.

An initial condition was generated using the data of Bradbury's earlier experiment (1965). Calculation was made to a downstream location of about 100 θ. The results for the jet spreading rate, centerline velocity decay, and the eddy Reynolds number defined by Eq. (3.2.14) are shown in Figs. 5.11 to 5.13, respectively. The predictions of the standard $K-\varepsilon$ model are included in these figures for comparison. In both sets of predictions, x_o is taken to be -6θ. The present model performs extremely well for all three quantities compared. The standard $K-\varepsilon$ model, on the other hand, predicts well only in the initial part of the flow and departs from the data further downstream. This is expected because, as demonstrated earlier, the standard $K-\varepsilon$ model works well for flows with small β (the first zone) but poorly for flows with large β. The serious disagreement between the data and the standard $K-\varepsilon$ model prediction for the eddy Reynolds number seen in Fig. 5.13 reveals that the standard model is unable to predict the shear stress level accurately. The low shear stress produces the slower spreading and velocity decay.

5.4.2 Mixing Layers

Another challenging test is the mixing layer. These flows do not have similar velocity profiles. However, the ratio of inertial force to driving force can be defined if we consider U_∞ to be the average of the two free stream velocities:

$$U_\infty = \frac{1}{2}\left(U_{\infty_1} + U_{\infty_2}\right) \tag{5.4.1}$$

and U_{1m} to be the difference between either free stream velocity and U_∞:

$$U_{1m} = \frac{1}{2}\left(U_{\infty_1} - U_{\infty_2}\right) \tag{5.4.2}$$

Thus, we take β to be $U_\infty/U_{1m} = (U_{\infty_1}+U_{\infty_2})/(U_{\infty_1}-U_{\infty_2})$. In these expressions, U_{∞_1} and U_{∞_2} are the free stream velocities on the high and low velocity sides, respectively. One side has a velocity excess; the other has a velocity defect. Both sides share the common U_∞ and have the same value of U_{1m}, and hence identical β's.

Another way of viewing a mixing layer is as follows. There exists a dividing streamline which, if not exactly coincident with, is very close to the line with velocity equal to U_∞. The high velocity side can be regarded as jet-like and the low velocity side as wake-like.

Using the velocities as defined in Eqs. (5.4.1) and (5.4.2), the ratio of inertial force to driving force, β, for the mixing layer is identical to the parameter used by Sabin (1965) to correlate the spreading parameter for flows with various velocity ratios.

In the calculation of mixing layers, we have to note that the results are very sensitive to the boundary conditions on the normal velocity, V, at both the top and bottom boundaries, as explained in Chapter III. In order to accurately compute these flows, therefore, both boundary conditions should be specified. However, in the thin shear-layer approximation, only one V boundary condition can be given. There is no way to improve the approximation other than to select a V boundary condition that is best for a particular problem. There are several ways to specify this boundary condition, including

$$V = 0 \quad \text{as} \quad y \to -\infty \quad \text{(low velocity side)} \tag{5.4.3}$$

$$U_{\infty_1} V_{\infty_1} + U_{\infty_2} V_{\infty_2} = 0 \tag{5.4.4}$$

or

$$\frac{d}{dx} \int_{-\infty}^{\infty} UV dy + V_{\infty_1}^2 - V_{\infty_2}^2 = 0 \tag{5.4.5}$$

In the above expressions, V_{∞_1} and V_{∞_2} are the normal velocities on the top and bottom boundaries, respectively. The last is derived from the y-momentum conservation equation and is the best condition for a "free" mixing layer, i.e., one that is not affected by wind-tunnel walls.

The V boundary condition determines the angle at which the mixing layer propagates and can be chosen to match the calculated flow angle to that observed experimentally; this differs from experiment to experiment. Fortunately, the spreading rate is only slightly affected by the V boundary conditions. In this work, only the spreading rate is of major concern; the flow angle will not be examined.

Mixing layers with various velocity ratios are computed with both the present model and the standard K-ε model. Calculations were carried out until a self-similar solution was achieved. Figure 5.14 shows the comparison between the predicted spreading rates and those of various experiments for the range of $1 < \beta < 9$. The present model performs better than the standard K-ε model. Figures 5.15(a), (b) and (c) compare the shear stress profiles of the model predictions and the data for three different velocity ratios (R = 0, 0.3, and 0.61), respectively.

5.5 Galilean Invariance -- A Frame-Invariant Form of the Model

The description of a phenomenon must be the same in all inertial frames of reference. That is, the equations governing the physics should be identical whether the reference frame is stationary or is moving at a constant speed. To be more specific, the equations must be form-invariant under the Galilean tranformation

$$\vec{x}' = \vec{x} - \vec{V}t \qquad (5.5.1)$$

where $\vec{x}'$ and $\vec{x}$ are the coordinates in the new and old reference frames, respectively. The new reference frame has a constant relative velocity $\vec{V}$ with respect to the old frame. The Navier-Stokes equations, for example, are Galilean invariant in this sense.

It is essential that the turbulence model be Galilean-invariant. Otherwise, the model will give different results in various inertial reference frames. The model developed for plane free shear flows in this chapter is not Galilean-invariant because the parameter β on which the model constants depend contains U_∞, which changes with the frame of reference. This would restrict use of the model to reference frames in which the flow appears steady. For example, for jet flows, the reference frame has to be stationary with respect to the nozzle that produces the jet and, for wake flows, stationary with respect to the body that generates the wake. For all other reference frames, the present model would be invalid.

A look at the analysis indicates that the lack of Galilean invariance of the model arises from our assumption of a steady flow. When the reference frame is changed, the flow appears unsteady and the analysis of Sec. 5.2 is no longer adequate. Therefore, in order to obtain Galilean invariance, we must consider unsteady flows.

The momentum integral equation for an unsteady flow is:

$$\frac{\delta_{1/2}}{U_{1m}^2}\frac{\partial U_{1m}}{\partial t} f - \frac{1}{U_{1m}}\frac{\partial \delta_{1/2}}{\partial t}\eta f' + \frac{\delta_{1/2}}{U_{1m}}\frac{U_\infty}{U_{1m}}\frac{\partial U_{1m}}{\partial x} f + \frac{\delta_{1/2}}{U_{1m}}\frac{\partial U_{1m}}{\partial x} f^2$$
$$- \frac{\partial \delta_{1/2}}{dx}\frac{U_\infty}{U_{1m}}\eta f' - \left(\frac{\delta_{1/2}}{U_{1m}}\frac{\partial U_{1m}}{\partial x} + \frac{\partial \delta_{1/2}}{\partial x}\right) f' \int_0^\eta f d\eta = \beta' \qquad (5.5.2)$$

where U_{1m} and $\delta_{1/2}$ are now functions of both x and t. We must redefine the parameter β as

$$\beta = \frac{\frac{D\delta_{1/2}}{Dt}}{U_{1m}\left(\frac{\partial \delta_{1/2}}{\partial x}\right)} = \frac{\frac{DU_{1m}}{Dt}}{U_{1m}\left(\frac{\partial U_{1m}}{\partial x}\right)} \qquad (5.5.3)$$

where

$$\frac{\bar{D}}{Dt} = \frac{\partial}{\partial t} + U_\infty \frac{\partial}{\partial x} \tag{5.5.4}$$

Combining Eqs. (5.5.2) and (5.5.3) gives

$$\frac{\delta_{1/2}}{U_{lm}} \frac{\partial U_{lm}}{\partial x} f(\beta + f) - \frac{\partial \delta_{1/2}}{\partial x} \beta \eta f' - \left(\frac{\delta_{1/2}}{U_{lm}} \frac{\partial U_{lm}}{\partial x} + \frac{\partial \delta_{1/2}}{\partial x} \right) f' \int_o^\eta f d\eta = g' \tag{5.5.5}$$

which is identical to Eq. (5.2.3). Moreover, the parameter β defined by (5.5.3) reduces to the previous definition, Eq. (5.2.1), for a steady flow. The remainder of the analysis is the same as that in Sec. 5.2 and will not be repeated here.

Therefore, in applying the present model to a general free shear flow, the definition of the parameter β given by Eq. (5.5.3) has to replace that of Eq. (5.2.1) This makes the model Galilean-invariant. No other changes are needed. Since the original equations with β given by Eq. (5.2.1) are simpler, the more complex analysis of this section need be used only when the flow is unsteady in the reference frame chosen.

5.6 Conclusions

In this chapter, plane free shear flows were studied. A zonal model was developed. Two zones were identified; they can be called the near and far fields, although that nomenclature is not accurate for all flows. This problem is a semantic one arising from the definition of a zone, and we shall suggest a clearer semantics in the final chapter. The difference in the turbulence transport mechanism in the two zones was discussed. Zonal models have been constructed for these two zones. A patching technique was used to represent the readjustment and to link the two zonal models. The new model predicts the change in physics by changing two constants. The requirement of Galilean invariance can be satisfied by use of a more general definition for β. Test results show that the model developed in this chapter performs much better than the standard K-ε model, but is no more difficult to apply or expensive to run for plane free shear flows.

Chapter VI

ZONAL MODELING FOR AXISYMMETRIC FREE SHEAR FLOWS

6.1 Introduction

In Chapter V, we built a new (zonal) model that works well for all usable cases of plane free shear flows. This new model improves the standard K-ε model significantly by allowing two of the constants to become functions of the parameter β. Axisymmetric flows were not considered in Chapter V, because there is a fundamental difference in the turbulence structure due to the lateral vortex stretching in axisymmetric flows as mentioned in Chapter III (Fig. 3.12). When vortex stretching is significant, it decreases the ratio of $|\overline{u'v'}|/K$ which determines a central constant in the K-ε model. In this chapter, we shall examine the vortex stretching effect in detail and incorporate its effects into the model for axisymmetric flows through a suitable nondimensional parameter.

The standard K-ε model was tuned to plane shear flows. As a result, boundary layers and plane pure jets are well represented by this model. However, to predict axisymmetric flows, some modifications are required. Most of the modifications shown in the literature involve changing either $C_{\varepsilon 1}$ or $C_{\varepsilon 2}$. For example, Launder et al. (1972) added correction terms in $C_{\varepsilon 2}$ and C_μ:

$$C_{\varepsilon 2} = 1.92 - 0.0667\ p$$

and

$$C_\mu = 0.09 - 0.04\ p$$

where

$$p = \left[\frac{\delta_{1/2}}{2U_{1m}}\left(\frac{dU_{CL}}{dx} - \left|\frac{dU_{CL}}{dx}\right|\right)\right]^{0.2}$$

Here, U_{1m} is the centerline velocity. McGuirk and Rodi (1977) suggested

$$C_{\varepsilon_1} = 1.14 - 5.31 \frac{\delta_{1/2}}{U_{CL}} \frac{dU_{CL}}{dx}$$

Morse (1977) used

$$C_{\varepsilon_1} = 1.4 - 3.4 \left(\frac{K}{\varepsilon} \frac{\partial U}{\partial x} \right)^3_{CL}$$

No convincing physical explanation is provided to justify any of these modifications. Moreover, when these corrections are used, the generality of the model ability to predict plane and axisymmetric flows is destroyed. It is not known whether the correction should be used for flows intermediate between plane and axisymmetric. Moreover, these modifications were primarily tuned to pure jets; they do not predict wakes well. In his extended $K-\varepsilon$ model, in which C_μ is a function of the ratio of the turbulence production and dissipation rates, Rodi (1972) included a modification for axisymmetric flows similar to that of Launder at el. (1972) described above. This gives predictions for axisymmetric flows better than the ones mentioned above. However, the predicted profiles do not agree well with data.

In this chapter, we will use the zonal approach to develop a model for axisymmetric flows. We want to maintain the ability to handle both plane and axisymmetric cases. Therefore, we shall often refer to the plane flow model developed in Chapter V. Our objective is to create a general model which treats plane flows as one special case and axisymmetric flows as another.

6.2 Analysis and Physics

An analysis similar to the one for plane flows (Sec. 5.2) can be carried out for axisymmetric flows. To briefly illustrate several key points, consider a steady axisymmetric jet in a uniform stream with arbitrary free stream velocity. Using dimensional analysis, we find

$$\beta = \frac{U_\infty}{U_{1m}} = F\left(\frac{x - x_0}{\theta} \right) \qquad (6.2.1)$$

and

$$\frac{\delta_{1/2}}{\theta} = G\left(\frac{x - x_o}{\theta}\right) \tag{6.2.2}$$

Here, θ is the momentum thickness for axisymmetric flows defined by Eq. (3.3.4). F and G are universal functions for all axisymmetric jets. Indeed, Rodi (1975), using Eqs. (6.2.1) and (6.2.2), collapsed the jet width and centerline velocity data of three experiments (Fig. 3.13).

We can apply the similarity expressions used in Chapter V for streamwise velocity and turbulent shear stress. Substituting them into the momentum equation, we have

$$\frac{\delta_{1/2}}{U_{1m}} \frac{dU_{1m}}{dx} f\,(\beta+f) - \frac{d\delta_{1/2}}{dx} \beta\eta f' - \left(\frac{\delta_{1/2}}{U_{1m}} \frac{dU_{1m}}{dx} + 2\,\frac{d\delta_{1/2}}{dx}\right) \frac{f'}{\eta} \cdot \int_o^\eta f\eta d\eta = \frac{1}{\eta}\,(\eta g)' \tag{6.2.3}$$

The momentum integral equation, after the similarity transformation, reads

$$\frac{\delta_{1/2}}{U_{1m}} \frac{dU_{1m}}{dx} = q' \frac{d\delta_{1/2}}{dx} \tag{6.2.4}$$

where

$$q' = -\frac{2I_2' + 2I_1'\beta}{2I_2' + I_1'\beta} \tag{6.2.5}$$

and I_1' and I_2' are defined by Eq. (3.3.6). Combining Eqs. (6.2.3) and (6.2.4) results in

$$\frac{d\delta_{1/2}}{dx}\left[q'\beta f + q' f^2 - \beta\eta f' - (q'+2)\,\frac{f'}{\eta}\int_o^\eta f\eta d\eta\right] = \frac{1}{\eta}\,(\eta g)' \tag{6.2.6}$$

Since β and $\delta_{1/2}$ are related by Eqs. (6.2.1) and (6.2.2), the shear stress can be considered a function of β alone.

Strictly speaking, the parameter $\beta = U_\infty/U_{1m}$ can be used only in steady flows. In general, $\beta = (\bar{D}\delta_{1/2}/Dt)/(U_{1m}\,\partial\delta_{1/2}/\partial x)$ should be used to allow Galilean invariance. This point was discussed in the last chapter.

The axisymmetric wake can be analyzed in a similar manner. Let us assume that the turbulence transport mechanism is independent of the sign of mean velocity gradient and only a function of β. As in plane flows, β has two extreme values: zero and infinity. These correspond to a pure jet and a far wake, respectively. A co-flowing jet or wake will develop between these two limits. They may start from a state close to a pure jet (small β) and eventually arrive at the asymptotic far wake state (large β). Therefore, the zonal idea used in plane flows can as well be applied here. We shall first consider these two extremes (or zones).

The first zone ($\beta = 0$) represents a pure jet. This flow spreads linearly. Its spreading rate is the greatest among axisymmetric flows. Due to the rapid spreading and small radius of curvature of the flow, there exists a significant strain in the circumferential direction. This strain tends to stretch the vortex rings which form in the shear layer. For this effect to be important, two criteria must be met. Firstly, the jet has to have a radius that is not large in comparison with the shear layer width. Secondly, the flow has to spread rapidly. Otherwise, the straining will be weak.

The stretching of vortex rings reduces the ratio of $|\overline{u'v'}|/K$. This conclusion is reached on the basis of experimental data. No physical or mathematical derivation is available at the present time. For a given turbulence intensity, the vortex stretching causes the shear stress to decrease. For axisymmetric pure jets, in which the effect of vortex stretching is the strongest, the ratio of $|\overline{u'v'}|/K$ in the equilibrium region is reduced to about 0.23 (vs. 0.3 for the plane flows, cf. Fig. 3.12).

The second zone ($\beta \to \infty$) is an asymptotic far wake. In this zone the spreading rate is very slow. The vortex stretching effect is therefore small. Indeed, in the review of Antonia and Bilger's (1973) axisymmetric co-flowing jet experiment in Chapter III, we found that $|\overline{u'v'}|/K$ is close to 0.3 in the equilibrium region far downstream. The physics of this far-field zone is nearly identical to that of the plane asymptotic far wake.

The turbulence diffusion enhancement as β increases seems to be the same for axisymmetric flows as for plane flows.

6.3 Construction of Zonal Models

Our approach will again be to model the extremes first, then the readjustment.

6.3.1 Zonal Model for the Limiting Case $\beta \to 0$

As before, the standard K-ε model is first tested to determine what modification, if necessary, is needed. The results for the global parameters are:

$$\frac{d\delta_{1/2}}{dx} = 0.121$$

$$\frac{d\left(J^{1/2}/U_{1m}\right)}{dx} = 0.178$$

Both the spreading and velocity decay rates are over-predicted by more than 35% by the standard K-ε model. Mean velocity, turbulent kinetic energy and shear stress profiles are shown, respectively, in Figs. 6.1 to 6.3 and compared with experimental data. While the mean velocity and kinetic energy profiles show reasonable agreement with the data, the shear stress is significantly over-predicted, i.e., the ratio $|\overline{u'v'}|/K$ is too high for this flow. The reason is that $C_\mu = 0.09$ in the standard K-ε model $|\overline{u'v'}|/K$ at appproximately 0.3 in the region where production is in balance with dissipation. However, as emphasized above, $|\overline{u'v'}|/K$ is reduced by the effect of vortex stretching and is 0.23 rather than 0.3. To reflect this value of $|\overline{u'v'}|/K$ in the model, it appears that the value of C_μ should be decreased.

From the shear stress and eddy viscosity formulation, as described in Chapter II, we have

$$\left(\frac{|\overline{u'v'}|}{K}\right)^2 = C_\mu \frac{P}{\varepsilon} \qquad (6.3.1)$$

where $P = -\overline{u'v'}\,\partial U/\partial y$ is the production rate of the turbulence. Knowing that $|\overline{u'v'}|/K \approx 0.23$ in the region where production is approximately equal to dissipation for axisymmetric pure jet, we set

$$C_\mu = 0.05 \qquad (6.3.2)$$

for this flow. With this new value of C_μ, the predicted global parameters are

$$\frac{d\delta_{1/2}}{dx} = 0.089$$

$$\frac{d(J^{1/2}/U_{1m})}{dx} = 0.132$$

which are in excellent agreement with Eqs. (3.3.1) and (3.3.2) that correlate the data. The various profiles generated by using $C_\mu = 0.05$ are also presented in Figs. 6.1 to 6.3. All three profiles match the data very well.

The zonal model for this zone is, therefore, the standard K-ε model with a change in model constant C_μ to account for the vortex stretching. No other modification is needed.

6.3.2 Zonal Model for the Limiting Case $\beta \to \infty$

A far-field wake or co-flowing jet represents this zone. As noted above, due to the slow spreading, the effect of vortex stretching is negligible in this zone, and the physics of the flow is nearly the same as that of plane cases. Therefore, the zonal model of the plane asymptotic far wake was adopted for the axisymmetric counterpart. This allows maintenance of the generality of the new model. No tuning of model constants is needed or performed in this zone.

6.3.3 Model for the Readjustment Region

As stated earlier, our intent is to produce a general model for free shear flows. Therefore, we want to keep the model for axisymmetric flows as consistent as possible with that for plane flows. Furthermore, the changes with β appear to be the same for both plane and axisymmetric flows. For these reasons, we shall keep the variation of the model constants $C_{\varepsilon 1}$ and σ_k between the two zones the same as in plane flows, i.e., we use Eqs. (5.3.3) to (5.3.7). This leaves us only

one more linking to be made (for the model constant C_μ) before the zonal model for axisymmetric flows is completed.

In going from the first zone to the second, the stretching diminishes. The model constant C_μ should increase from 0.05 to 0.09. This transitional stage can be represented by sliding C_μ between the two extreme values. Before constructing the blending function for C_μ, let us examine what controls the stretching of vortices.

As discussed in Sec. 6.2, the flow has to be small in the normal direction and has to spread rapidly in order for the stretching effect to be significant. This means that the vortex stretching should be a function of the spreading rate, $d\delta_{1/2}/dx$, and the radius of curvature of the vortex ring. From these and dimensional arguments, an appropriate parameter appears to be:

$$S = \frac{R_{1/2}}{\delta_{1/2}} \frac{1}{d\delta_{1/2}/dx} \tag{6.3.3}$$

where $R_{1/2}$ is the radius of curvature of the vortex line passing through the point of $\delta_{1/2}$. The smaller this parameter, the more stretching there is. For plane flows, S is infinite and there is no stretching. For axisymmetric flows, $R_{1/2} = \delta_{1/2}$ and S is inversely proportional to the spreading rate. For general three-dimensional flows, for example a rectangular jet, S is smaller at the corners due to the small radius of curvature. This gives more stretching and hence smaller shear stress near the corners. Consequently, the spreading near the corners slows down and the flow will eventually become axisymmetric. This is at least qualitatively correct.

The smallest observed value of S occurs in the axisymmetric pure jet and is 11.3. Therefore, we propose that the sliding function for model constant C_μ be:

$$C_\mu = 0.05 + 0.04\ \lambda_2 \quad , \qquad S \geq 11.3 \tag{6.3.4}$$

where $0 \leq \lambda_2 \leq 1$ is the readjustment parameter. Further study may be needed if a value of S below 11.3 occurs in any flow. λ_2 is governed by the first-order differential equation:

$$\frac{d\lambda_2}{dS} = C_s(1 - \lambda_2) \tag{6.3.5}$$

where C_s is a constant that needs to be tuned. The solution to Eq. (6.3.5) is:

$$\lambda_2 = 1 - e^{-C_s(S-11.3)} \tag{6.3.6}$$

The last task is to determine the constant C_s. The tuning is done by computing a co-flowing jet and comparing the results with the data in Figs. 3.13 and 3.14. An initial condition was created by using Antonia and Bilger's (1973) experimental data for a co-flowing jet with the jet nozzle velocity to free stream velocity equal to 4.5. It was determined that

$$C_s = 0.1 \tag{6.3.7}$$

gives the best results. The agreement for the jet spreading rate and centerline velocity decay rate can be seen in Figs. 6.4 and 6.5. The K-ε model prediction is included in these figures for comparison.

6.4 Tests of the Zonal Model

We have constructed a new model for axisymmetric free shear flows with Eqs. (5.3.3), (5.3.4) and (6.3.4) and are ready to test the model.

6.4.1 Co-Flowing Jets

It was decided to simulate another axisymmetric co-flowing jet. The initial condition is based on the data of another co-flowing jet of Antonia and Bilger (1973). This jet has a ratio of nozzle velocity to free stream velocity equal to 3. Computation was carried out to about 150 θ downstream. The spreading rate and centerline velocity decay are presented in Figs. 6.6 and 6.7, respectively. Good agreement with experimental results is obtained for both quantities. Predictions of the standard K-ε model for the same flow are also shown for comparison. Although giving reasonable spreading rate, the standard K-ε model fails to predict the velocity decay rate accurately.

6.4.2 Wakes

Axisymmetric wakes provide a challenge to the present model because these flows were not used in the determination of the model constants. Chevray's (1968) wake experiment is used for this test. The computation uses the data at $x/D = 6$ as an initial condition. Comparisons of the prediction by the present model and experimental data for the spreading rate and decay rate of centerline velocity deficit are shown in Figs. 6.8 and 6.9. Excellent agreement is achieved. The standard $K-\varepsilon$ model underpredicts both quantities; these results are also shown in the figures. The predicted turbulent kinetic energy and shear stress profiles at the last measuring station $(x/D = 18)$ are compared with the experimental data in Figs. 6.10 and 6.11. Good agreement is observed with the present model. The standard $K-\varepsilon$ model, on the other hand, predicts significantly lower values for both quantities; the low shear stress is responsible for the slow spreading and velocity decay seen in Figs. 6.8 and 6.9.

6.5 Conclusions

In this chapter, axisymmetric jets and wakes were studied. The turbulence model for these flows is closely connected with the plane flow model. Vortex stretching was identified as the principal difference between axisymmetric and plane flows. It reduces the shear stress and, thereby, the integral parameters of the flow. Incorporation of this effect into the model required a change of one model constant. The readjustment of this constant was accomplished as in the plane case. Excellent results for axisymmetric co-flowing jets and wakes were obtained with the present model.

This model reduces to plane flow model when there is no vortex stretching $(S \to \infty)$ and can be applied to general three-dimensional flows. Tests of this model for three-dimensional flows is therefore required. However, in order to do so, initial conditions on a plane normal to the flow direction must be provided. This requires a set of experimental data that covers the initial plane. Unfortunately, no experimental data presently available give this information. Most of the data were taken only on two axes. For this reason, this model

cannot be tested for three-dimensional flows at present. Measurements providing the necessary data for jets and for wakes of noncircular and nonplanar cross sections are accordingly a next step toward further generalization of zonal models of free shear flows.

Chapter VII

DISCUSSION, CONCLUSIONS, AND RECOMMENDATIONS

7.1 Summary and Discussion

In this research, we developed zonal models for homogeneous and free shear flows. In each case, a linear first-order ordinary differential equation provides a good readjustment between zones. We have, therefore, not explored more complex readjustment models.

The homogeneous flows were modeled primarily to provide a quick test of the concept of zonal modeling. Details of the zonal models for three types of homogeneous flows are given in Table 2.1. The homogeneous flows show that accurate prediction can be achieved by adjusting the constants in the standard K-ε model. The accuracies of the two types of modeling are indicated in Table 7.1; the differences are based on the worst point on each curve. These results partially validate the OPINION by Kline (1981).

Table 7.1

Acccuracy Comparisons for the Predictions of Homogeneous Flows

Worst Point on Curve Agrees with Data Within	Percentage of Cases Accurate to the Limit			
	< 10%	< 25%	< 50%	> 50%
Zonal Models	86	10	4	0
Standard K-ε Models	16	16	17	51

The zonal model predicts all free shear flows within the uncertainty in the data. This model is given in detail in Table 7.2. Comparisons of the accuracy of the model of Table 7.2 with that of the standard K-ε model are shown in Table 7.3.

Table 7.2

Summary of Unified Zonal Model for Free Shear Flows

	Present Model	Standard K-ε Model
C_μ	$0.05 + 0.04\,\lambda_2$, $S \geq 11.3$	0.09
C_{ε_1}	$1.44 - 0.4\,\lambda_1$	1.44
C_{ε_2}	1.92	1.92
σ_K	$1.0 - 0.35\,\lambda_1$	1.0
σ_ε	1.3	1.3

$$\lambda_1 = 1 - e^{-C\beta} \quad , \quad \lambda_2 = 1 - e^{-C_s(S-11.3)}$$

$$C = 0.18 \quad , \quad C_s = 0.1$$

In general,

$$\beta = \frac{\left(\overline{D}\delta_{1/2}/Dt\right)}{U_{1m}\left(\partial\delta_{1/2}/\partial x\right)} \quad , \quad S = \frac{R_{1/2}}{\delta_{1/2}} \frac{1}{\left(d\delta_{1/2}/dx\right)}$$

For steady flows, β simplifies to:

$$\beta = \frac{U_\infty}{U_{1m}}$$

Table 7.3

Accuracy Comparisons for the Predictions of Free Shear Flows

Worst Point on Curve	Percentage of Cases Accurate to the Limit			
Agrees with Data Within	> 10%	> 25%	> 50%	> 50%
Unified Zonal Model	100	0	0	0
Standard K-ε Model	39	25	32	4

As Tables 7.2 and 7.3 show, the zonal modeling concept not only succeeds but also provides significant and unexpected results.

First, while the models apply to the "zones" of free shear flows, it is possible to connect these models to yield a single model containing two non-dimensional parameters. This unified model predicts all the available free shear flow data, including plane and axisymmetric jets and wakes and mixing layers.

Second, the work enlightened us significantly about the underlying physics of free shear flows and the governing parameters needed to represent the effects observed.

These gains leave two questions that need discussion. The semantics introduced initially does not describe the results adequately and needs improvement. We also need to know whether the physical insights are particular to this set of flows or more general.

The semantic question centers on the definition of the word "zone." We defined a zone to be one or more flow regions which could be modeled by a single model including particular values of the parameters. In the homogeneous flows, this description fits the situation precisely; three types of strains needed three different zonal models. For the free shear flows, the situation is more complex. Zones representing the near and far fields were created and linked using a simple readjustment model. From that point onward, the modeling process almost took on a life of its own. The readjustment from the near to the far field employs a velocity-ratio parameter β. However, in both pure jets and mixing layers there is only a single value of this parameter (β) throughout the flow. We found further that the far field of the axisymmetric jet is well modeled by the plane far-field model. This made it natural to determine why the near field of the axisymmetric jet is not well modeled. Vortex stretching was identified as the probable cause. Once a parameter, S, accounting for the effect of vortex stretching was introduced, the unified model emerged.

The free shear flows do not constitute a zone in the sense initially defined. We ended with three basic models connected by two parameters. The basic models (the physical situations they represent

might best be called "flow states") do not represent physical regions but parts of flows with limiting values of the governing parameters β and S. In flows in which the parameters vary, the states are connected by what we originally called readjustments but might better be called "bridges."

These ideas suggest use of two sets of words. At an elemental level, we might speak of a zone and a zonal model for that zone. Such an elemental zonal model might still have a readjustment region as from an initial to a final or from a near field to a far field. At a second level of organization, such as that of the final results for the class of free shear flows, where a single model containing parameters is found, we might speak of a "unified zonal model" for a defined "class".

What about the question of generality of the process? Inspection of the processes used herein suggests that they will generalize to at least some degree. The model-construction process is based on a search for inadequacies in existing models, identification of probable causes and finding simple modifications that model them. This process is likely to succeed as well for other flows; there is nothing special about the free shear flows. The latter were a good choice for this study, since there is a variety of cases in this class of flows.

This augurs well for the utility of zonal modeling as a method for creating accurate models of turbulent flows for engineering purposes. It also provides a tool for increasing our basic understanding of technically significant turbulent flows. Indeed, the most important result of this work may be the process suggested rather than the particular models developed.

7.2 Conclusions

We have shown that the zonal modeling concept can be applied to homogeneous turbulence and free shear flows. This is a proof of the concept and provides an indication of what might be expected from zonal modeling. However, this is only a very small portion of a much larger project that needs to be carried out; a great deal remains to be done. The zonal concept provides a logical framework within which simple and accurate turbulence models can be developed more easily than the

traditional way. The present research has laid a good groundwork for the project and we hope that the encouraging results obtained reflect what can be achieved with more complex flows.

Finally, although we cannot anticipate how far this project will carry us toward reliable and fast computations of practically important complex turbulent flows, we are confident that we will be able to achieve significantly more than has been done in the past.

7.3 Recommendations for Future Work

The followings are suggestions for future work in further testing the present unified model for other free shear flows, understanding the physics, and extending zonal modeling to more complex flows.

1. A three-dimensional free shear flow can provide a challenging test case for the present unified model. However, detailed measurements on an entire plane must be available to start the computation. No candidate flow has been measured with sufficient detail to meet these requirements. Therefore, experiments such as elliptic or rectangular jets with full measurements on a cross section for a minimum of two stations would be useful.

2. The two physical phenomena parameterized by β and S in the present model are mainly observed from the experimental results; the causes of the underlying effects are not understood. More fundamental research work, either experimental or analytical, that can address these causes might increase understanding of the nature of turbulence.

3. An extension of the present work to the study of free shear flows with density difference and/or scalar transport, such as heat or species, would make the zonal model more valuable in practical engineering application.

4. The readjustment parameters are solutions of first-order ordinary differential equations in the present study. In later development of the zonal modeling project, a similar format in readjustments can probably be used in a complex flow-field where patching of zonal models is required. This will make the task of creating zonal models for complex flow fields easier and more systematic.

References

Abramovich, G. N. (1968), The Theory of Turbulent Jets, The M.I.T. Press.

Andreopoulos, J., and Bradshaw, P. (1980), "Measurements of Interacting Turbulent Shear Layers in the Near Wake of a Flat Plate," J. Fluid Mech., **100**: 639-668.

Antonia, R. A., and Bilger, R. W. (1973), "An Experimental Investigation of an Axisymmetric Jet in a Co-Flowing Air Stream," J. Fluid Mech., **61**: 805-822.

Antonia, R. A., Prabhu, A., and Stephenson, S. E. (1975), "Conditionally Sampled Measurements in a Heated Turbulent Jet," J. Fluid Mech., **72**: 455-480.

Batchelor, G. K., and Proudman, I. (1954), "The Effect of Rapid Distortion of a Fluid in Turbulent Motion," Quart. J. Mech. and Appl. Math., **7**: 83-103.

Bilger, R. W. (1968), "The Turbulent Plane Jet-Wake," 3rd Austr. Conf. on Fluid Mech. and Hydraul., 159-162, Inst. Engrs., Australia.

Boussinesq, J. (1877), "Theorie de l'ecoulement Tourbiliant," Mem. Pre. par. div. Sav., 23, Paris.

Bradbury, L. J. S. (1965), "The Structure of a Self-Preserving Turbulent Plane Jet," J. Fluid Mech., **23**: 31-64.

Bradbury, L. J. S. (1967), "Simple Expressions for the Spread of Turbulent Jets," Aero. Quart., May 1967, 133-142.

Bradbury, L. J. S., and Riley J. (1967), "The Spread of a Turbulent Plane Jet Issuing into a Parallel Moving Airstream," J. Fluid Mech., **27**: 381-394.

Carmody, T. (1964), "Establishment of the Wake Behind a Disk," Trans. A.S.M.E., J. Basic Engng., **87**: 869-882.

Cebeci, T., and Bradshaw, P. (1977), Momentum Transfer in Boundary Layers, Chap. 7, Hemisphere Publishing Corp., Washington, D. C.

Champagne, F. H., Pao, Y. H., and Wygnanski, I. J. (1976), "On the Two-Dimensional Mixing Region," J. Fluid Mech., **74**: 209-250.

Chevray, R. (1968), "The Turbulent Wake of a Body of Revolution," Trans. A.S.M.E., J. Basic Engng., **90**: 275-284.

Chevray, C., and Kovasznay, L. S. G. (1969), "Turbulence Measurements in the Wake of a Thin Flat Plate," AIAA J., **7**: 1641-1643.

Gutmark, E., and Wygnanski, I. (1976), "The planar Turbulent Jet," J. Fluid Mech., **73**: 465-495.

Harsha, P. T. (1971), "Free Turbulent Mixing: A Critical Evaluation of Theory and Experiment," AEDC-TR-71-36.

Heskestad, G. (1965), "Hot-Wire Measurements in a Plane Turbulent Jet," J. Appl. Mech., **32**: 721-734.

Hill, P. G. (1965), "Turbulent Jets in Ducted Streams," J. Fluid Mech., **22**: 161-186.

Hinze, J. O. (1959), "Turbulence," McGraw-Hill, New York.

Jones, W. P., and Launder B. E. (1972), "The Prediction of Laminarisation with a 2-Equation Model of Turbulence," Int. J. Heat Mass Transfer, **15**: 301.

Kline, S. J., Cantwell, B. J., and Lilley, G. M. (1981), 1980-81 AFOSR-HTTM-Stanford Conference on Complex Turbulent Flows.

Launder, B. E., Morse, A. P., Rodi, W., and Spalding, D. B. (1972), "The Prediction of Free Shear Flows - A Comparison of Six Turbulence Models," NASA SP-311, 361-426.

Launder, B. E., and Spalding, D. B. (1972), Mathematical Models of Turbulence, Academic Press, London and New York.

Lee, M. J., and Reynolds, W. C. (1985), "Numerical Experiments on the Structure of Homogeneous Turbulence," Ph.D. thesis, Stanford University, Report No. TF-24.

Liepmann, H. W., and Laufer, J. (1947), "Investigations of Free Turbulent Mixing," NACA Tech. Note, No. 1257.

Maczynski, J. F. J. (1962), "A Round Jet in an Ambient Co-Axial Stream," J. Fluid Mech., **13**: 597-608.

McGuirk, J. J., and Rodi, W. (1977), "The Calculation of Three-Dimensional Free Jets," Symposium on Turbulent Shear Flows, Pennsylvania State University.

Miles, J. B., and Shih, J.-S. (1968), "Similarity Parameter for Two-Stream Turbulent Jet-Mixing Region," AIAA J., **6**: 1429-1430.

Morse, A. P. (1977), "Axisymmetric Turbulent Shear Flows with and without Swirl," Ph.D. Thesis, London University, England.

Newman, B. G. (1966), "Turbulent Jets and Wakes in a Pressure Gradient," in Fluid Mechanics of Internal Flow (G. Sovran, ed.), Elsevier, 170-201.

Patel, R. P. (1973), "An Experimental Study of a Plane Mixing Layer," AIAA J., **11**: 67-71.

AD-A181 177 ZONAL MODELS OF TURBULENCE AND THEIR APPLICATION TO FREE SHEAR FLOWS(U) STANFORD UNIV CA THERMOSCIENCES DIV K TZUOO ET AL NOV 86 TF-27 F49620-86-K-0008 2/2

UNCLASSIFIED F/G 20/4 NL

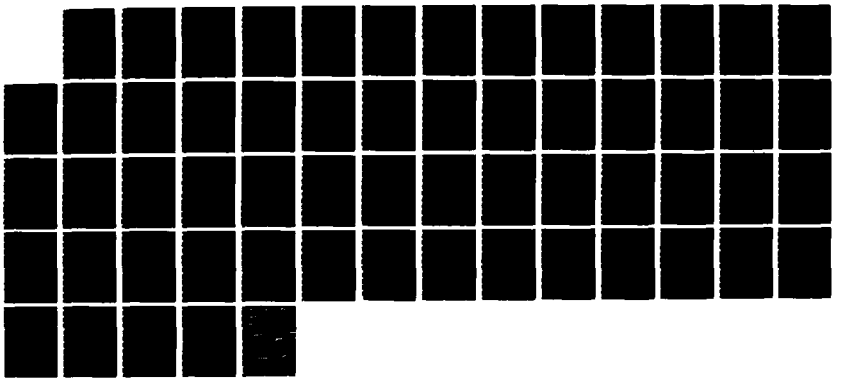

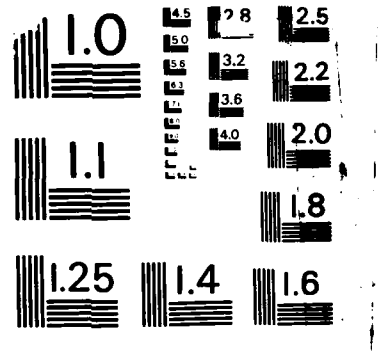

MICROCOPY RESOLUTION TEST CHART

NATIONAL BUREAU OF STANDARDS - 1963 - A

Patel, V. C., and Scheuerer, G. (1982), "Calculation of Two-Dimensional Near and Far Wakes," AIAA J., **20**: 900-907.

Paullay, A. J., Melnik, R. E., Rubel, A., Rudman, S., and Siclari, M. J. (1985), "Similarity Solutions for Plane and Radial Jets Using a K-ε Turbulence Model," A.S.M.E. J. Fluids Eng'g, March, 1985.

Pot, P. J. (1979), "Measurements in a 2-D Wake and in a 2-D Wake Merging into a Boundary Layer," Data Report, NLR TR-79063 U, The Netherlands.

Prandtl, L. (1925), "Bericht Uber Untersuchungen Zur Ausgebildeten Turbulenz," ZAMM, 5, 136.

Ramaprian, B. R., Patel, V. C., and Sastry, M. S. (1982), "The Symmetric Turbulent Wake of a Flat Plate," AIAA J., **20**, 1228-1235.

Reynolds, W. C. (1976), "Computation of Turbulent Flows," Ann. Rev. Fluid Mech., **8**: 183-208.

Reichardt, H. (1965), "Zur Problematik der Turbulenten Strahlausbreitung in Einer Grundströmung," Mitteilungen aus dem Max-Planck-Institüt für Strömungsforschung No. 35.

Rodi, W. (1972), "The Prediction of Free Turbulent Boundary Layers by Use of a Two-Equation Model of Turbulence," Ph.D. Thesis, London University, England.

Rodi, W. (1975), "A Review of Experimental Data of Uniform-Density Free Turbulent Boundary Larers," Studies in Convection, Vol. 1, Academic Press.

Rodi, W. (1980), "Turbulence Models and Their Application in Hydraulics," IAHR Publication, Delft.

Rogallo, R. S. (1981), "Numerical Experiments in Homogeneous Turbulence," NASA Report, TM 81315.

Sabin, C. M. (1965), "An Analytical and Experimental Study of the Plane, Incompressible, Turbulent Free-Shear Layer With Arbitrary Velocity Ratio and Pressure Gradient," Trans. A.S.M.E., J. Basic Engng., **86**: 421-428.

Schlichting, H. (1979), Boundary-Layer Theory, Seventh Edition, McGraw-Hill, New York.

Spencer, B. W., and Jones, B. G. (1971), "Statistical Investigation of Pressure and Velocity Fields in the Turbulent Two-Stream Mixing Layer," AIAA Paper, No. 71-613.

Tennekes, H., and Lumley, J. L. (1972), A First Course in Turbulence, MIT Press, Cambridge, Massachusetts.

Thomas, R. M. (1973), "Conditional Sampling and Other Measurements in a Plane Turbulent Wake," J. Fluid Mech., **57**: 549-582.

Townsend, A. A. (1949), "The Fully Developed Turbulent Wake of a Circular Cylinder," Australian J. Sci. Res., **2**: 451-468.

Townsend, A. A. (1956), The Structure of Turbulent Shear Flow, Cambridge University Press, Cambridge.

Uberoi, M. S., and Freymuth, P. (1969), "Spectra of Turbulence in Wakes Behind Circular Cylinders," Phys. Fluids, **12**: 1359-1363.

Uberoi, M. S., and Freymuth, P. (1970), "Turbulent Energy Balance and Spectra of the Axisymmetric Wake," Phys. Fluids, **13**: 2205-2210.

White, F. M. (1974), Viscous Fluid Flow, McGraw-Hill, New York.

Wygnanski, I., and Fiedler, H. (1969), "Some Measurements in the Self-Preserving Jet," J. Fluid Mech., **38**: 577-612.

Wygnanski, I., and Fiedler, H. (1970), "The Two-Dimensional Mixing Region," J. Fluid Mech., **41**: 327-363.

Yule, A. J. (1971), "Two-Dimensional Self-Preserving Turbulent Mixing Layers at Different Free Stream Velocity Ratios," Aero. Res. Counc., Rep. and Memo. No. 3683.

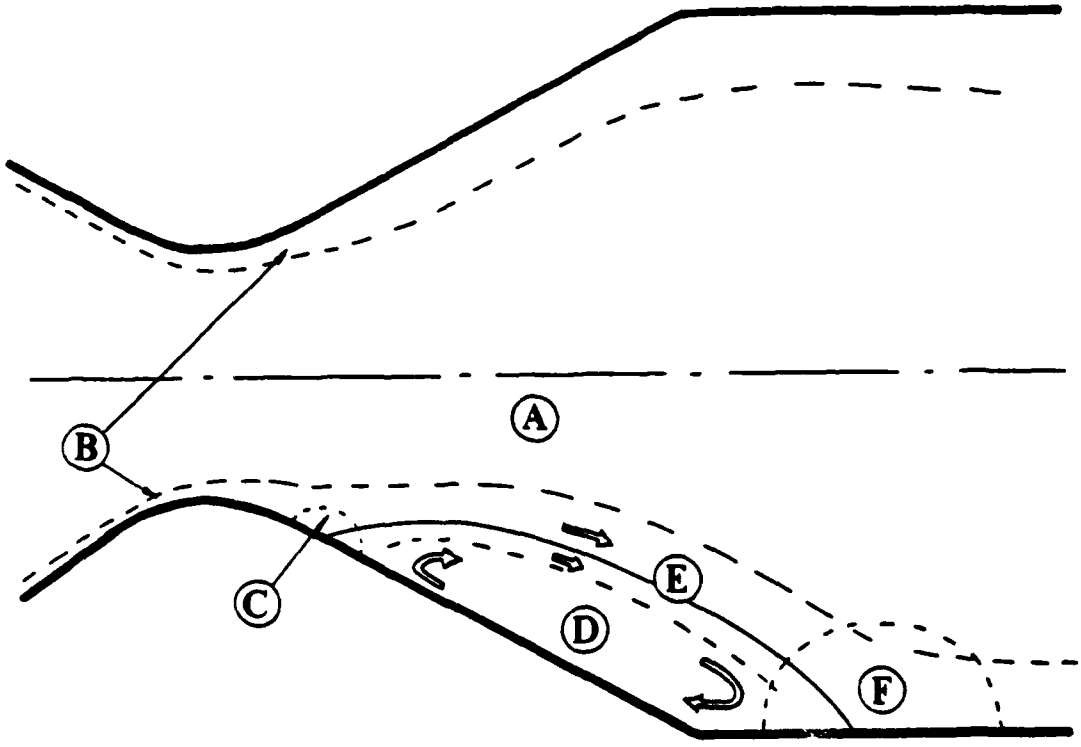

A : Potential Flow

B : Attached Boundary Layer

C : Detachment

D : Recirculation

E : Free Shear Layer

F : Reattachment

Fig. 1.1. Flow zones in a diffuser flow with separation.

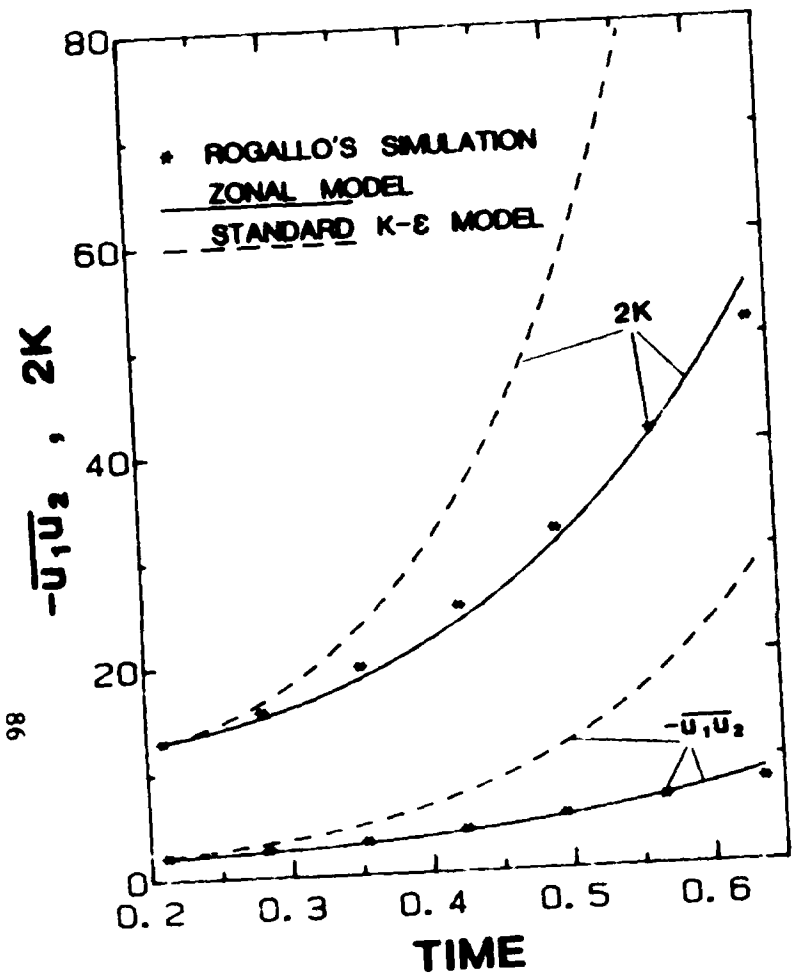

(a)

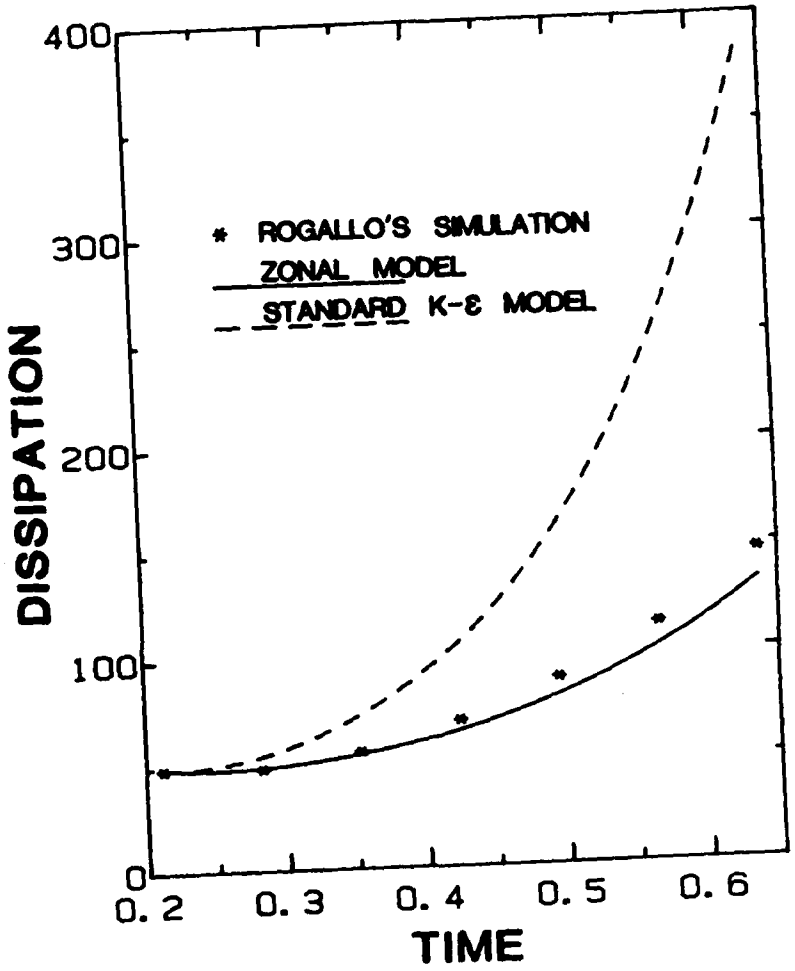

(b)

Fig. 2.1. Homogeneous shear flow case 1, $dU/dy = 20\sqrt{2}$, $\nu = 0.01/\sqrt{2}$. Comparison of zonal model and standard K-ε model with Rogallo's simulation.

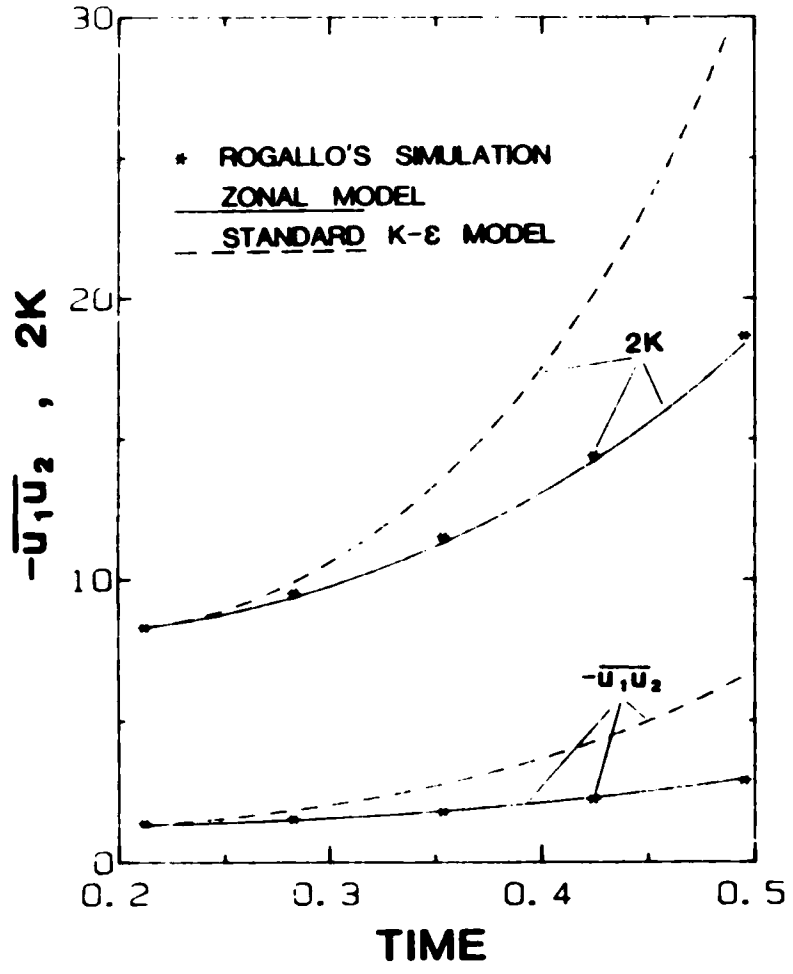

(a)

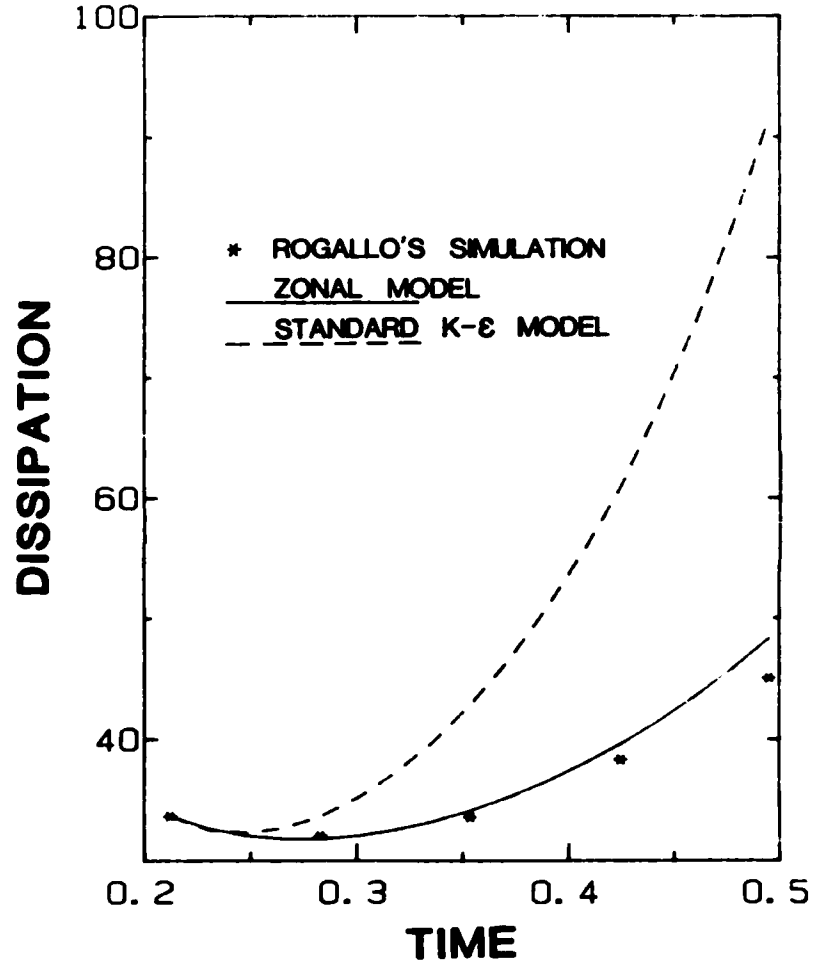

(b)

Fig. 2.2. Homogeneous shear flow case 2, $dU/dy = 20\sqrt{2}$, $\nu = 0.02/\sqrt{2}$. Comparison of zonal model and standard K-ε model with Rogallo's simulation.

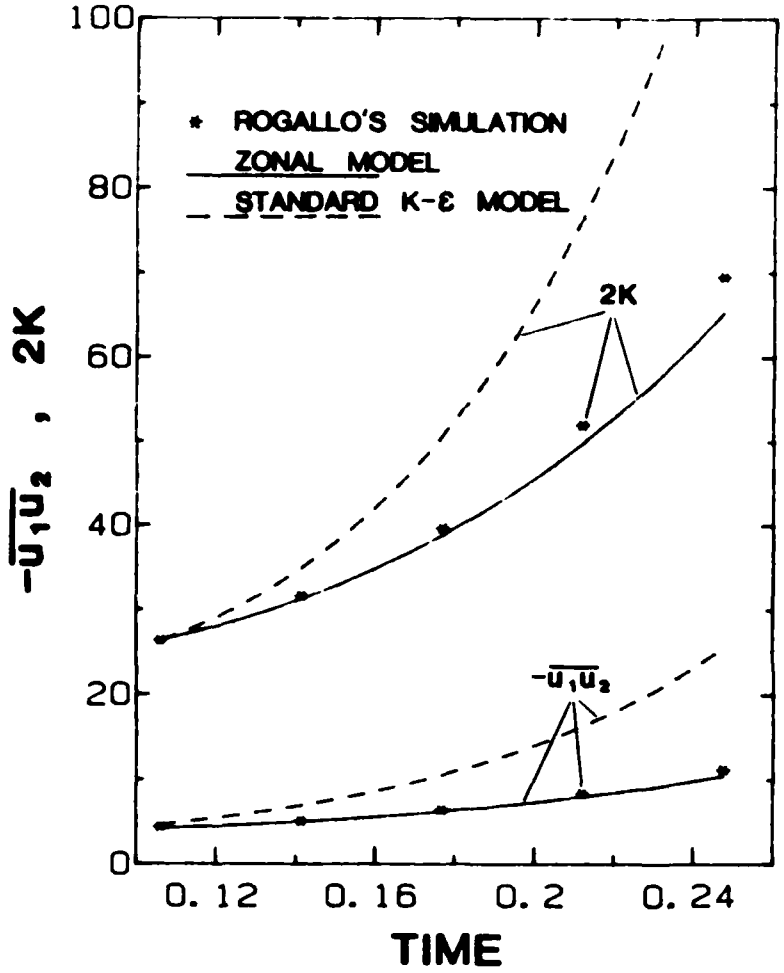

(a)

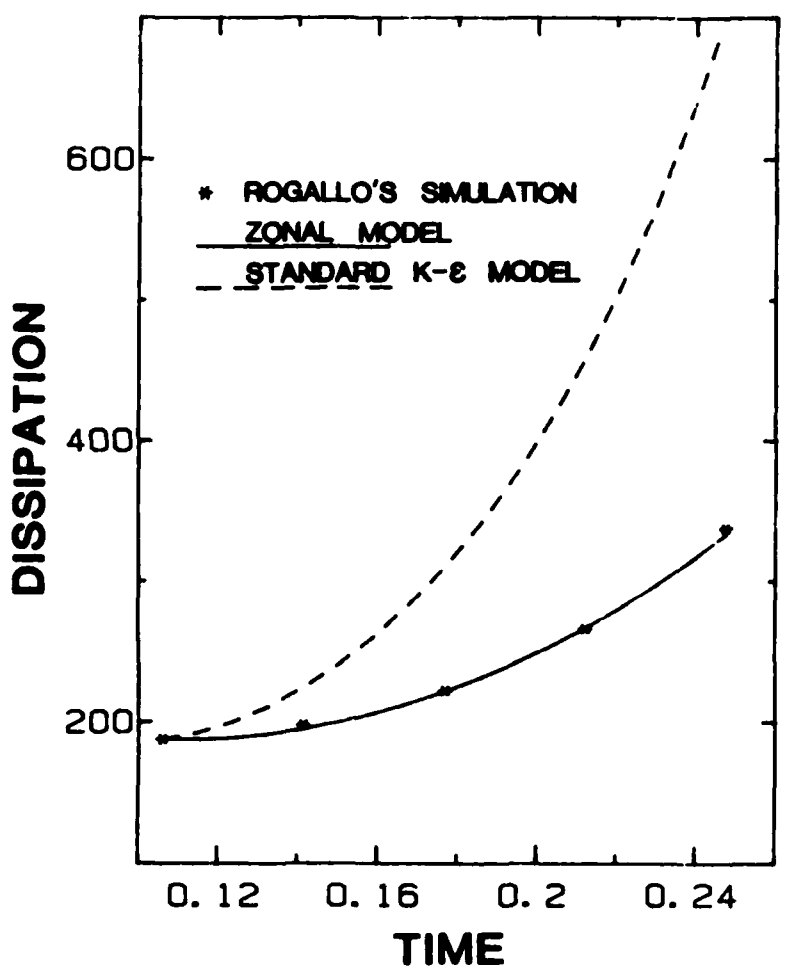

(b)

Fig. 2.3. Homogeneous shear flow case 3, $dU/dy = 40\sqrt{2}$, $\nu = 0.02/\sqrt{2}$. Comparison of zonal model and standard K-ε model with Rogallo's simulation.

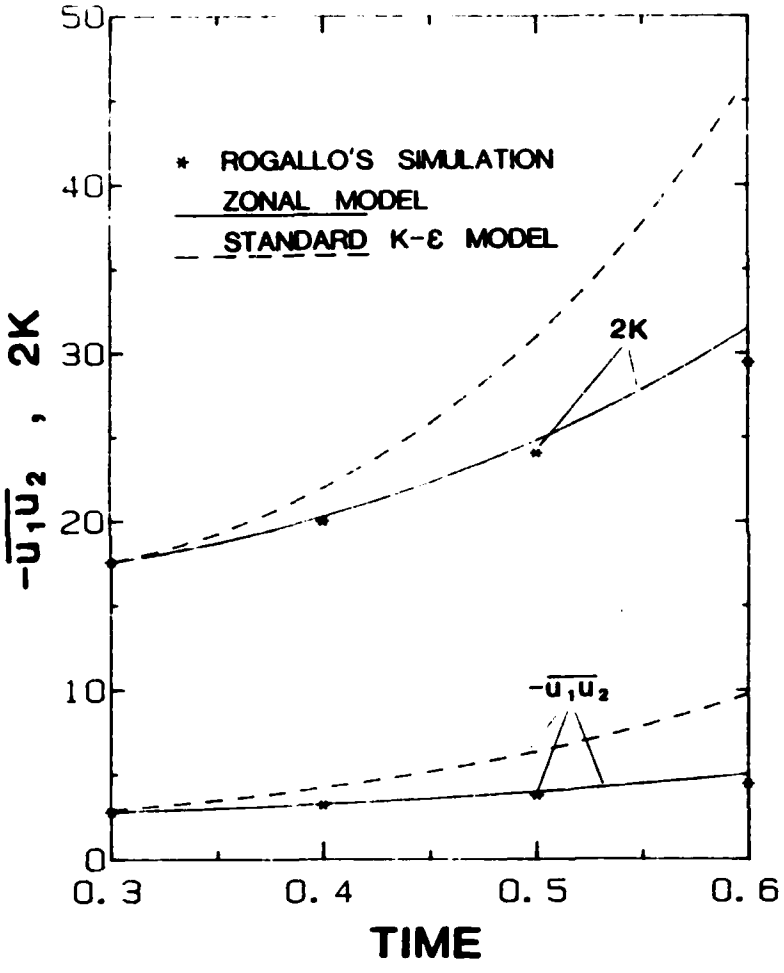

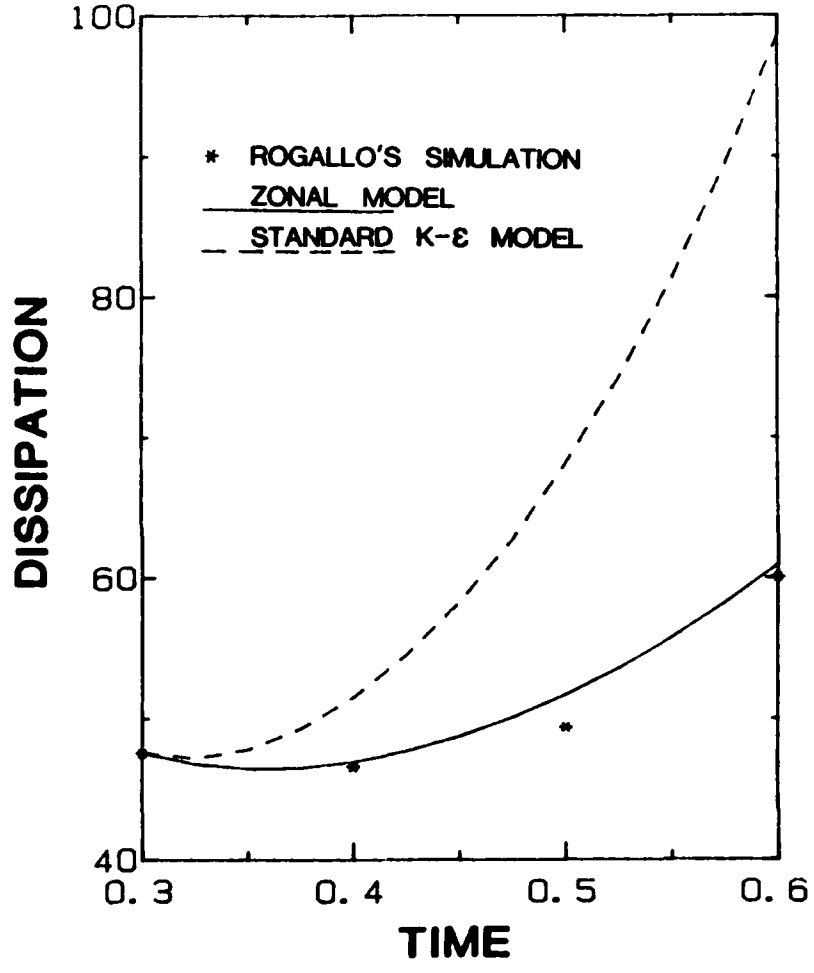

(b)

Fig. 2.4. Homogeneous shear flow case 4, dU/dy = 20, ν = 0.005. Comparison of zonal model and standard K-ε model with Rogallo's simulation.

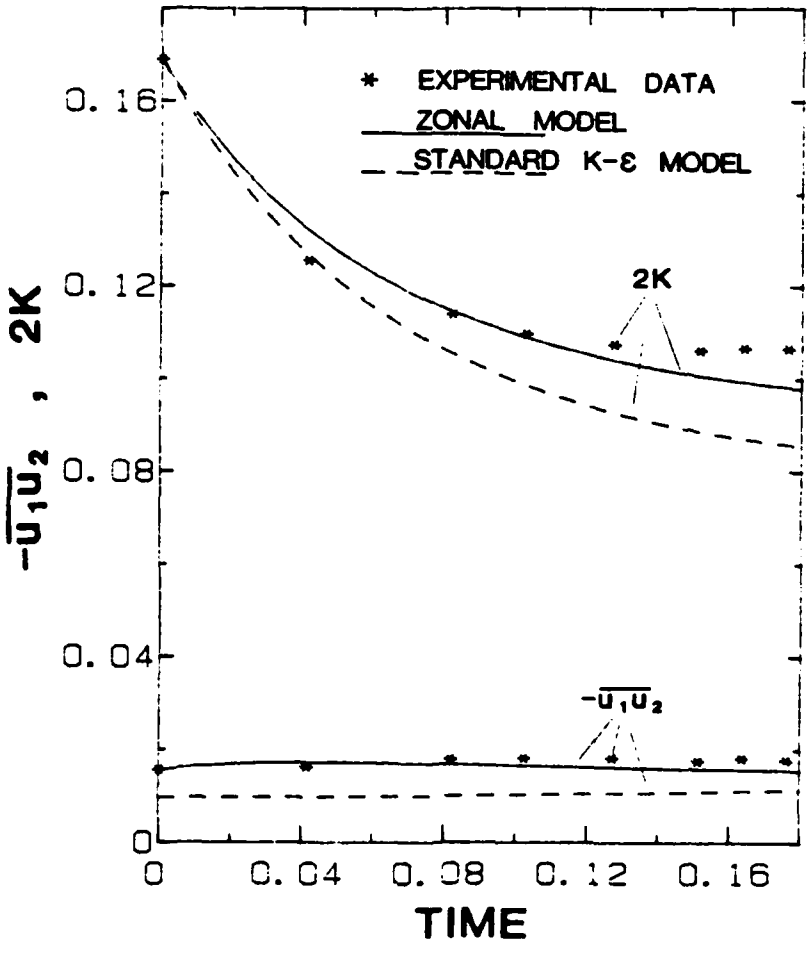

Fig. 2.5. Homogeneous shear flow, case 376A in 80-81 Stanford Conference, dU/dy = 12.9. Comparison of zonal model and standard K-ε model with experimental data.

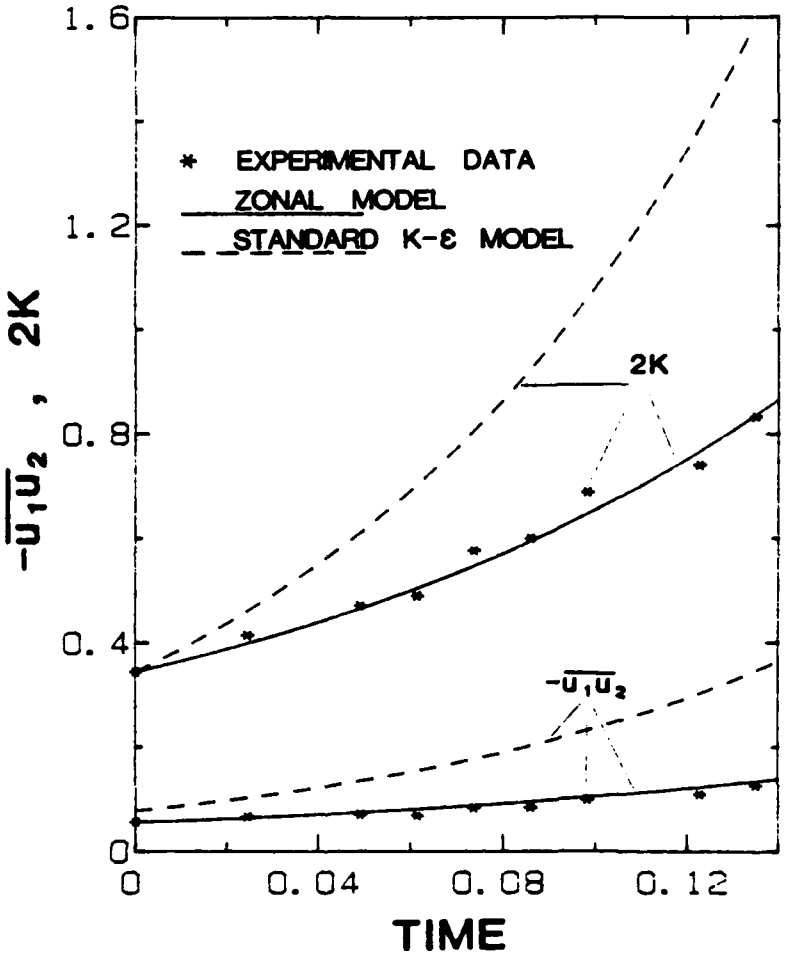

Fig. 2.6. Homogeneous shear flow, case 376B in 80-81 Stanford Conference, dU/dy = 48. Comparison of zonal model and standard K-ε model with experimental data.

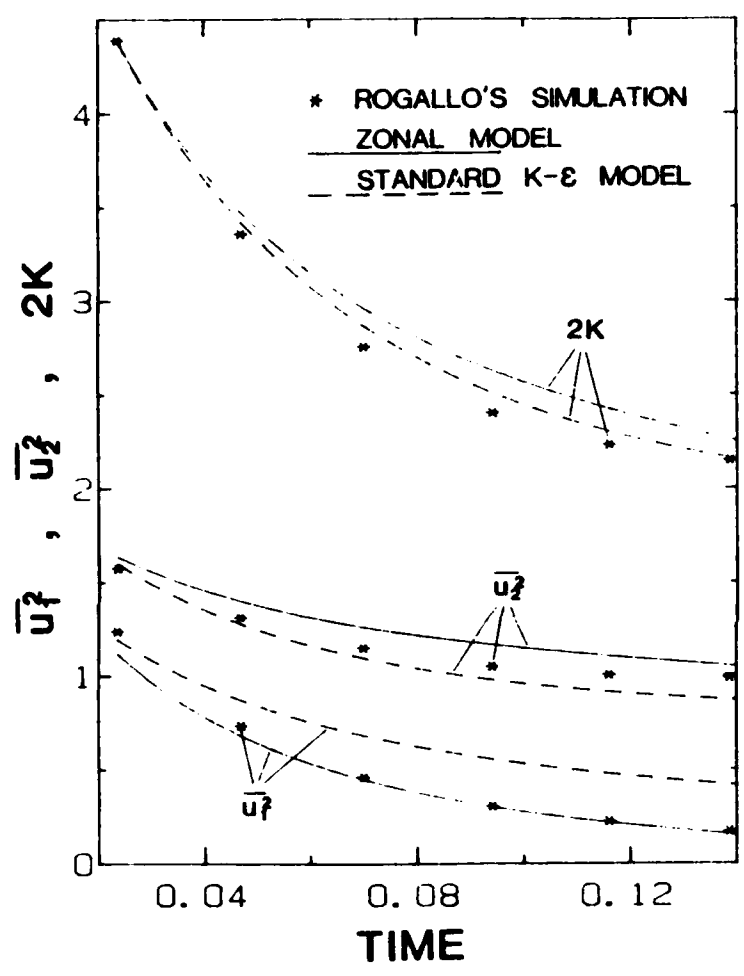

(a)

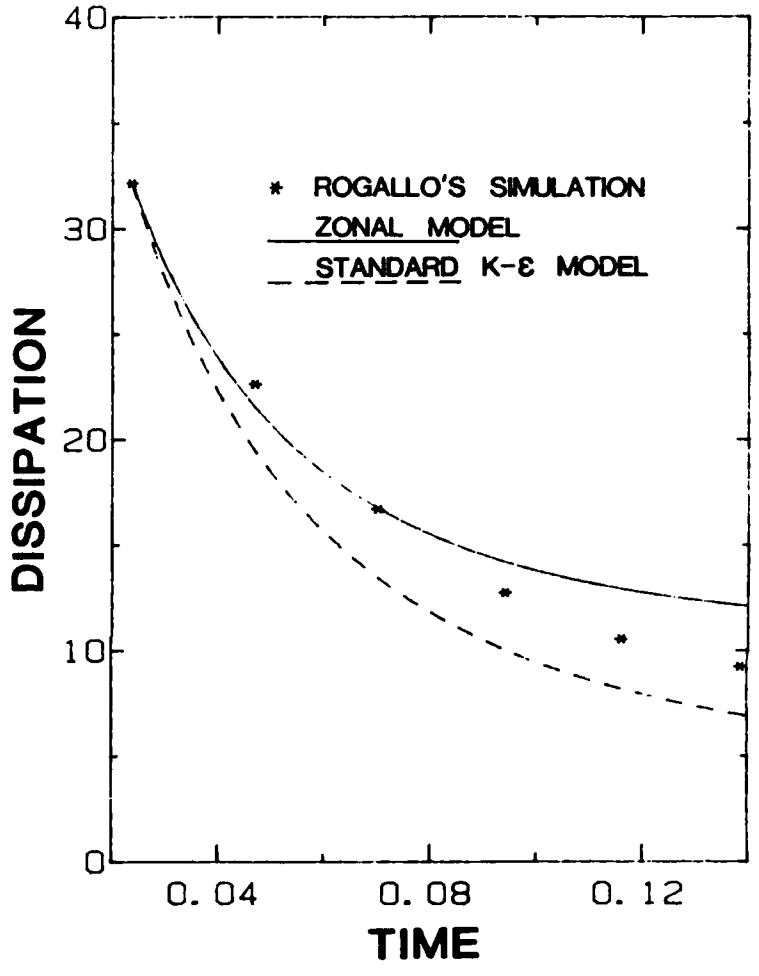

(b)

Fig. 2.7. Homogeneous axisymmetric strain case 1, $dU/dx = 10$, $\nu = 0.01/\sqrt{2}$. Comparison of zonal model and standard K-ε model with Rogallo's simulation.

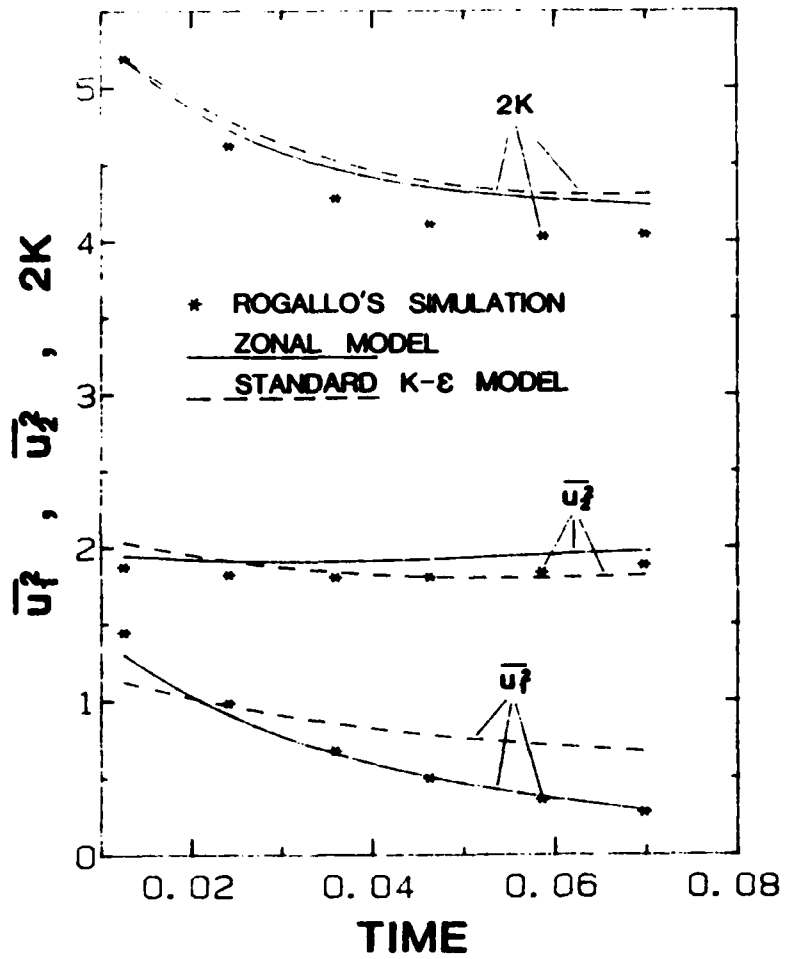

(a)

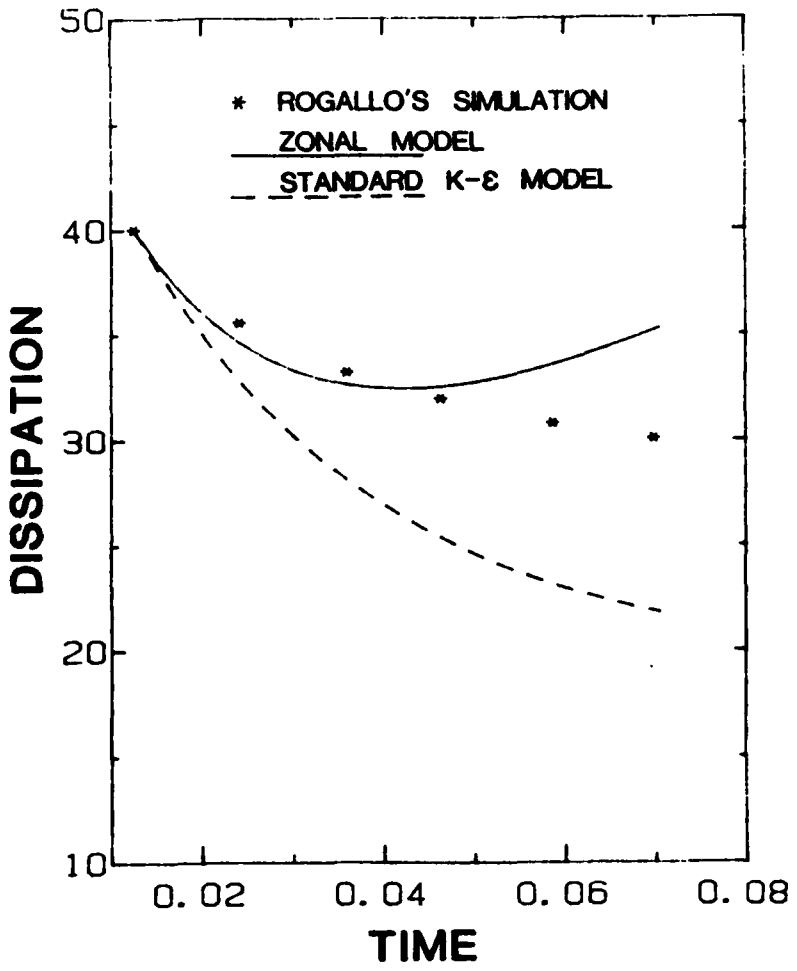

(b)

Fig. 2.8. Homogeneous axisymmetric strain case 2, $dU/dx = 20$, $\nu = 0.01/\sqrt{2}$. Comparison of zonal model and standard K-ε model with Rogallo's simulation.

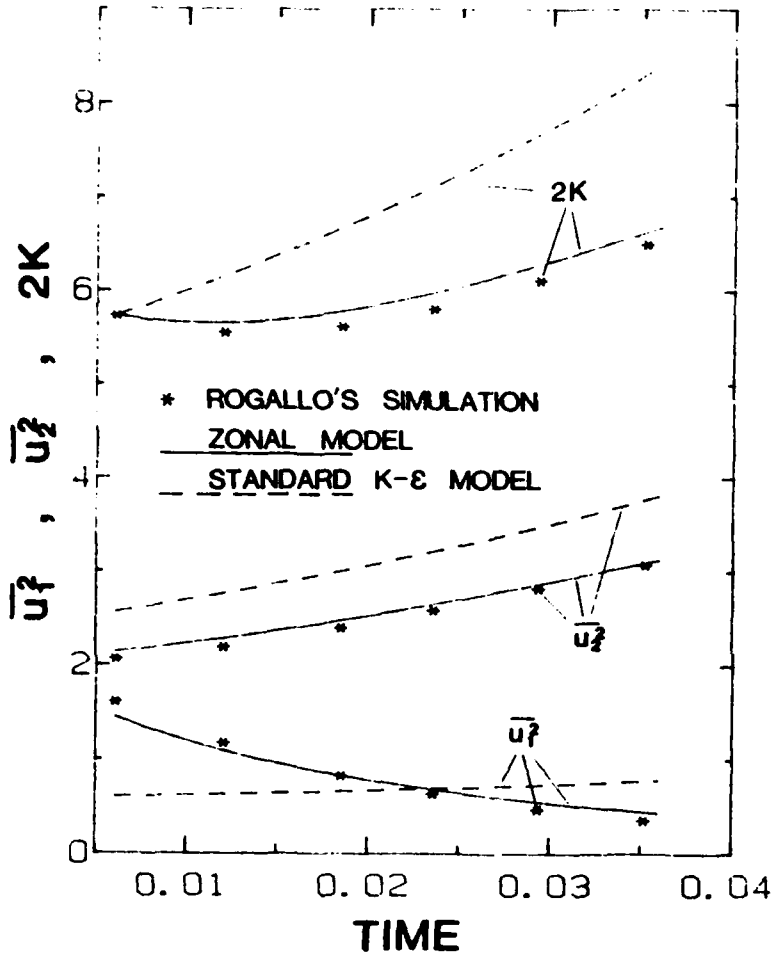

(a)

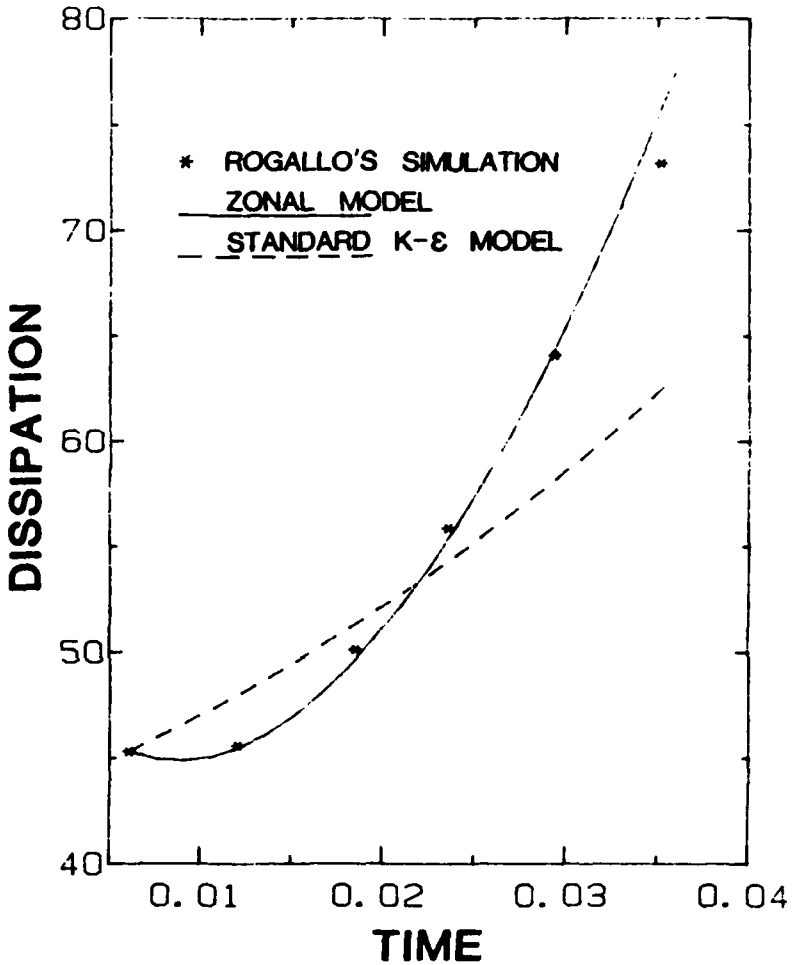

(b)

Fig. 2.9. Homogeneous axisymmetric strain case 3, $dU/dx = 40$, $\nu = 0.01/\sqrt{2}$. Comparison of zonal model and standard K-ε model with Rogallo's simulation.

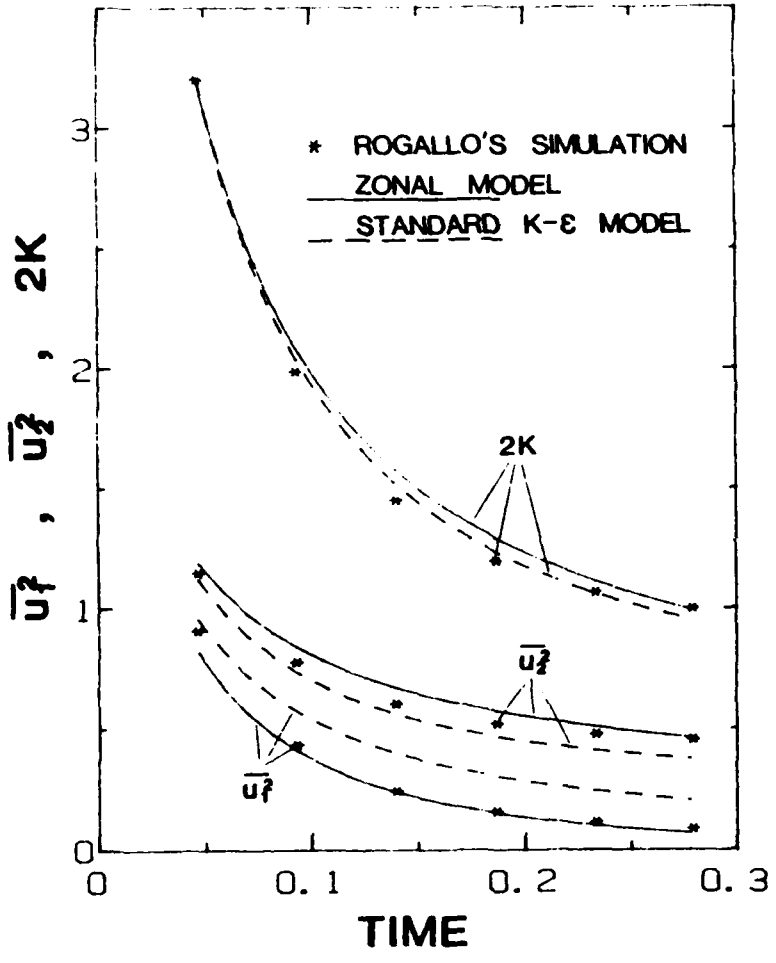

(a)

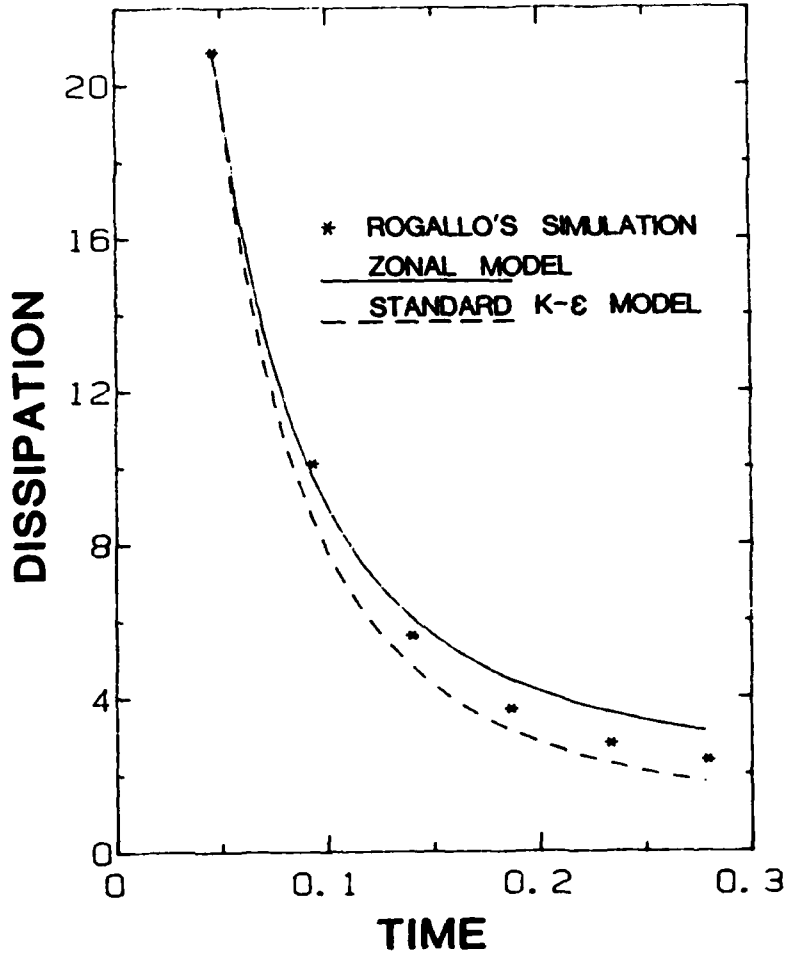

(b)

Fig. 2.10. Homogeneous axisymmetric strain case 4, $dU/dx = 5$, $\nu = 0.01/\sqrt{2}$. Comparison of zonal model and standard K-ε model with Rogallo's simulation.

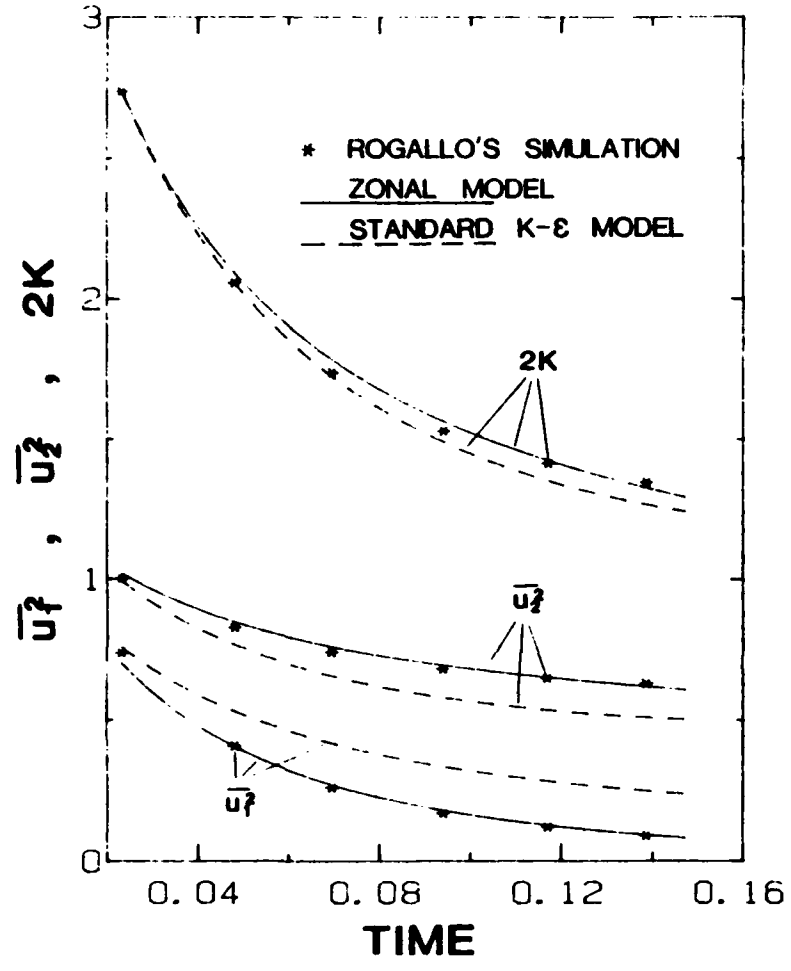

(a)

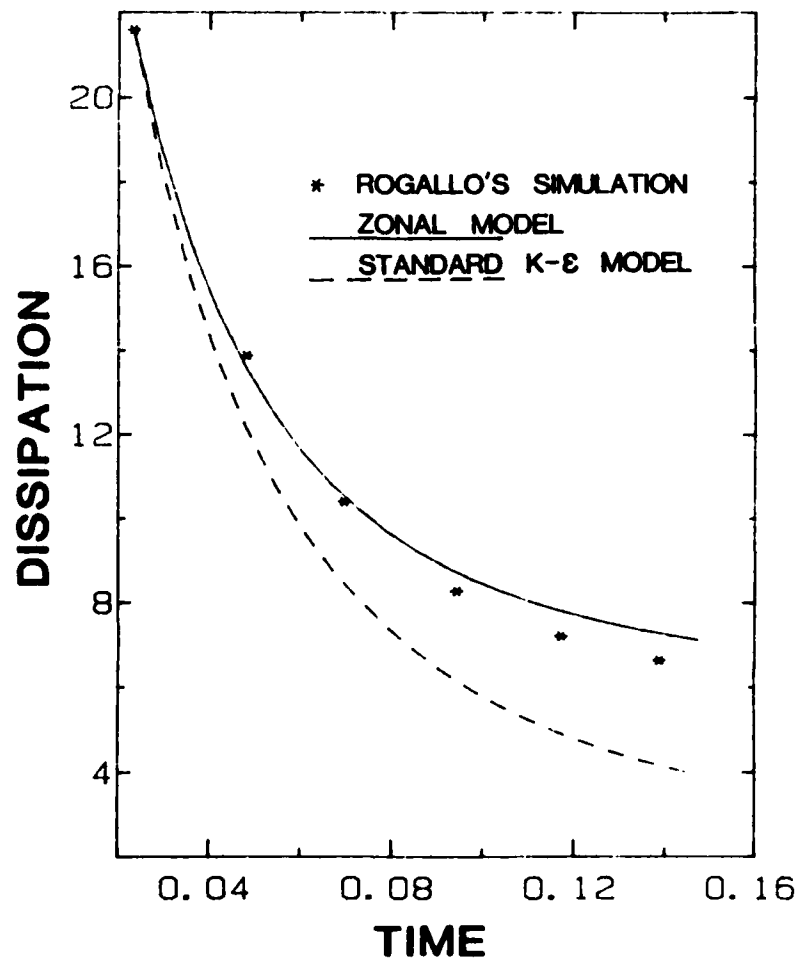

(b)

Fig. 2.11. Homogeneous axisymmetric strain case 5, $dU/dx = 10$, $\nu = 0.02/\sqrt{2}$. Comparison of zonal model and standard K-ε model with Rogallo's simulation.

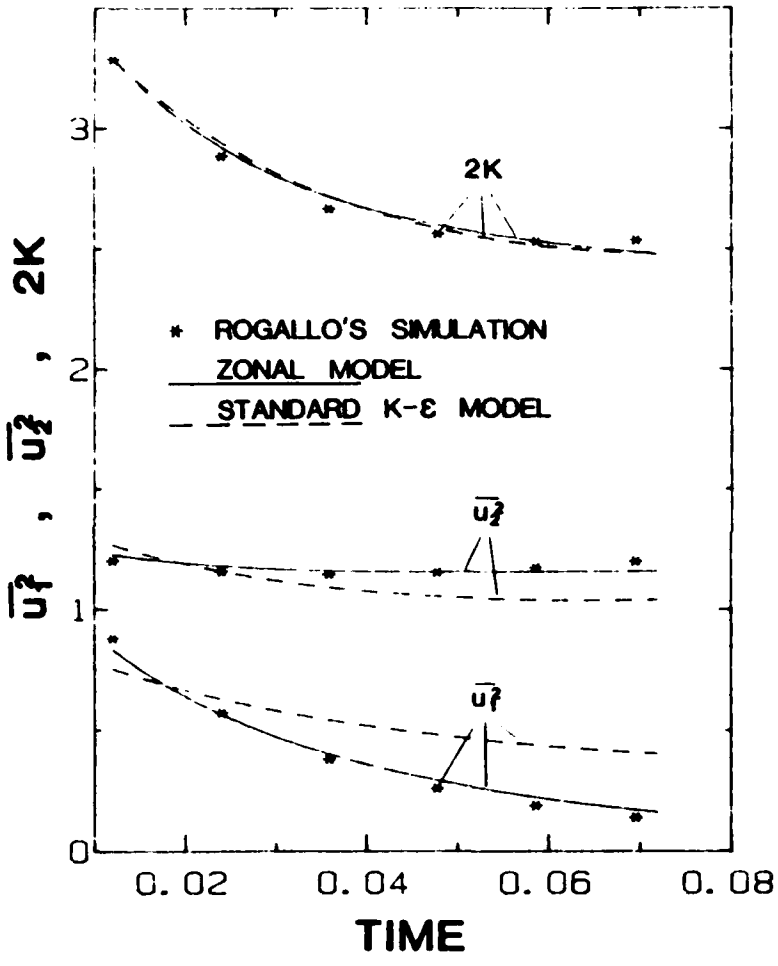

(a)

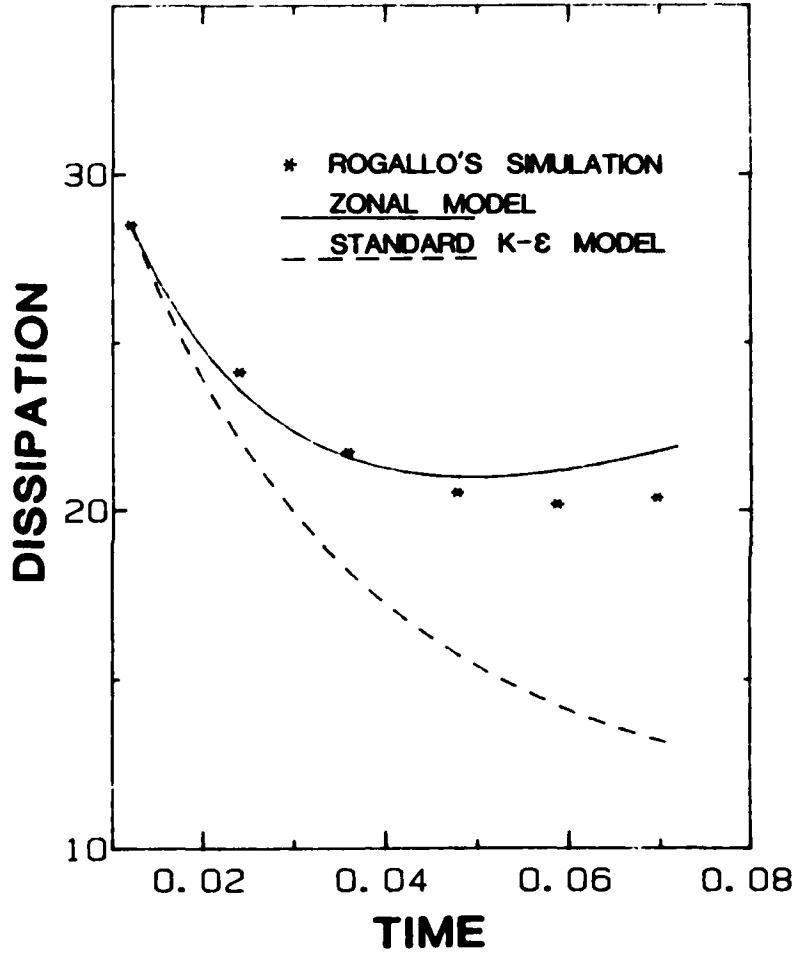

(b)

Fig. 2.12. Homogeneous axisymmetric strain case 6, $dU/dx = 20$, $\nu = 0.02/\sqrt{2}$. Comparison of zonal model and standard K-ε model with Rogallo's simulation.

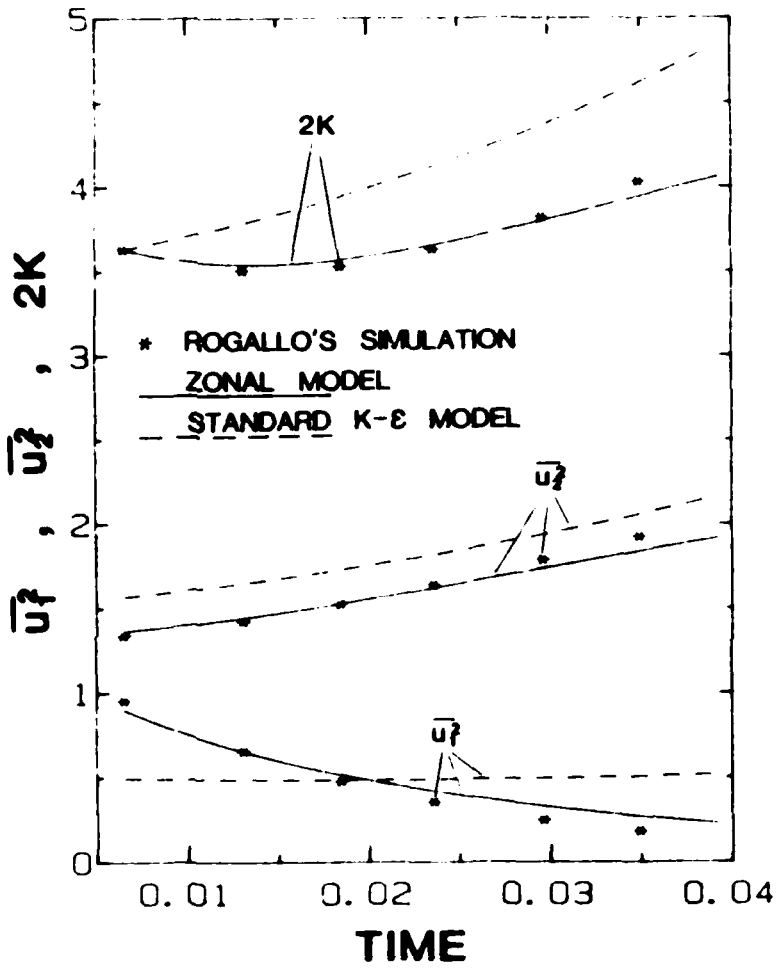

(a)

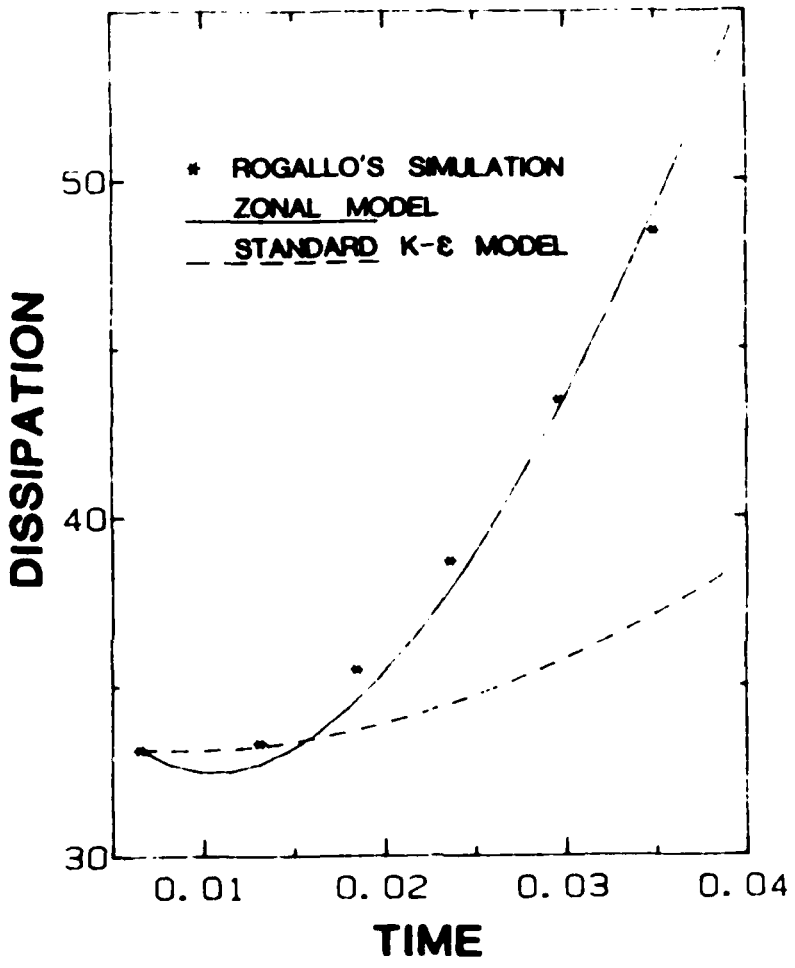

(b)

Fig. 2.13. Homogeneous axisymmetric strain case 7, $dU/dx = 40$, $\nu = 0.02/\sqrt{2}$. Comparison of zonal model and standard K-ε model with Rogallo's simulation.

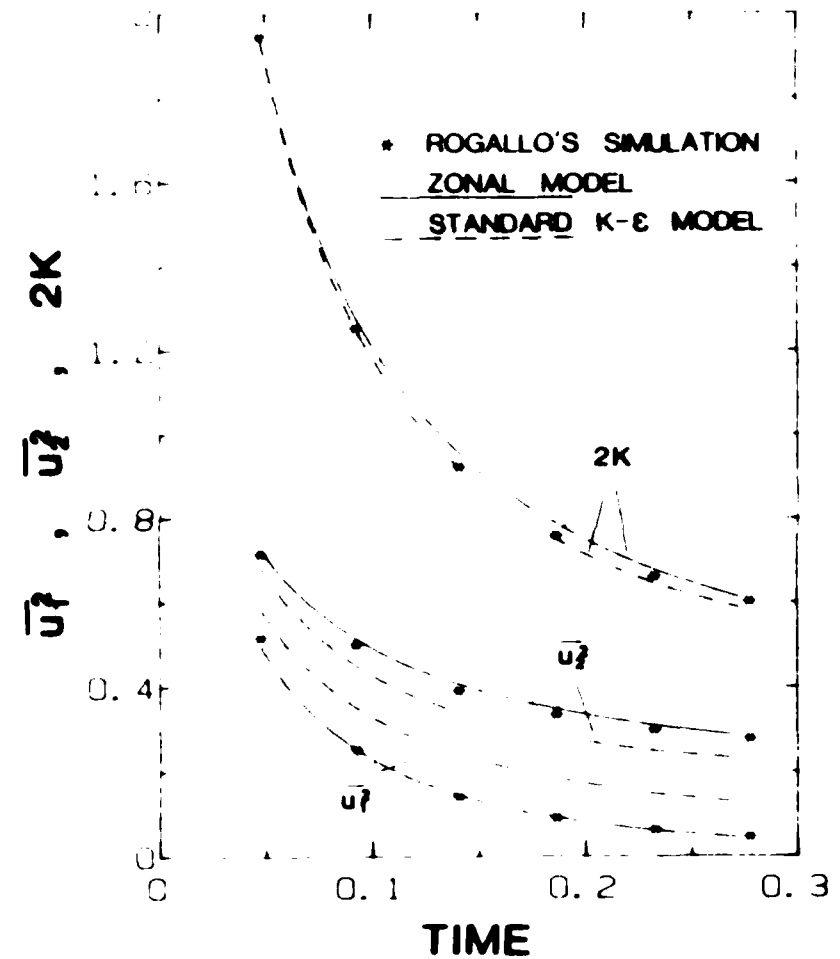

(a)

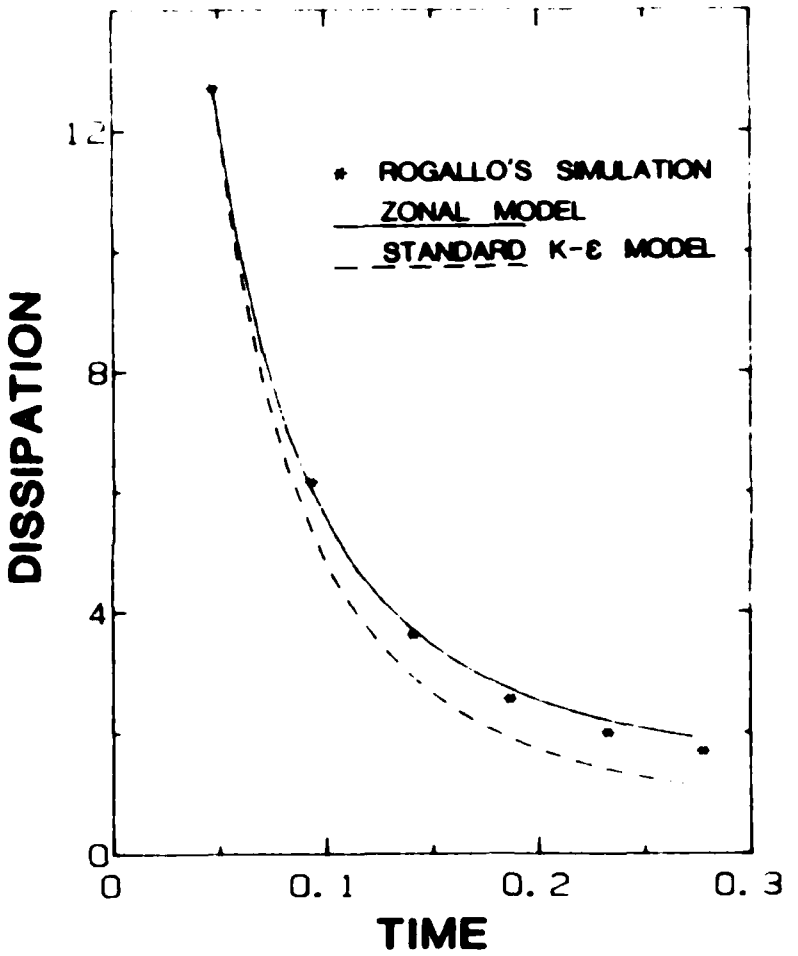

(b)

Fig. 2.14. Homogeneous axisymmetric strain case 8, $dU/dx = 5$, $\nu = 0.02/\sqrt{2}$. Comparison of zonal model and standard K-ε model with Rogallo's simulation.

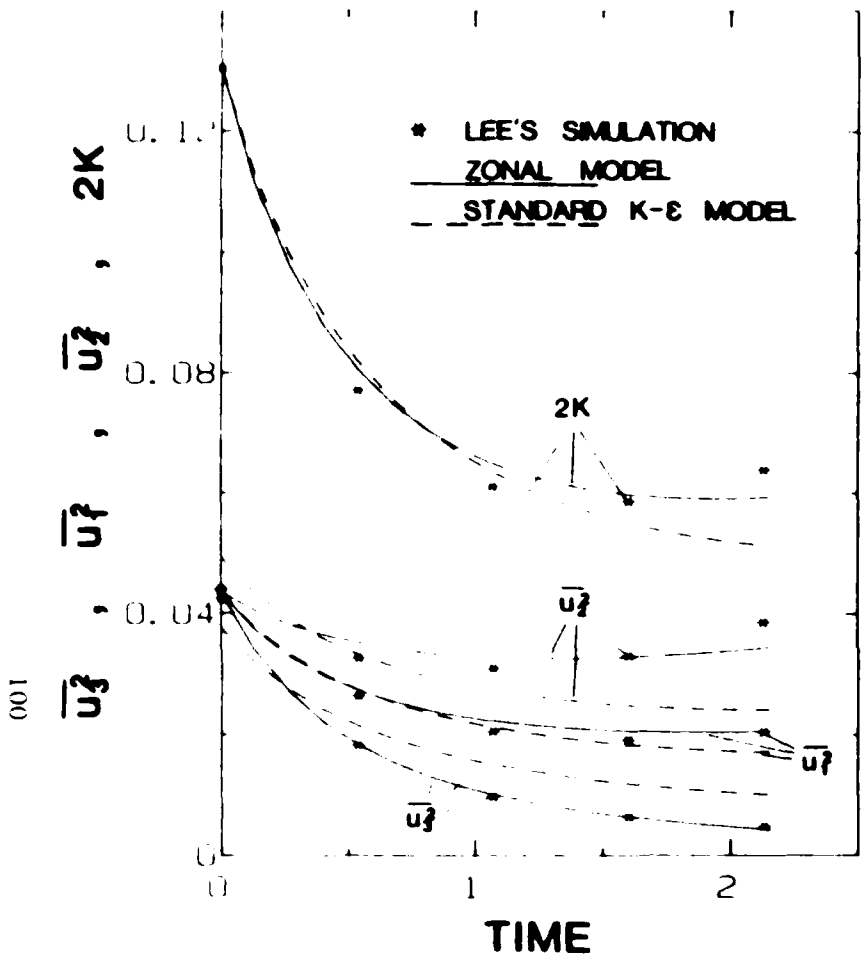

(a)

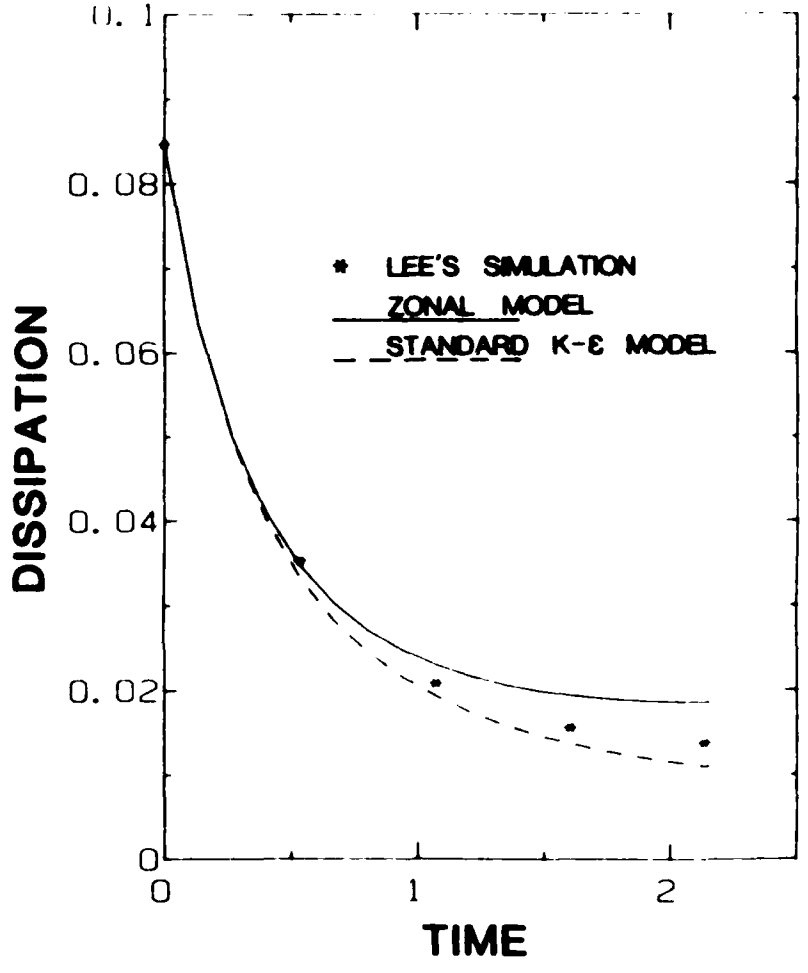

(b)

Fig. 2.15. Homogeneous plane strain case 1, $dW/dz = 0.65$, $\nu = 4.299 \times 10^{-3}$. Comparison of zonal model and standard K-ε model with Lee and Reynolds' simulation.

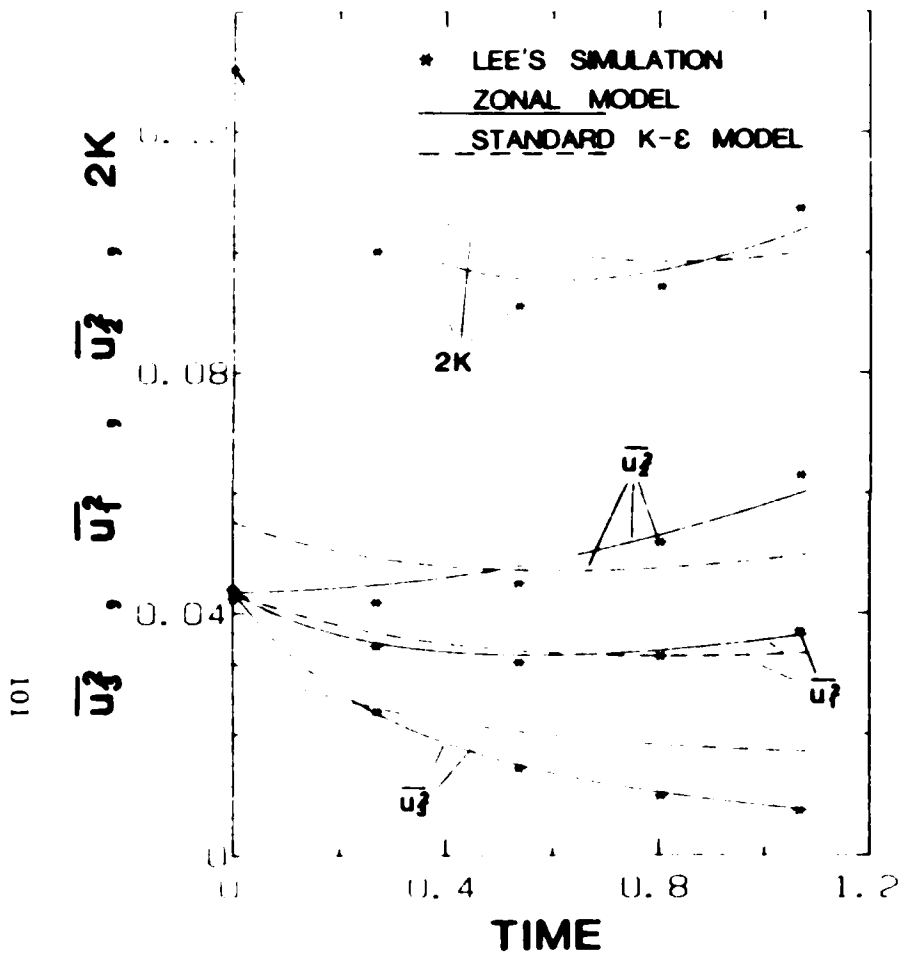

(a)

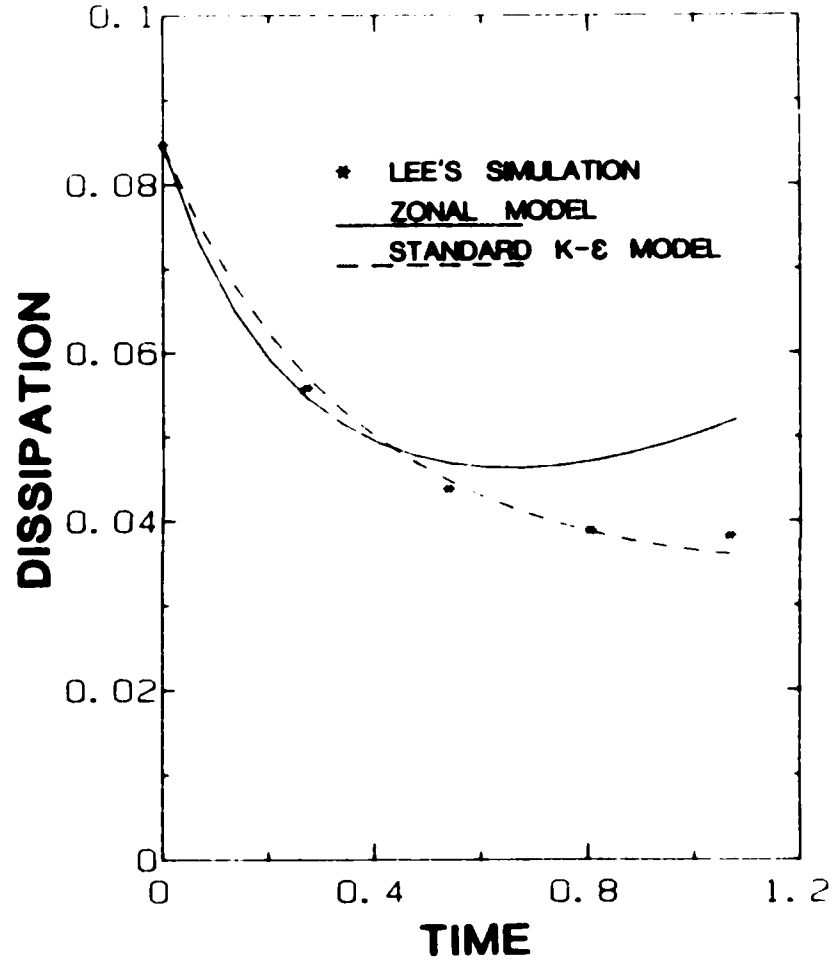

(b)

Fig. 2.16. Homogeneous plane strain case 2, $dW/dz = 1.3$, $\nu = 4.299 \times 10^{-3}$. Comparison of zonal model and standard K-ε model with Lee and Reynolds' simulation.

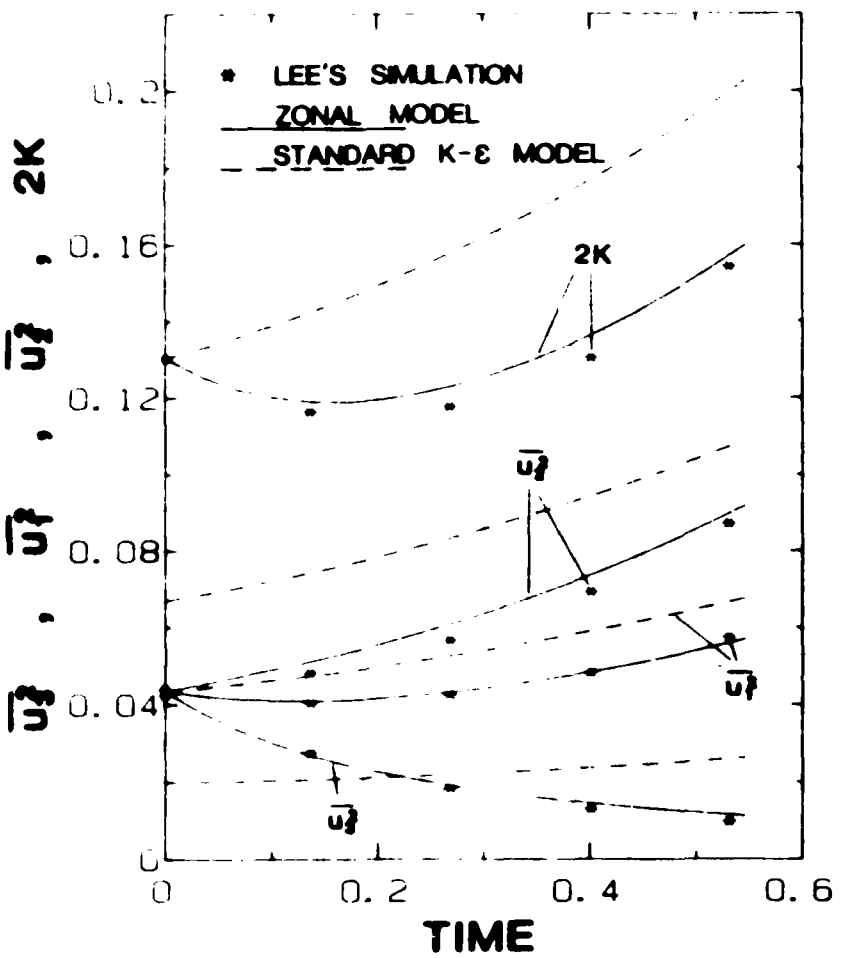

(a)

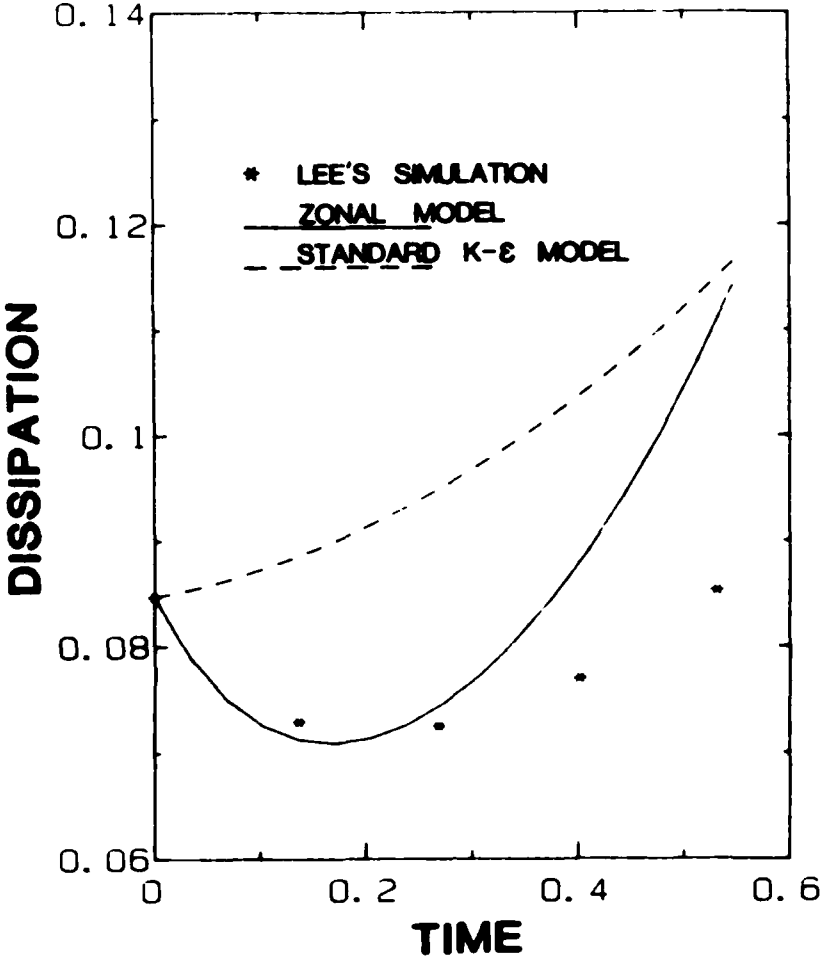

(b)

Fig. 2.17. Homogeneous plane strain case 3, $dW/dz = 2.6$, $\nu = 4.299 \times 10^{-3}$. Comparison of zonal model and standard K-ε model with Lee and Reynolds' simulation.

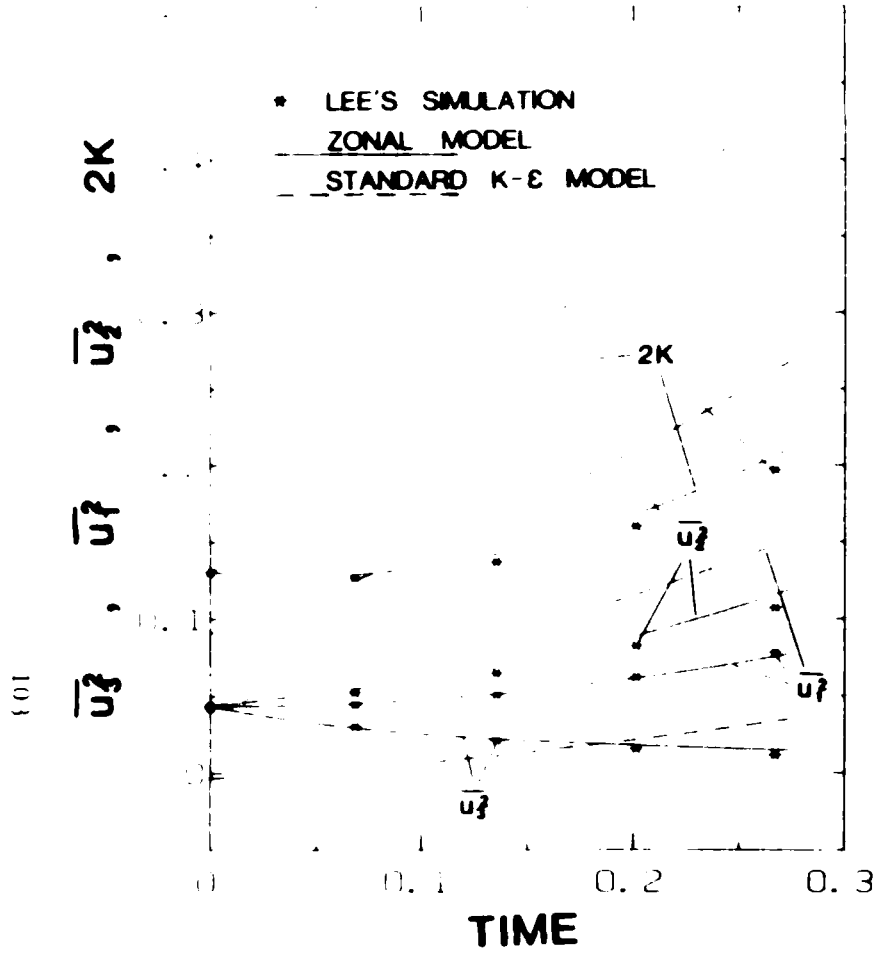

(a)

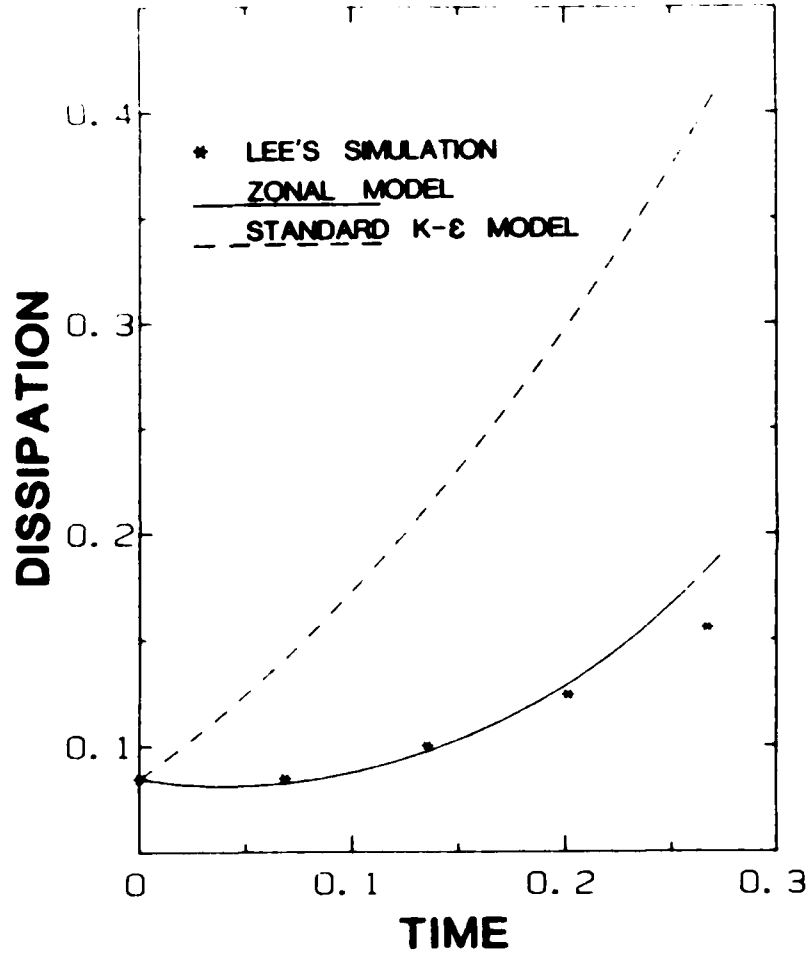

(b)

Fig. 2.18. Homogeneous plane strain case 4, dW/dz = 5.2, $\nu = 4.299 \times 10^{-3}$. Comparison of zonal model and standard K-ε model with Lee and Reynolds' simulation.

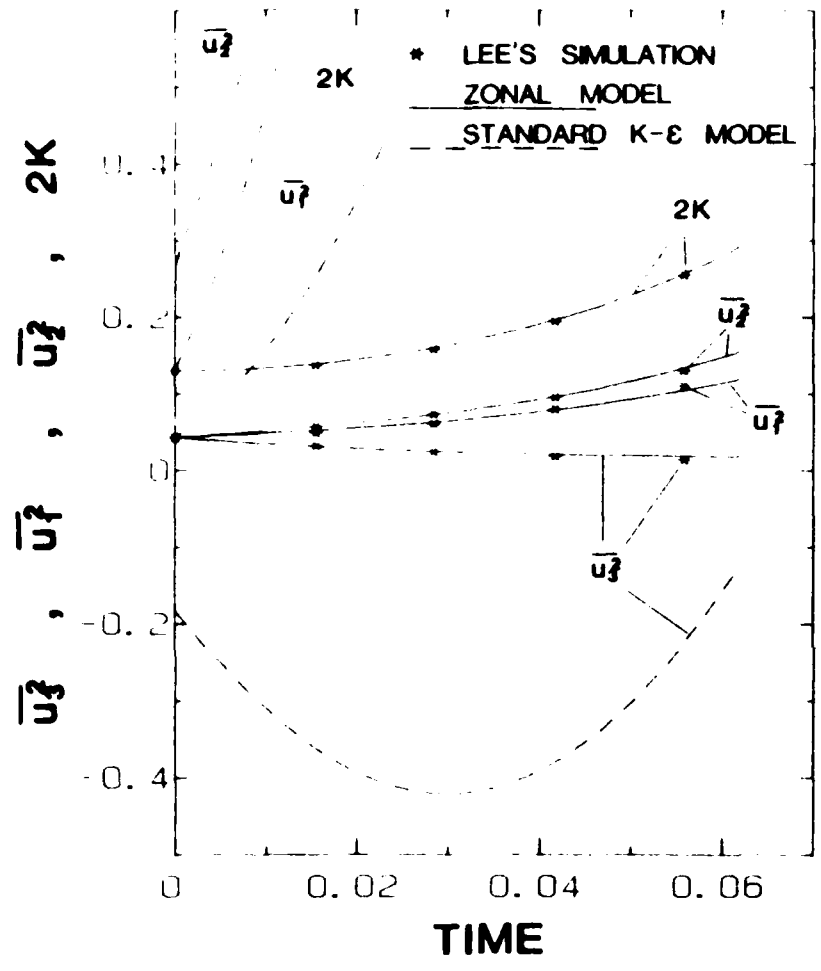

(a)

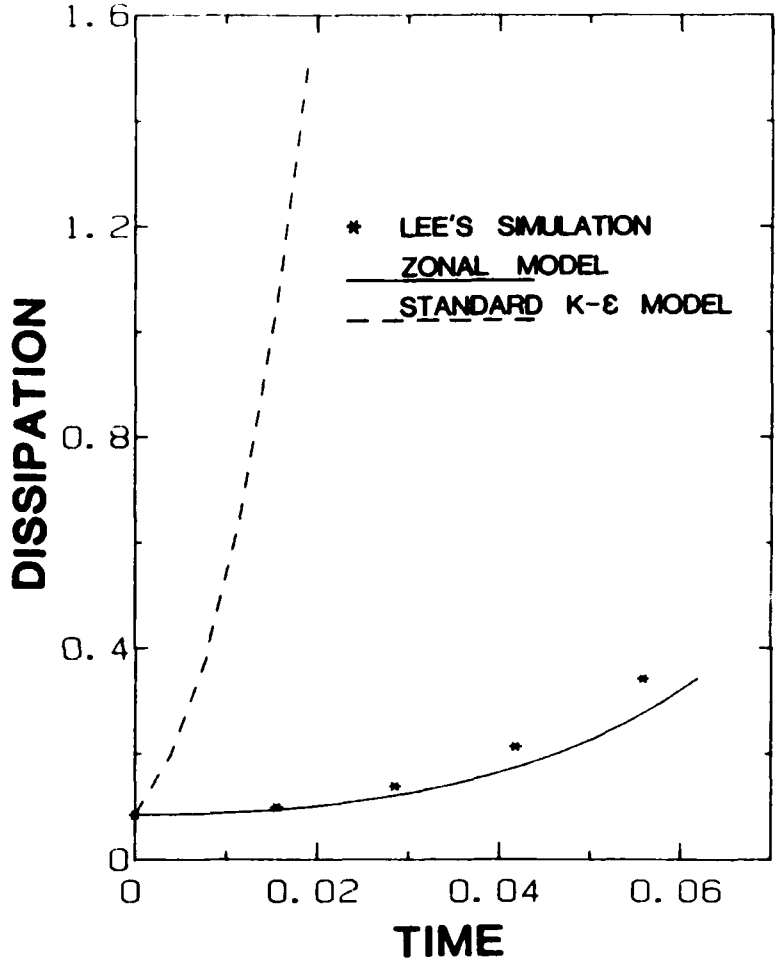

(b)

Fig. 2.19. Homogeneous plane strain case 5, dW/dz = 25, $\nu = 4.299 \times 10^{-3}$. Comparison of zonal model and standard K-ε model with Lee and Reynolds' simulation.

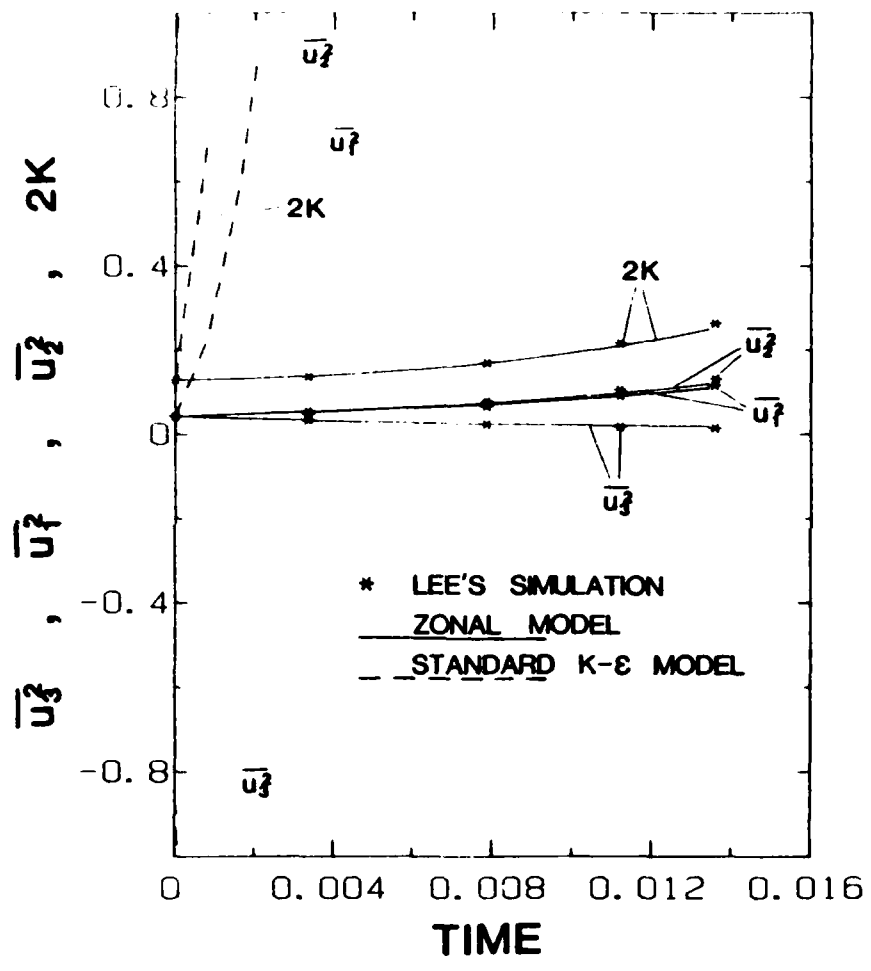

(a)

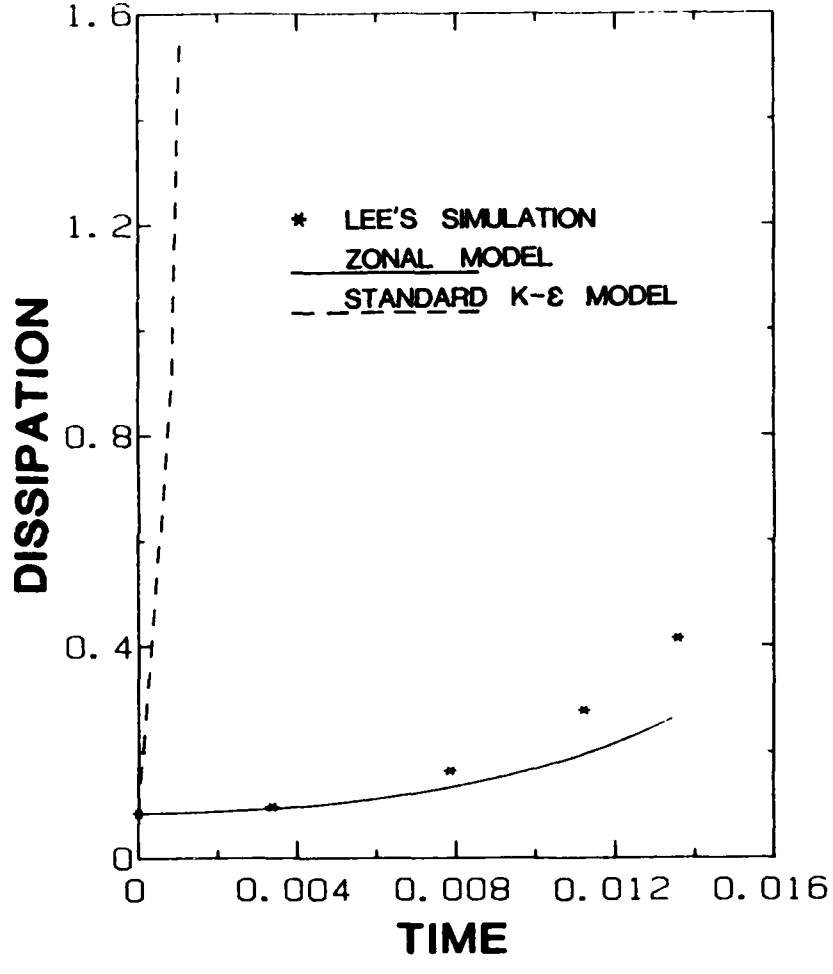

(b)

Fig. 2.20. Homogeneous plane strain case 6, dW/dz = 100, $\nu = 4.299 \times 10^{-3}$. Comparison of zonal model and standard K-ε model with Lee and Reynolds' simulation.

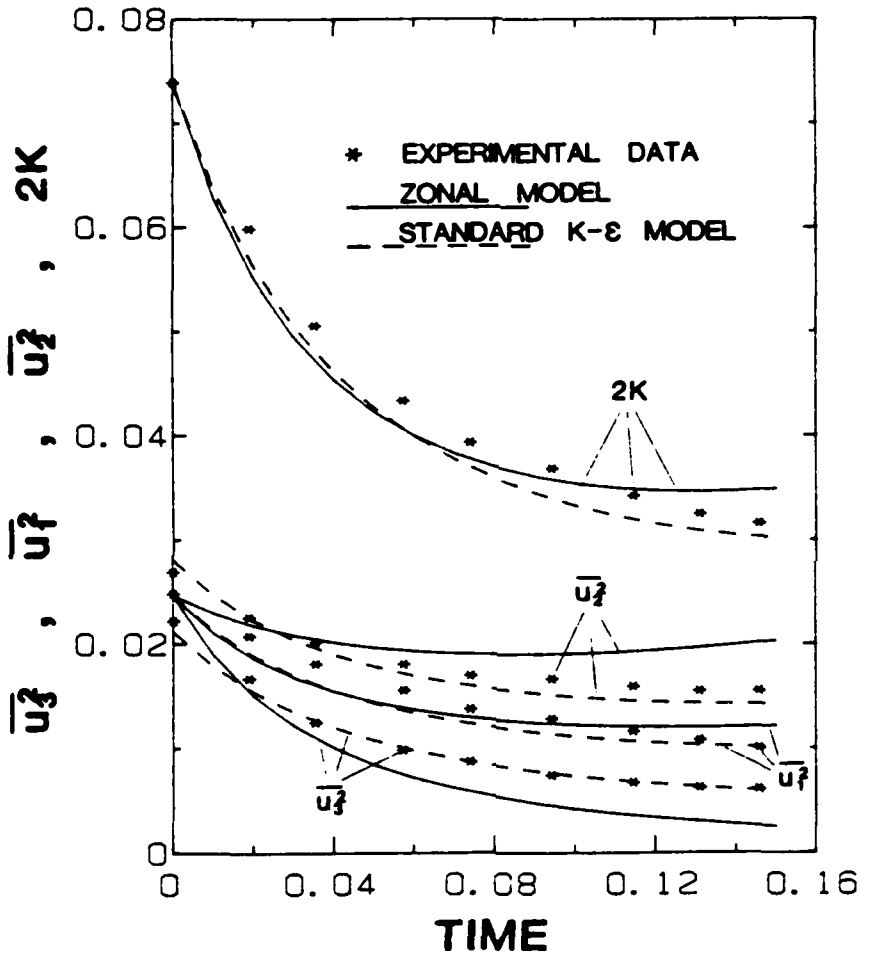

Fig. 2.21. Homogeneous plane strain, case 374A in 80-81 Stanford Conference, dW/dz = 9.44. Comparison of zonal model and standard K-ε model with experimental data.

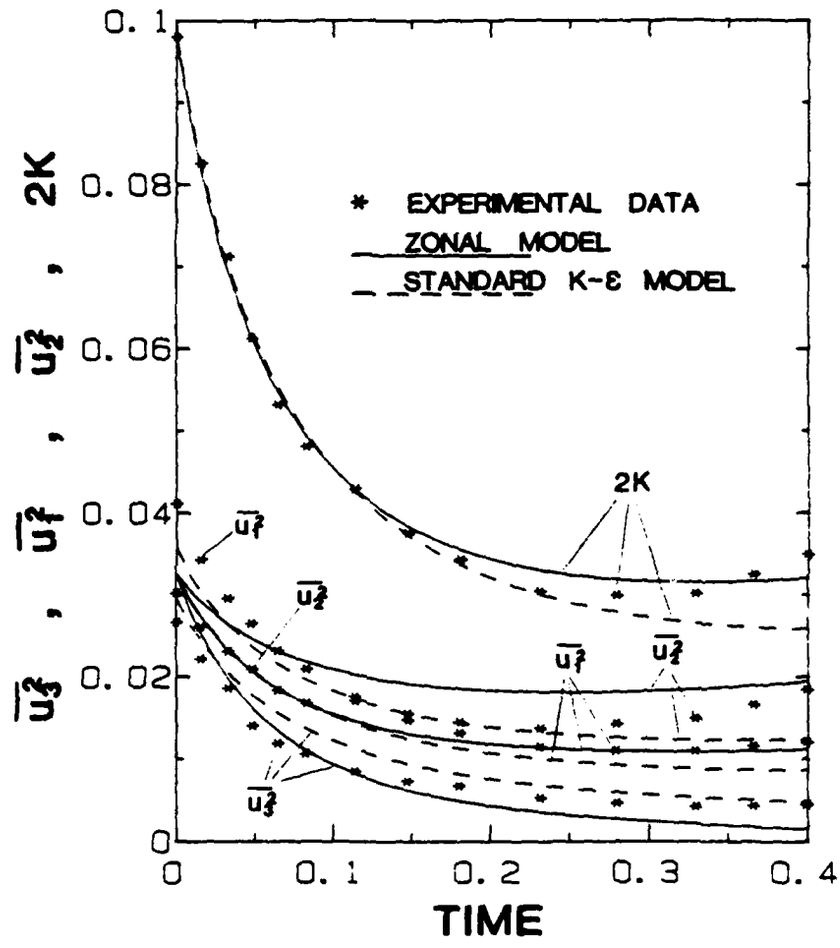

Fig. 2.22. Homogeneous plane strain, case 374B in 80-81 Stanford Conference, $dW/dz = 4.45$. Comparison of zonal model and standard K-ε model with experimental data.

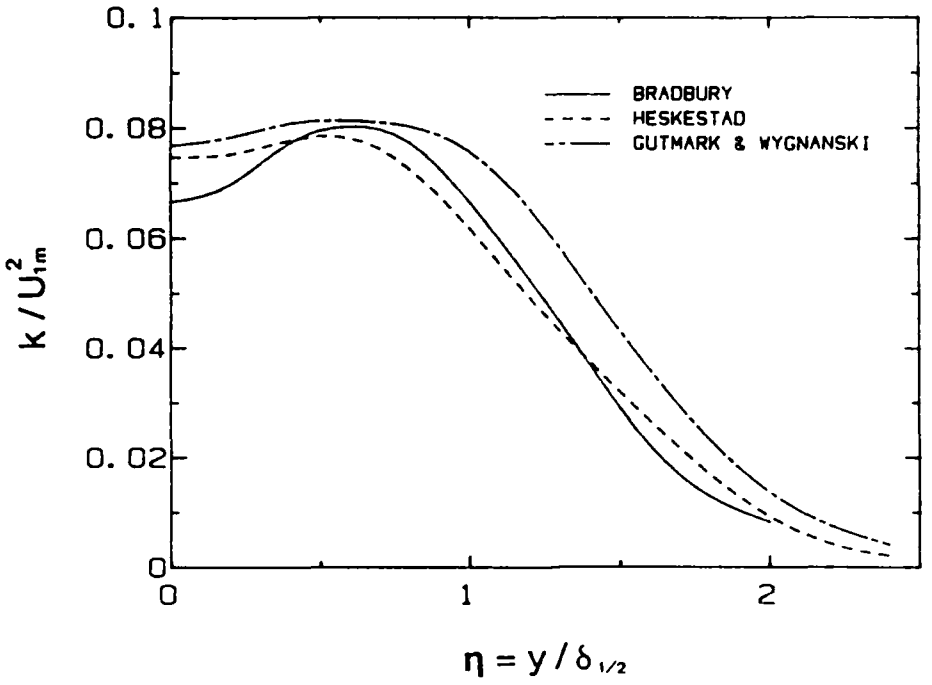

Fig. 3.1. Turbulent kinetic energy of plane pure jet.

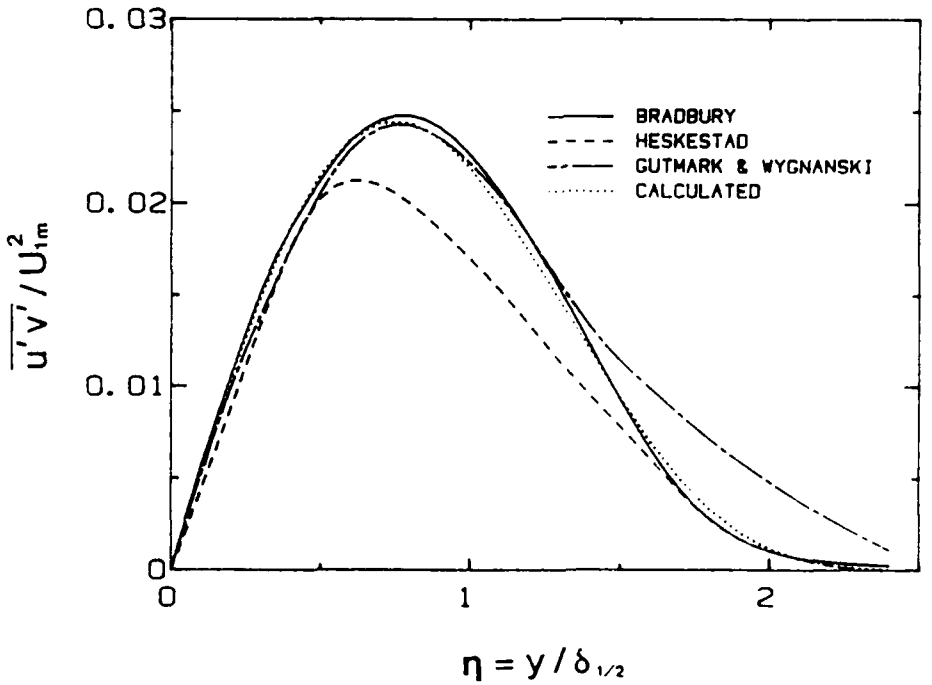

Fig. 3.2. Shear stress of plane pure jet.

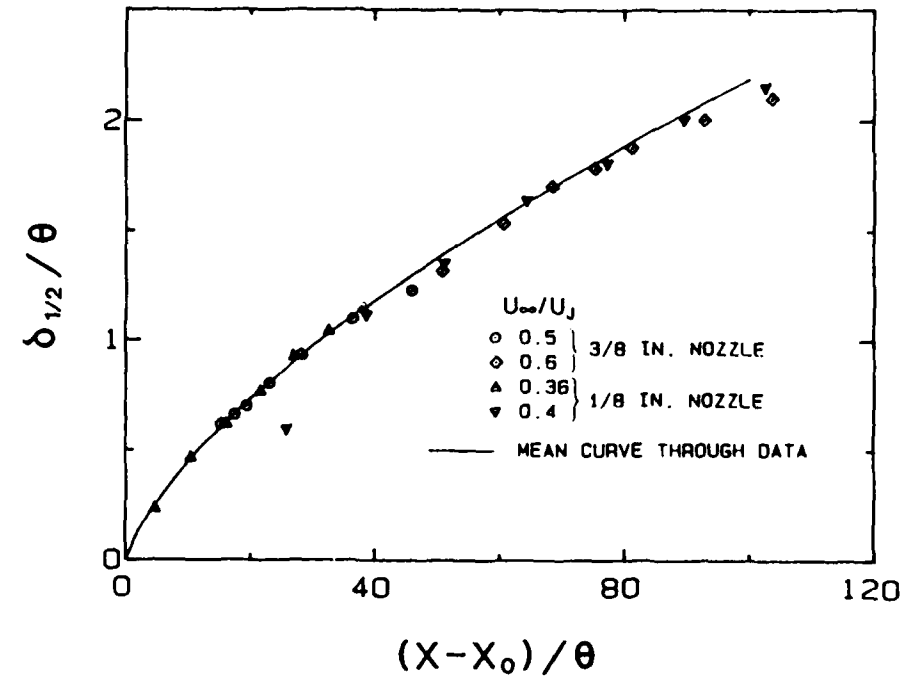

Fig. 3.3. Spreading rate of plane co-flowing jets.

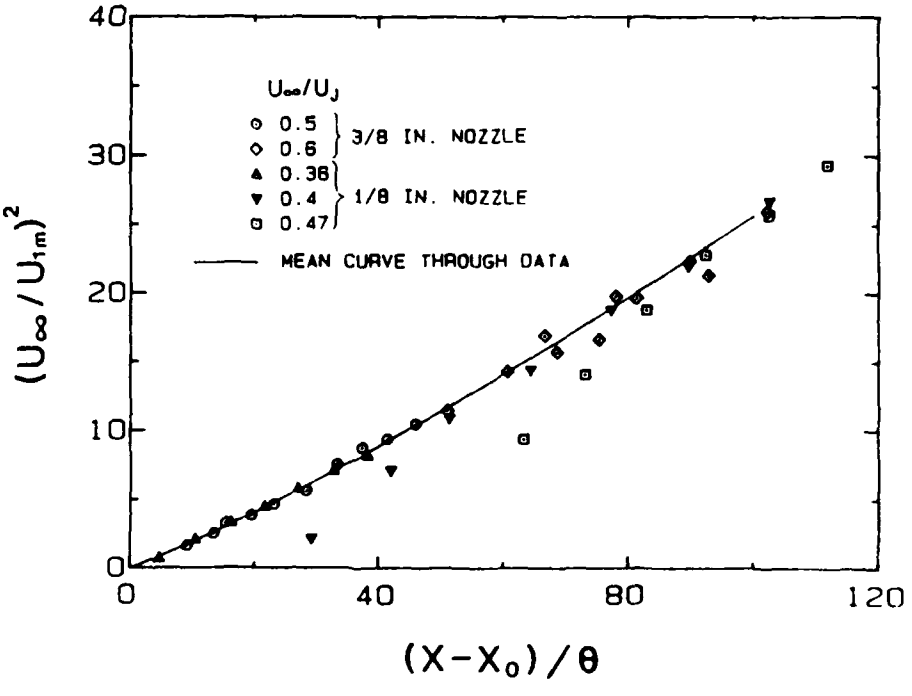

Fig. 3.4. Centerline velocity decay of plane co-flowing jets.

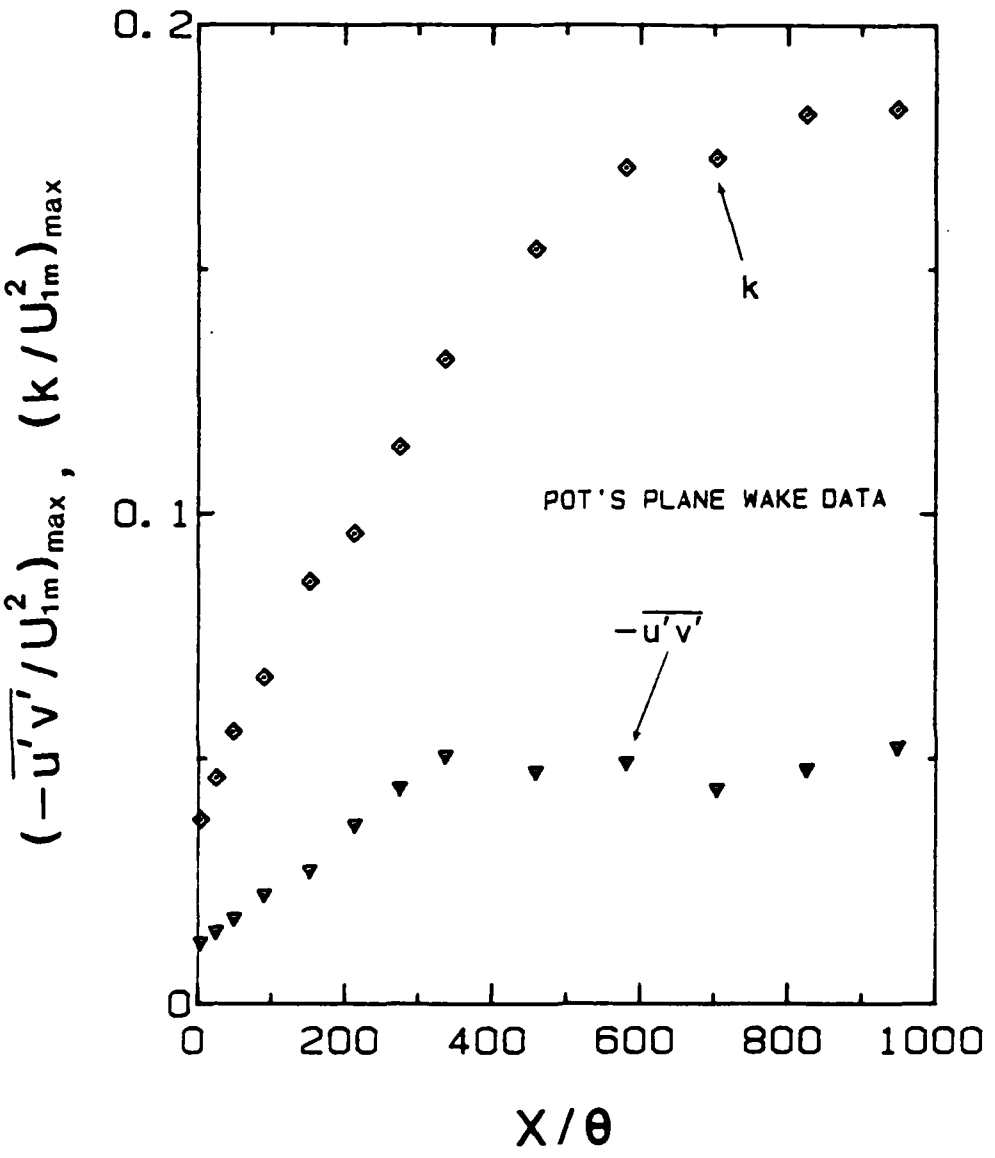

Fig. 3.5. Maximum shear stress and kinetic energy in a plane wake.

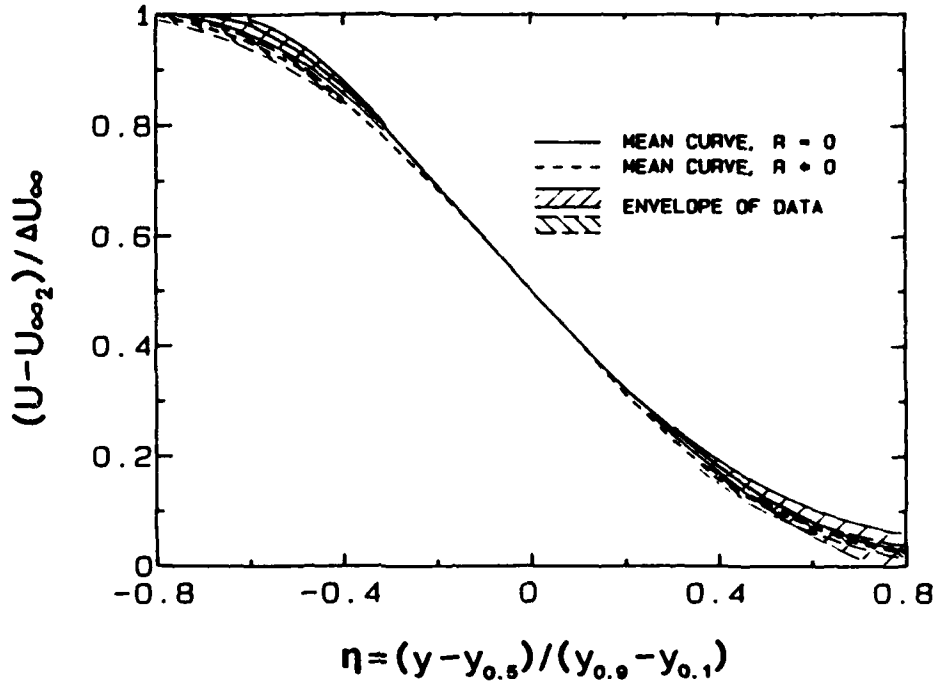

Fig. 3.6. Velocity profiles of mixing layers with zero and nonzero velocity ratios.

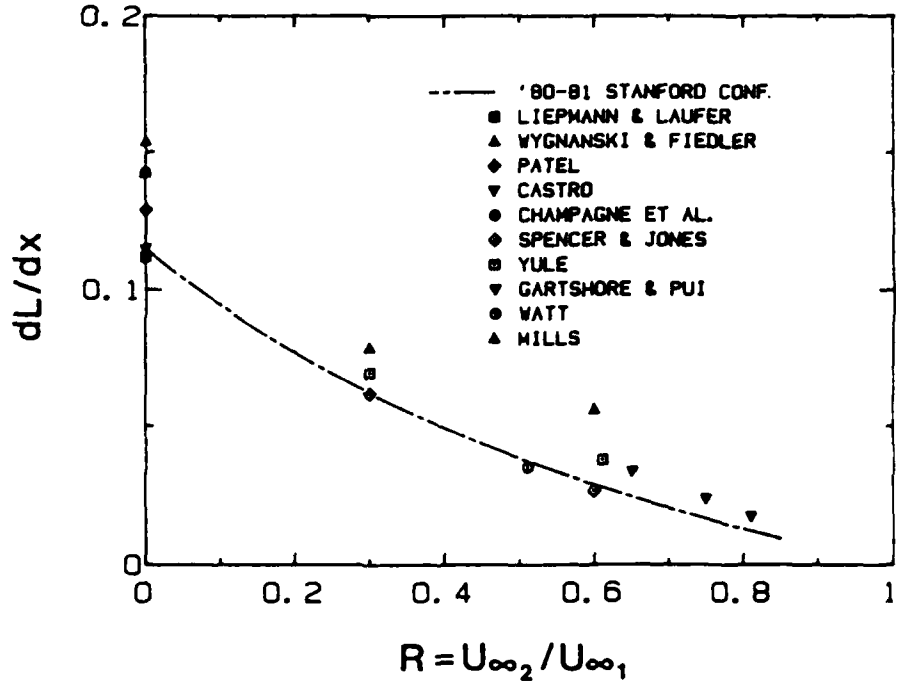

Fig. 3.7. Spreading rates of mixing layer flows.

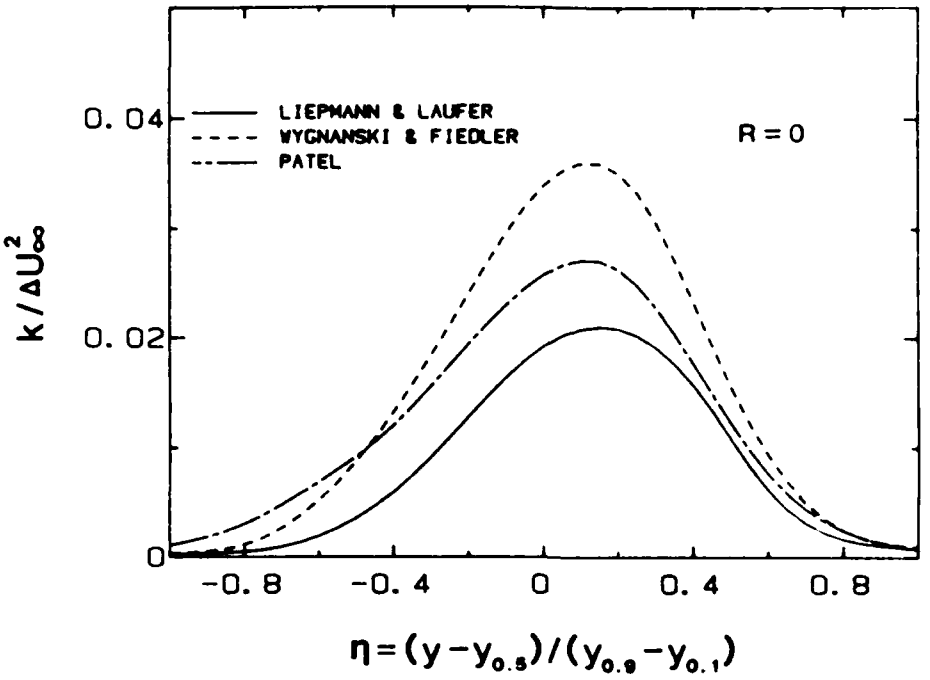

Fig. 3.8(a). Turbulent kinetic energy of mixing layers with zero velocity ratio.

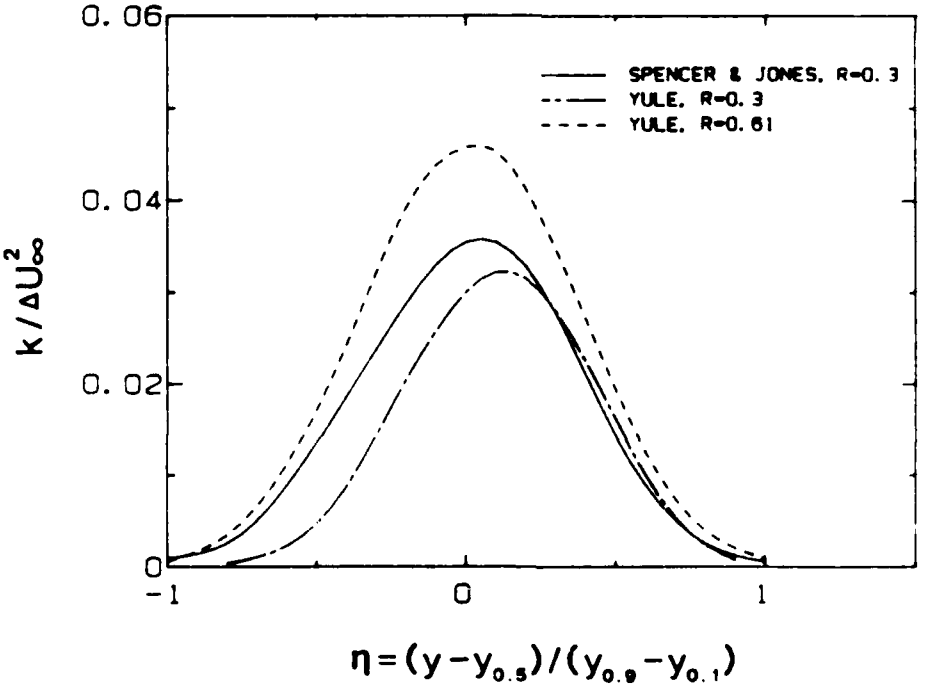

Fig. 3.8(b). Turbulent kinetic energy of mixing layers with two nonzero velocity ratios.

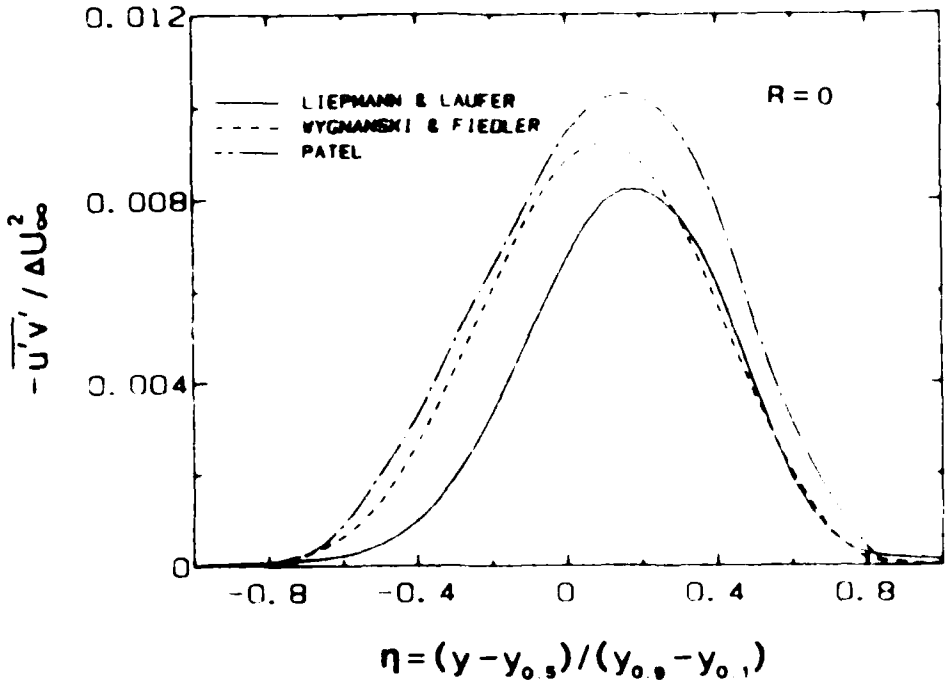

Fig. 3.9(a). Shear stress of mixing layers with zero velocity ratio.

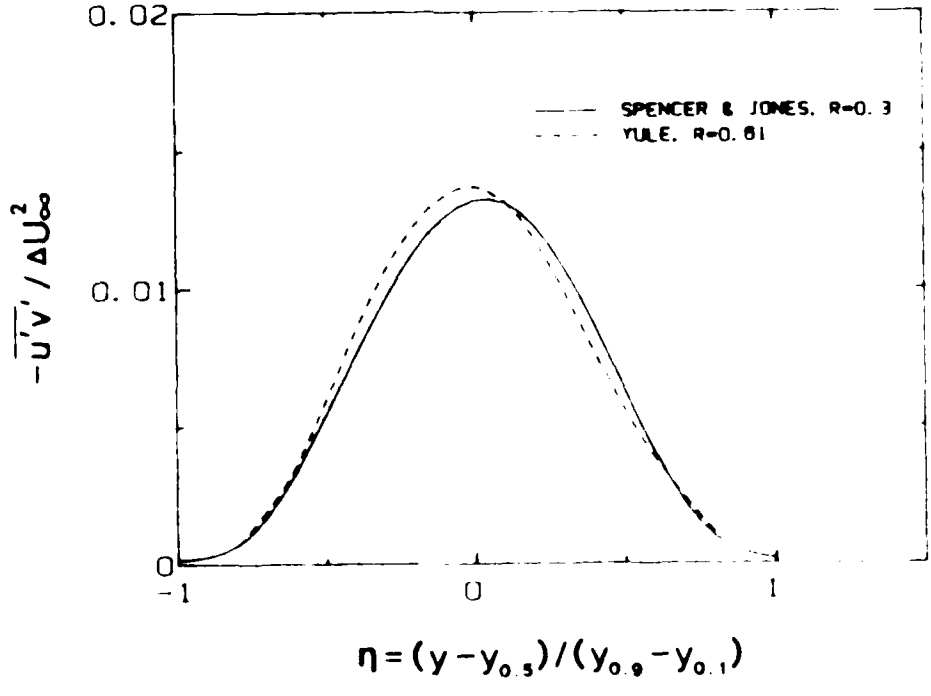

Fig. 3.9(b). Shear stress of mixing layers with two nonzero velocity ratios.

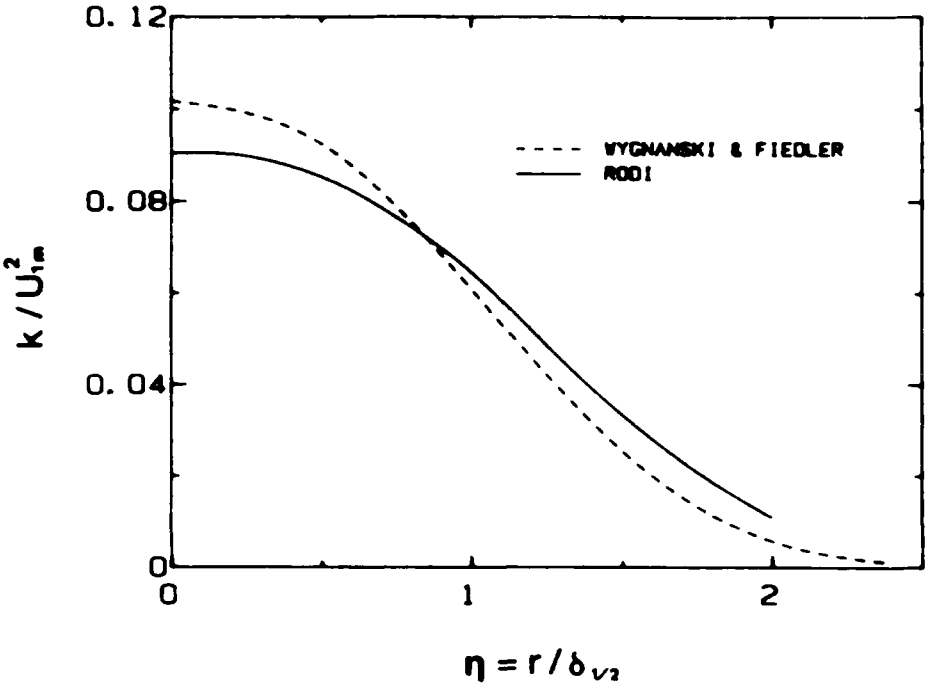

Fig. 3.10. Turbulent kinetic energy of axisymmetric pure jet.

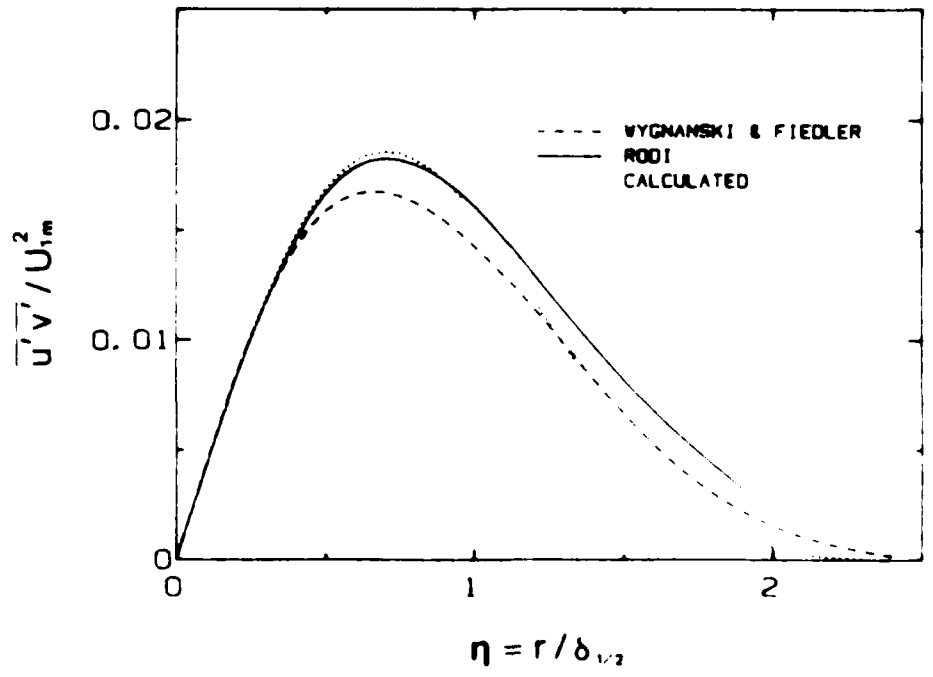

Fig. 3.11. Shear stress of axisymmetric pure jet.

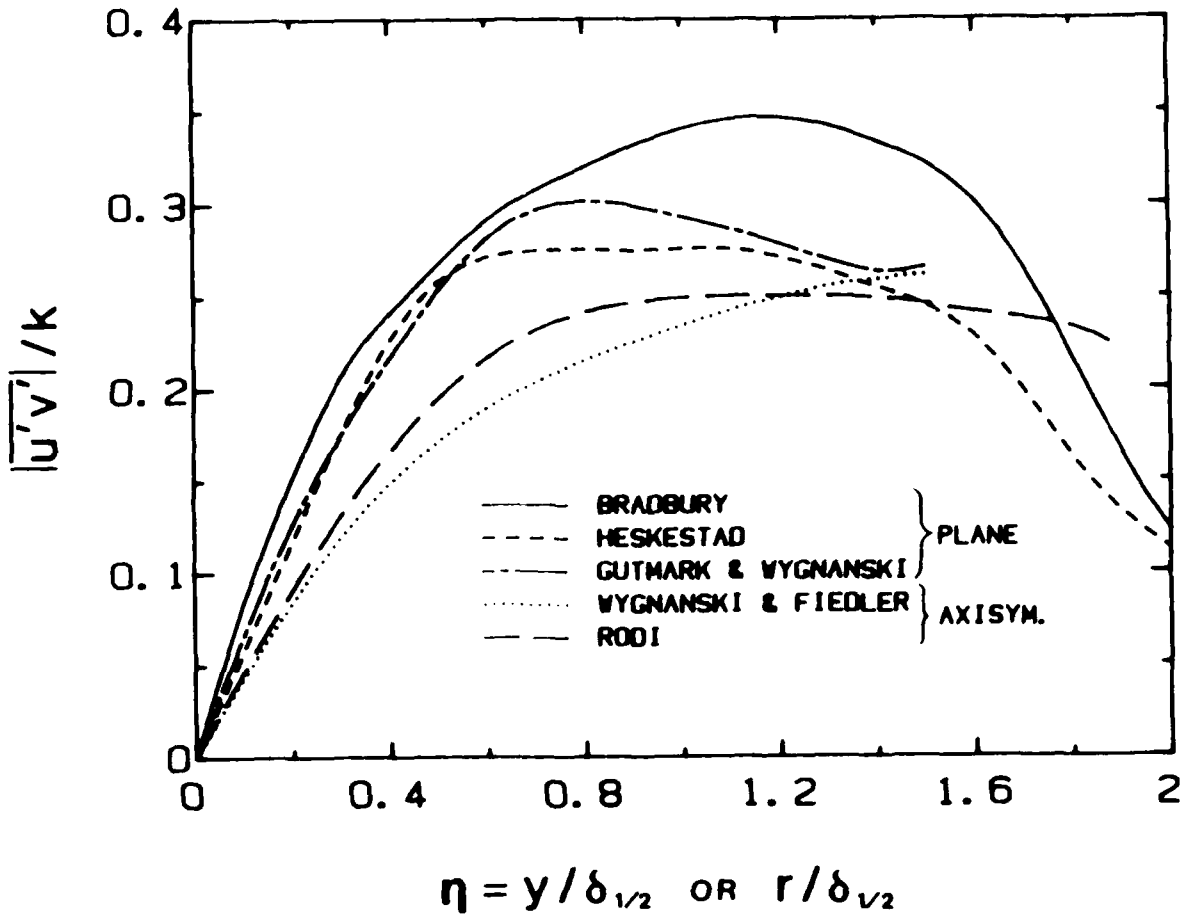

Fig. 3.12. Comparison of $|\overline{u'v'}|/K$ for plane and axisymmetric pure jet.

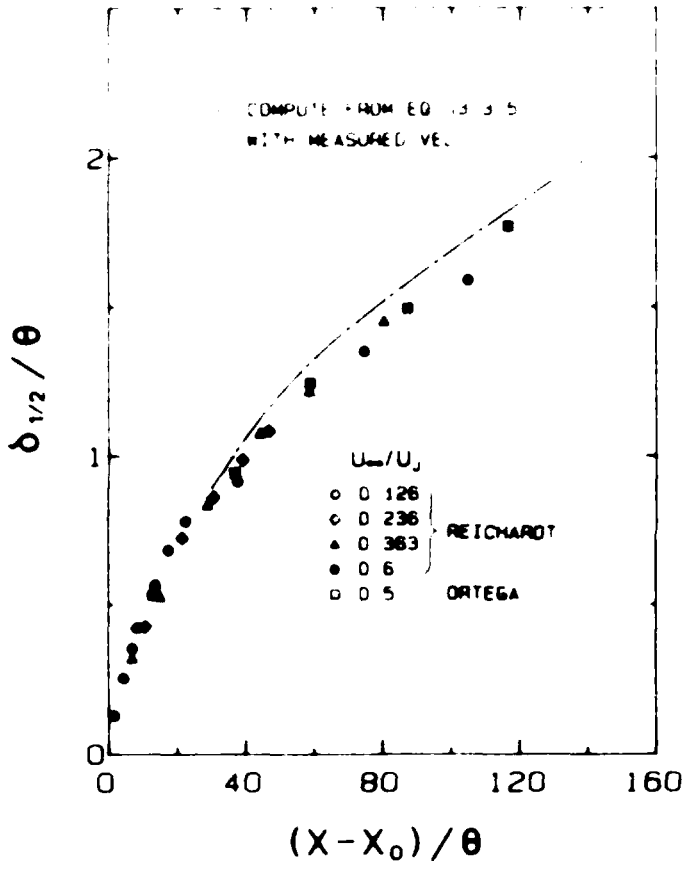

Fig. 3.13. Spreading rate of axisymmetric co-flowing jets.

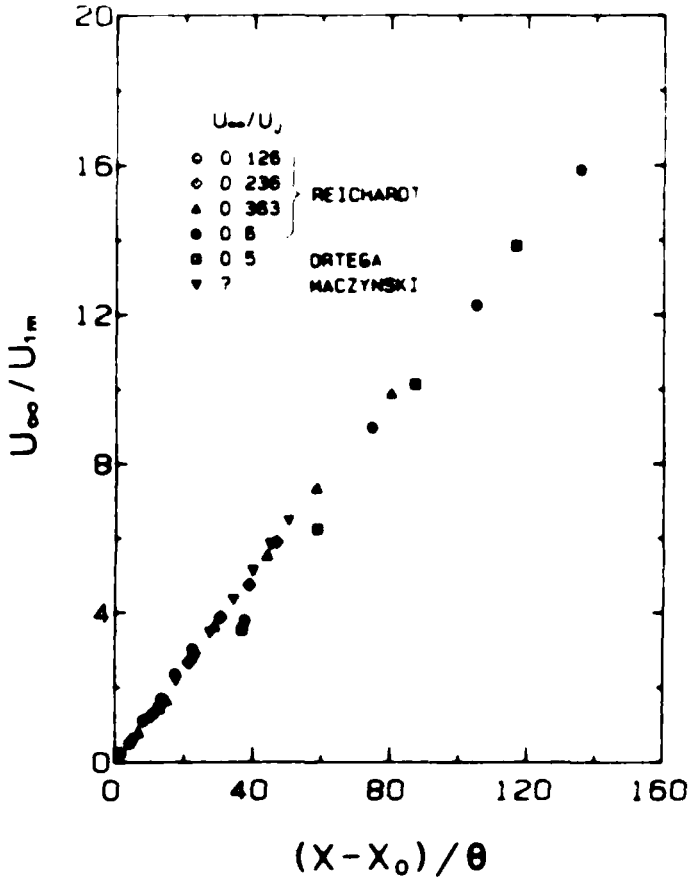

Fig. 3.14. Centerline velocity decay of axisymmetric co-flowing jets.

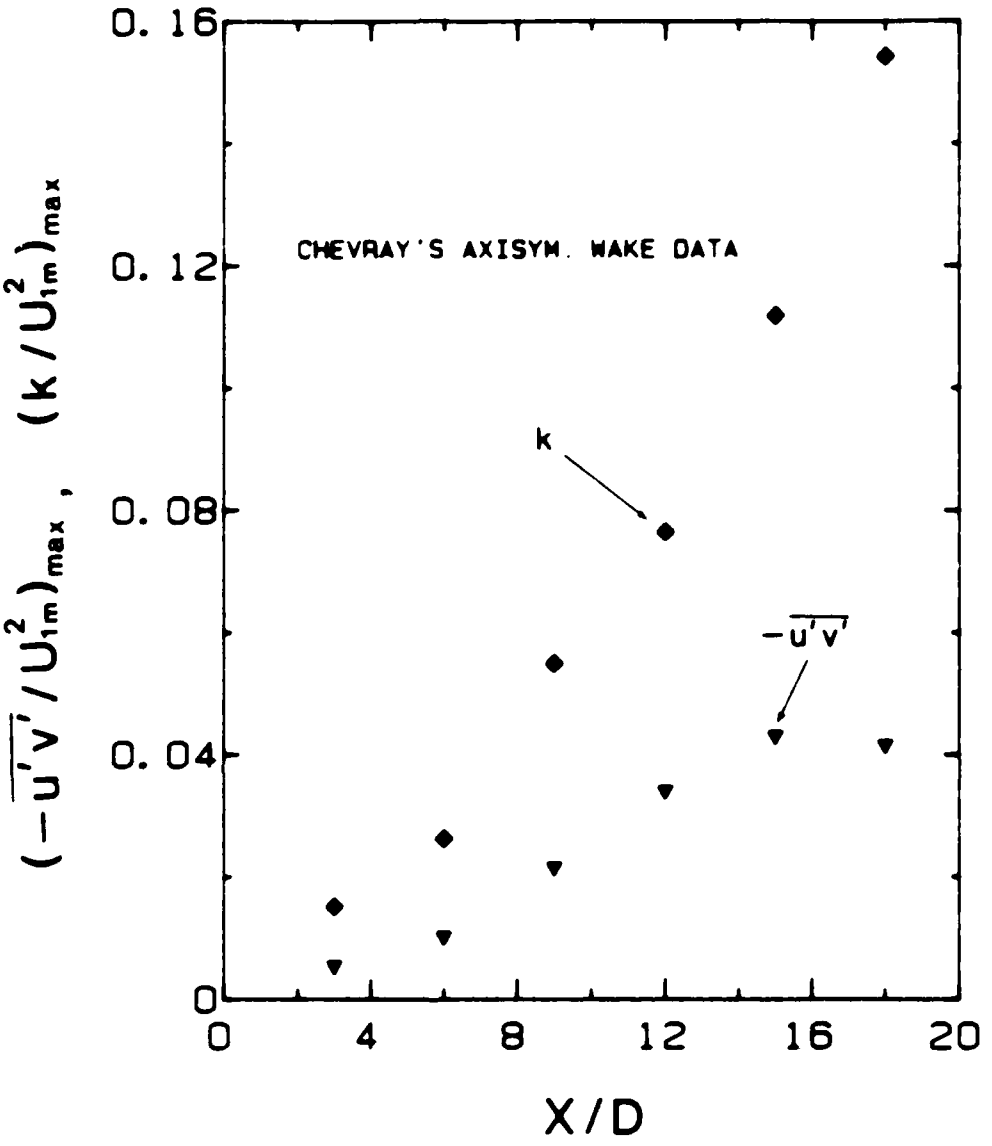

Fig. 3.15. Maximum shear stress and kinetic energy in an axisymmetric wake.

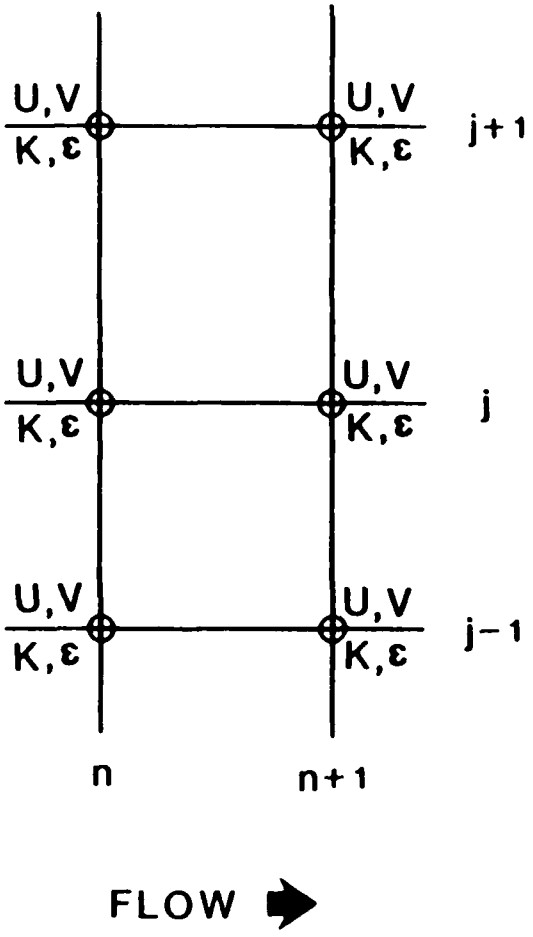

Fig. 4.1(a). Grid box used in Keller Box method.

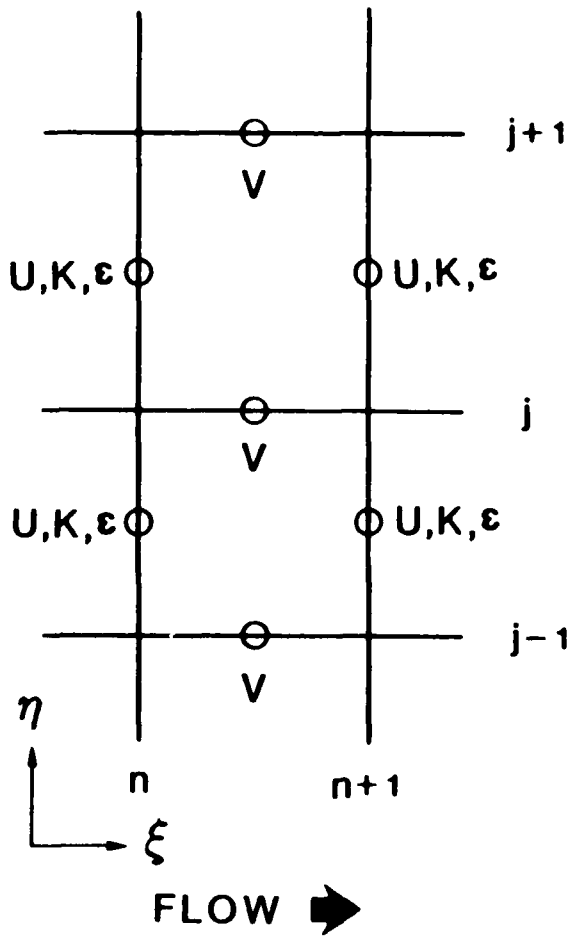

Fig. 4.1(b). Grid box used in the present scheme.

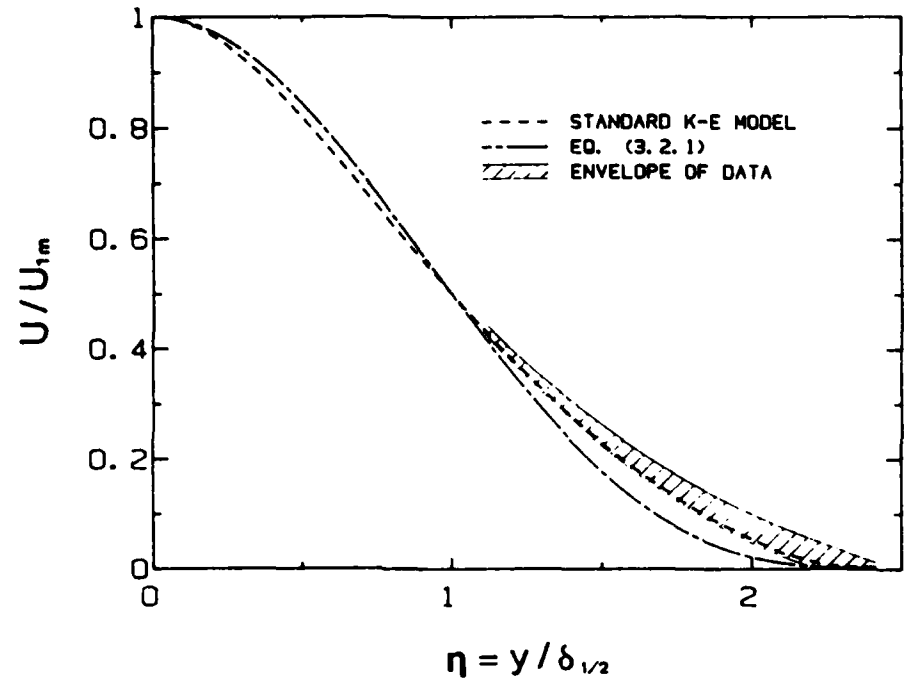

Fig. 5.1. Prediction of mean velocity for plane pure jet.

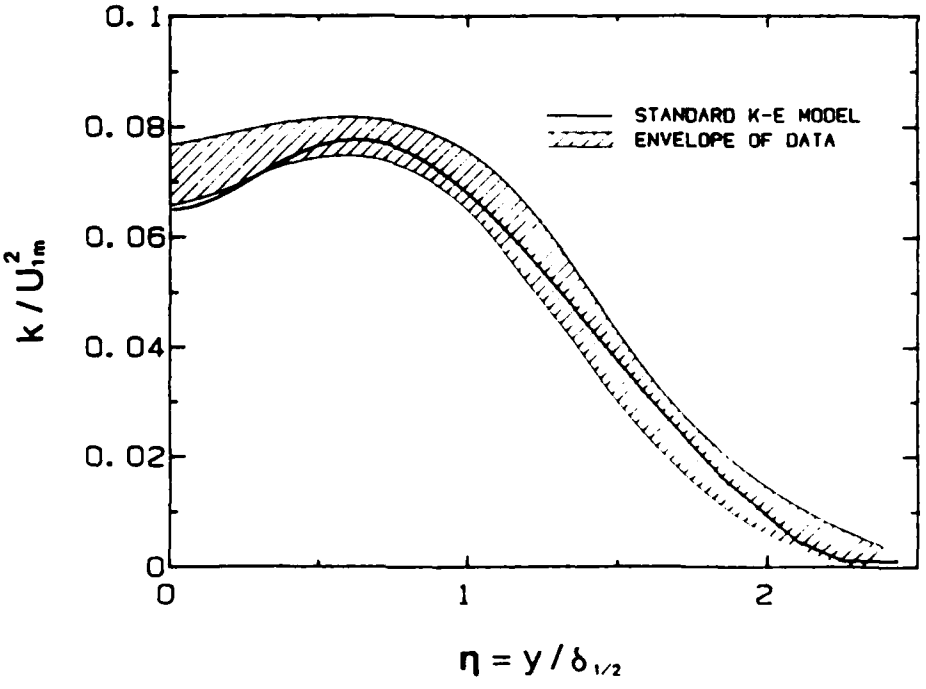

Fig. 5.2. Prediction of turbulent kinetic energy for plane pure jet.

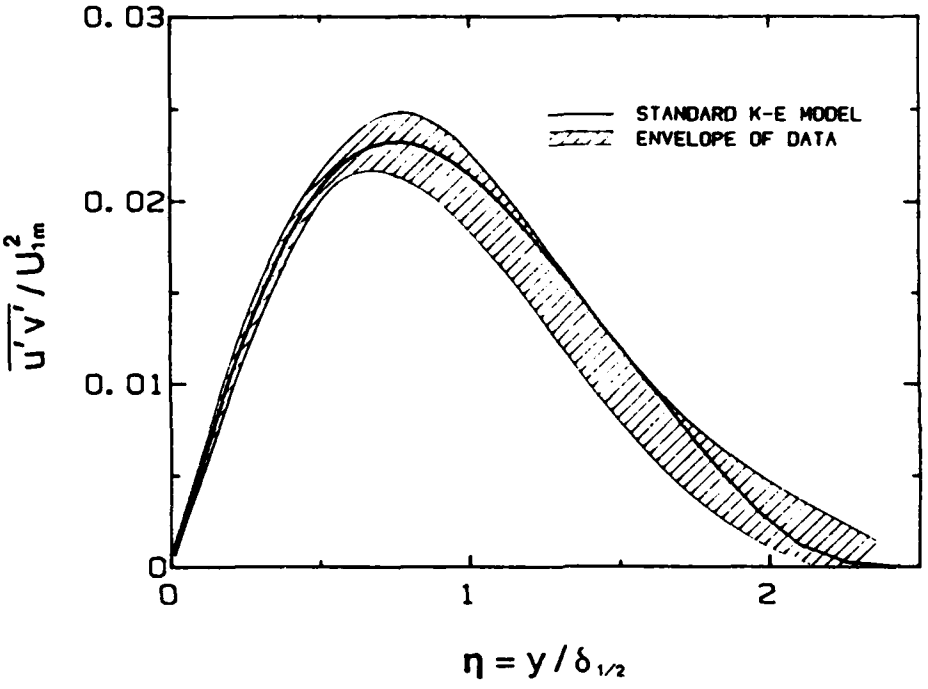

Fig. 5.3. Prediction of shear stress for plane pure jet.

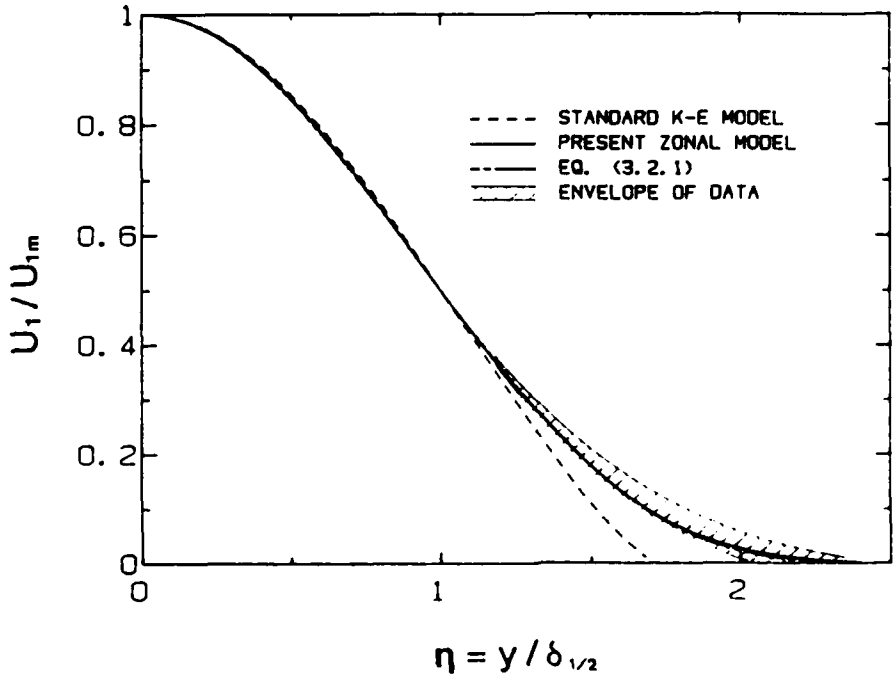

Fig. 5.4. Prediction of mean velocity for plane far-field wake.

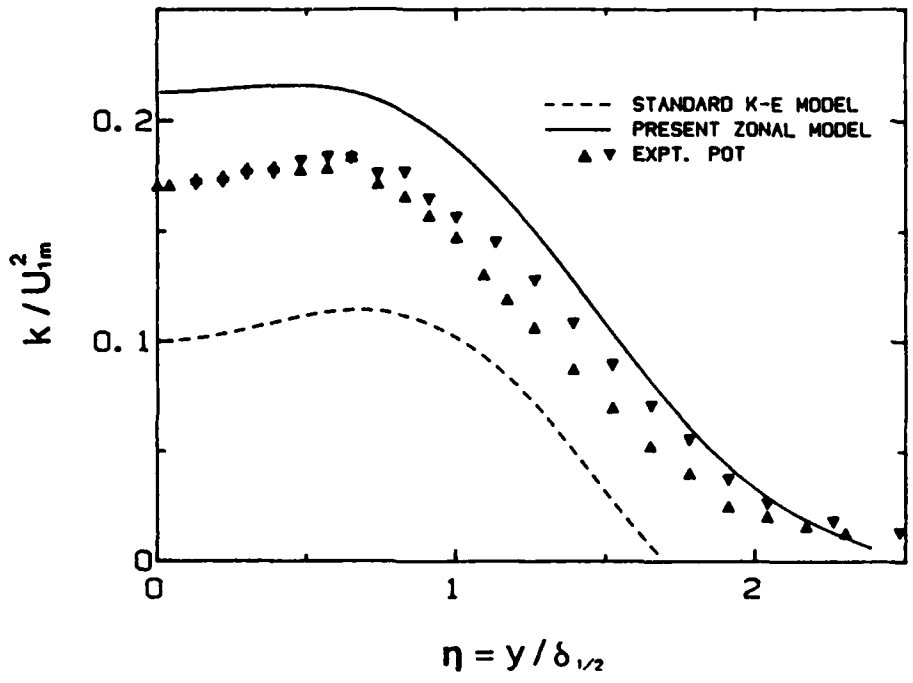

Fig. 5.5. Prediction of turbulent kinetic energy for plane far-field wake.

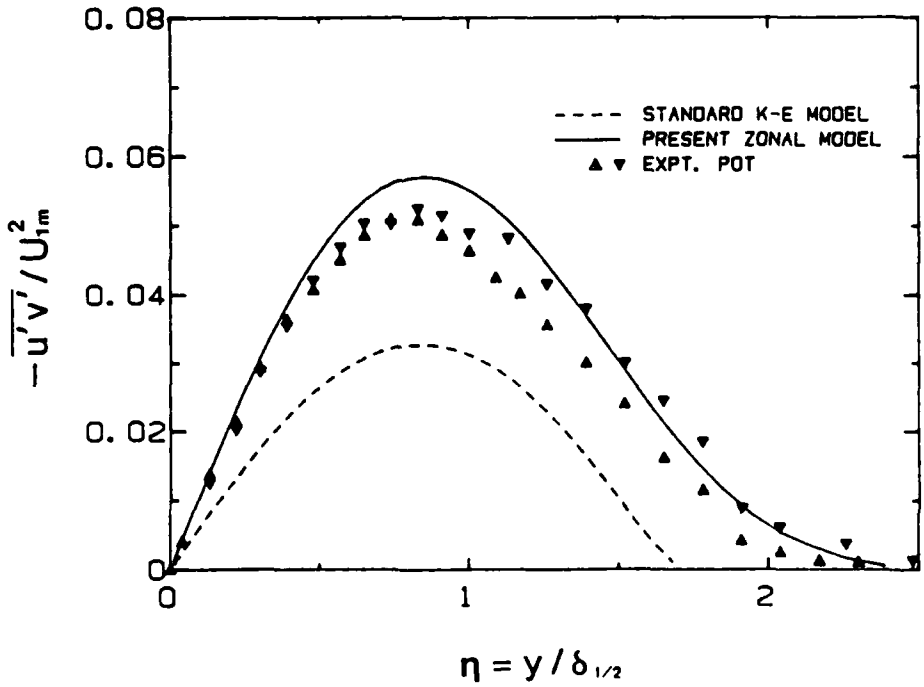

Fig. 5.6. Prediction of shear stress for plane far-field wake.

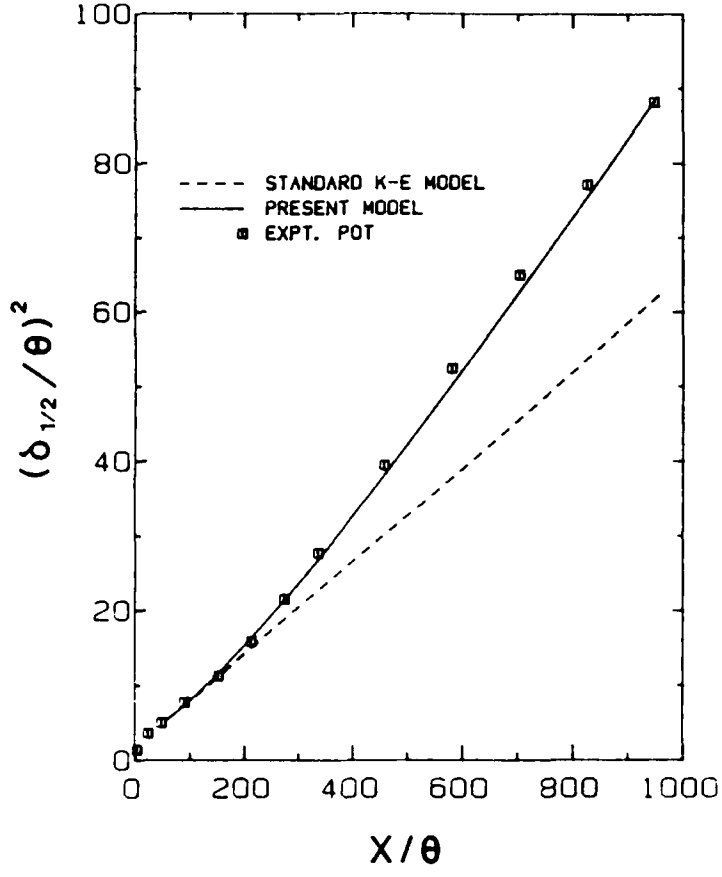

Fig. 5.7. Prediction of spreading rate for plane wake.

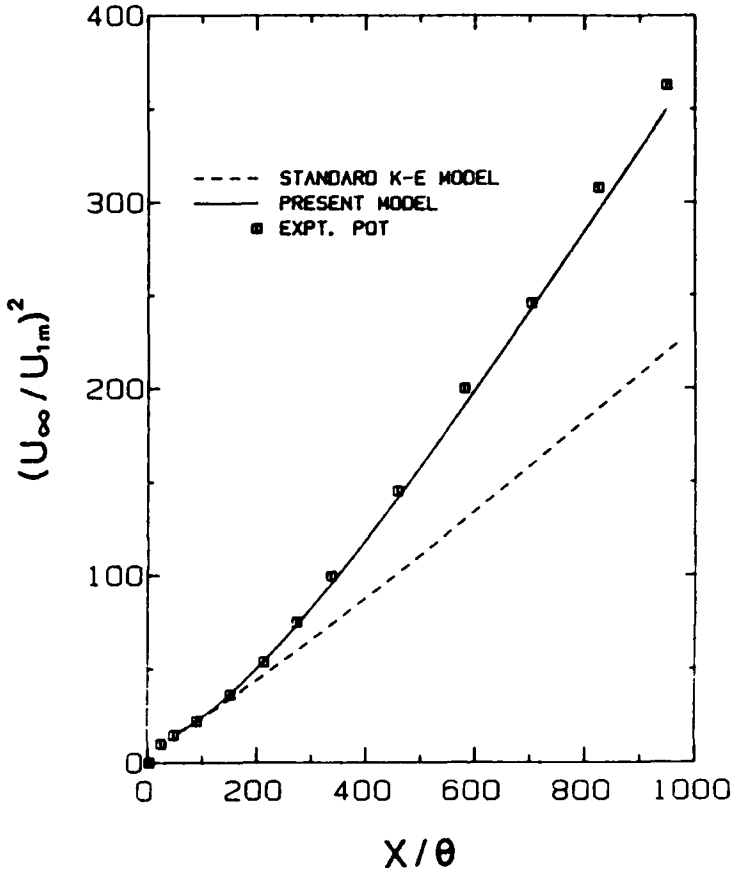

Fig. 5.8. Prediction of centerline-velocity-deficit decay for plane wake.

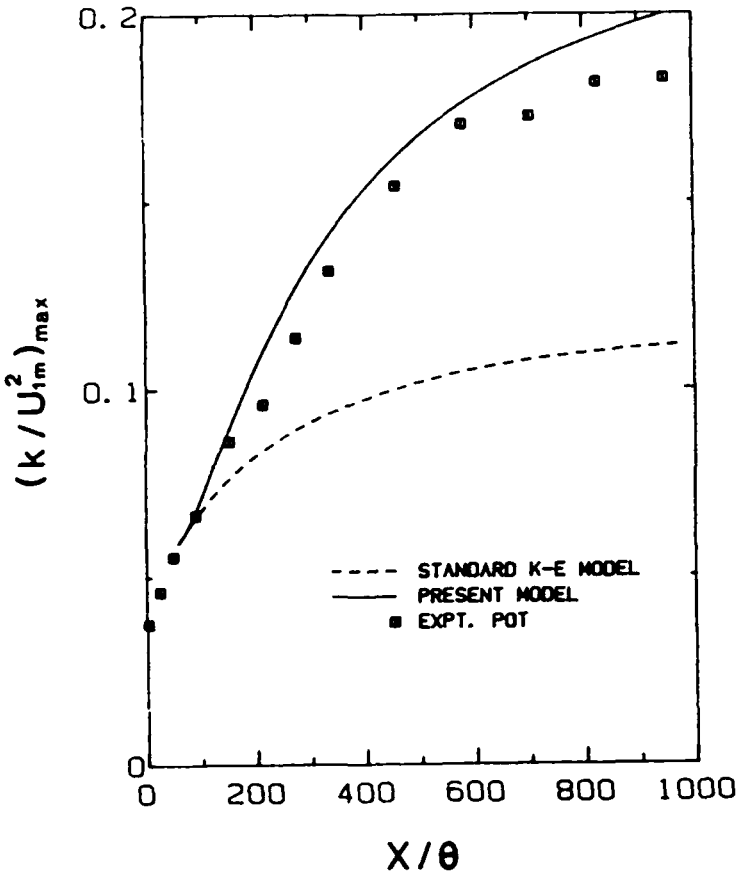

Fig. 5.9. Prediction of the maximum turbulent kinetic energy for plane wake.

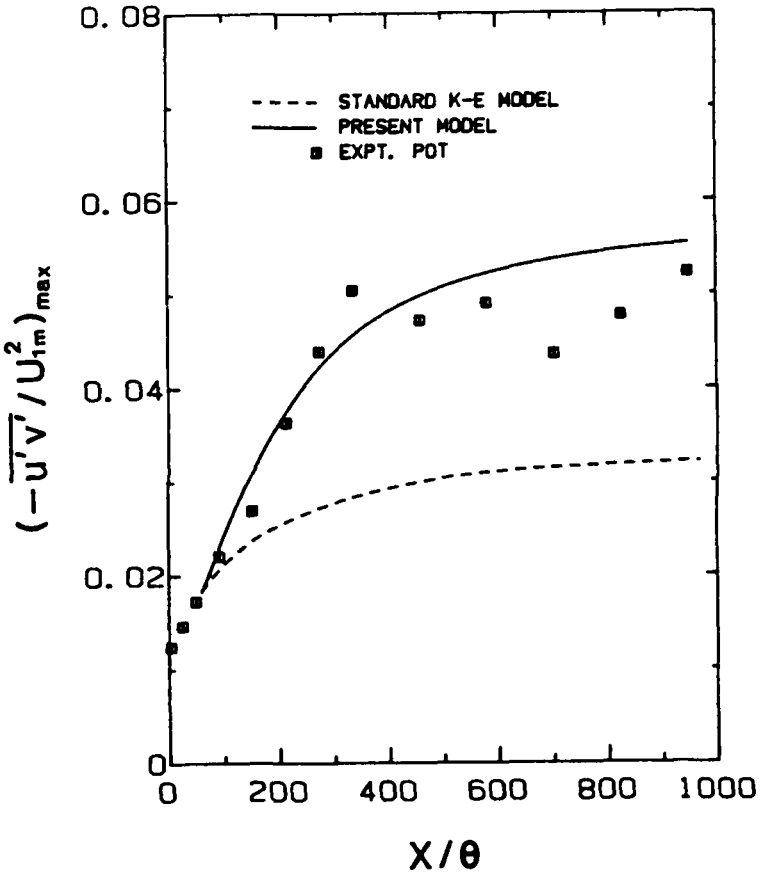

Fig. 5.10. Prediction of the maximum shear stress for plane wake.

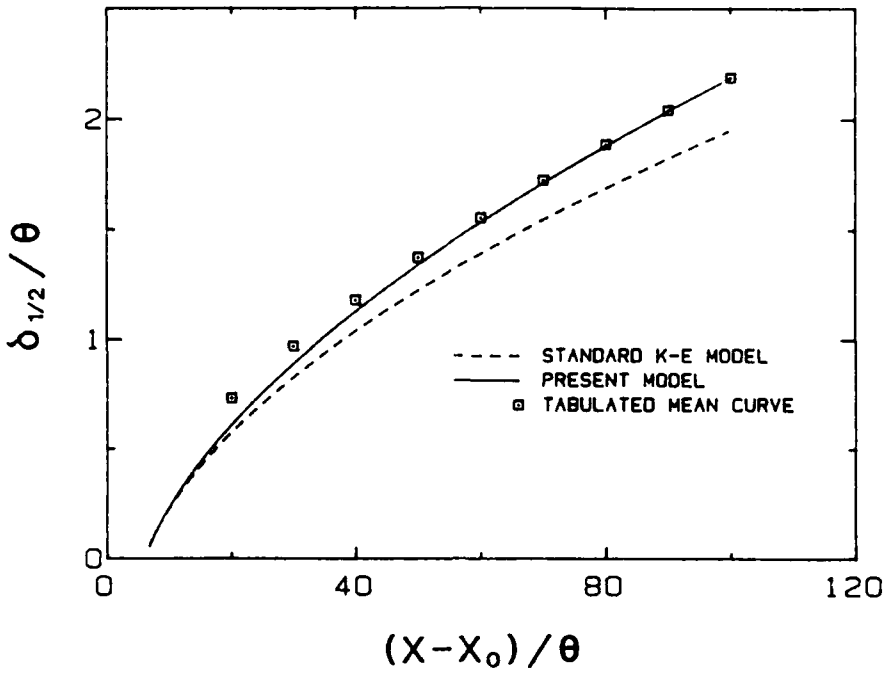

Fig. 5.11. Prediction of spreading rate for plane co-flowing jet.

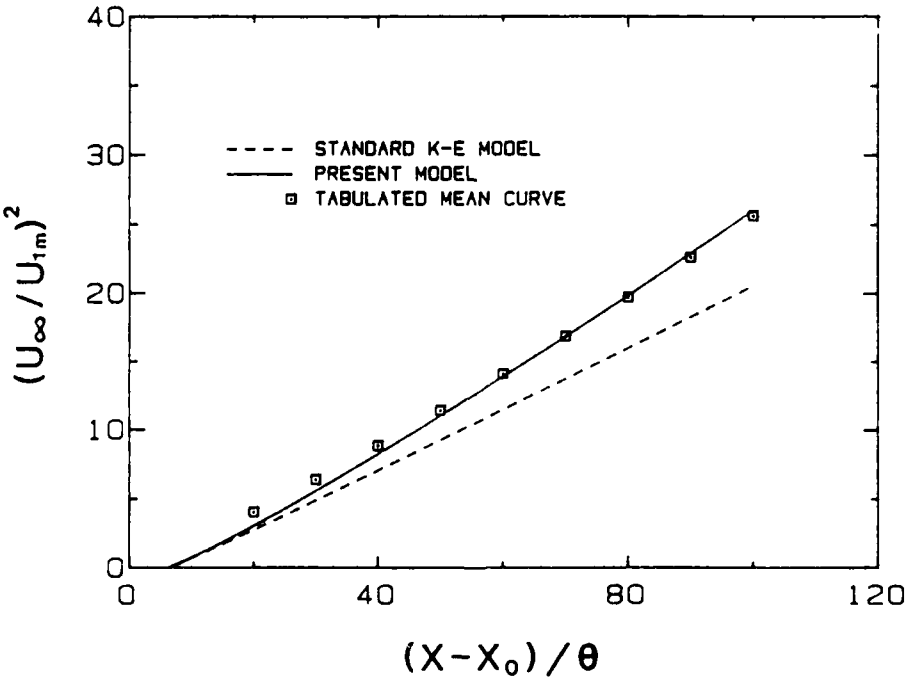

Fig. 5.12. Prediction of centerline-velocity decay for plane co-flowing jet.

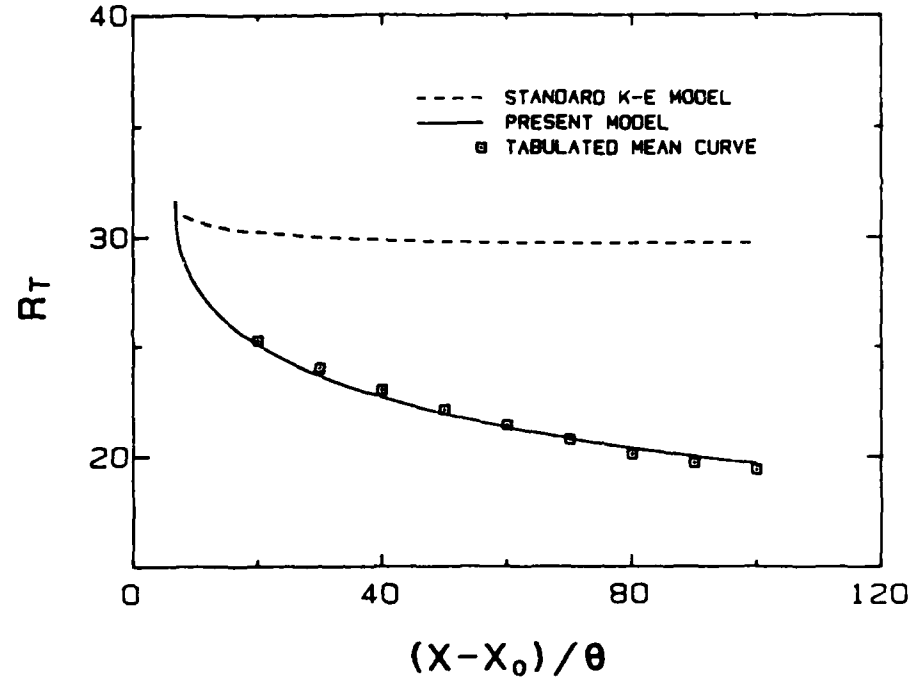

Fig. 5.13. Prediction of eddy Reynolds number for plane co-flowing jet.

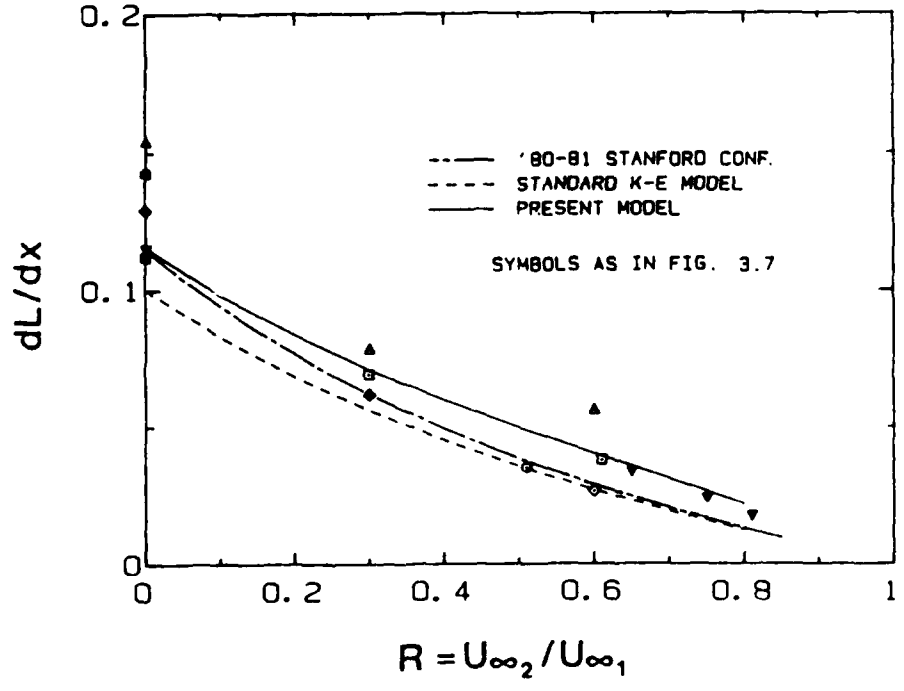

Fig. 5.14. Prediction of spreading rate for plane mixing layer.

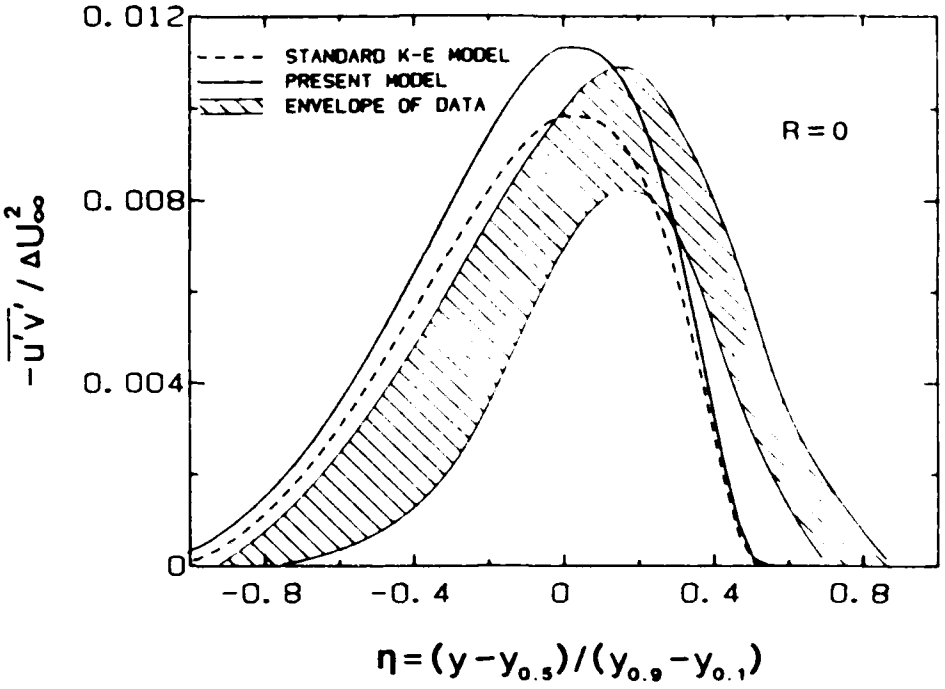

Fig. 5.15(a). Prediction of shear stress for plane mixing layer, R = 0.

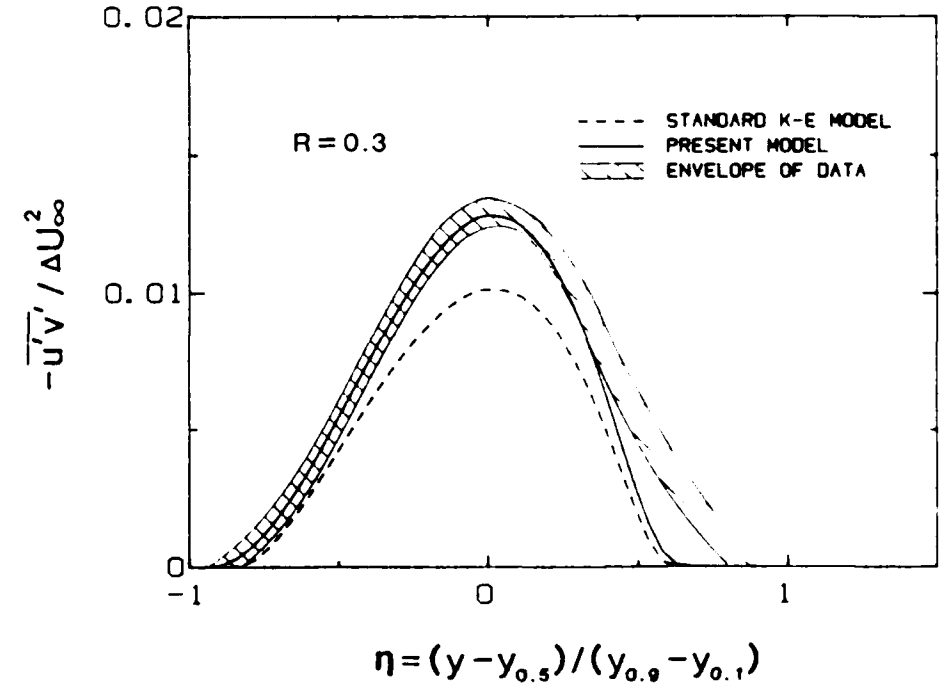

Fig. 5.15(b). Prediction of shear stress for plane mixing layer, R = 0.3.

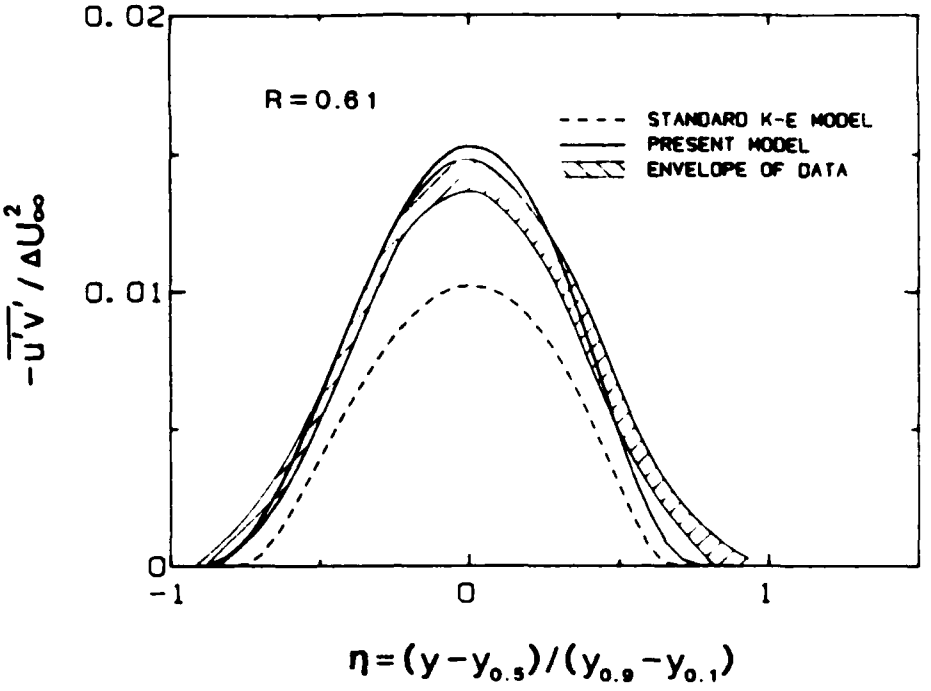

Fig. 5.15(c). Prediction of shear stress for plane mixing layer, R = 0.61.

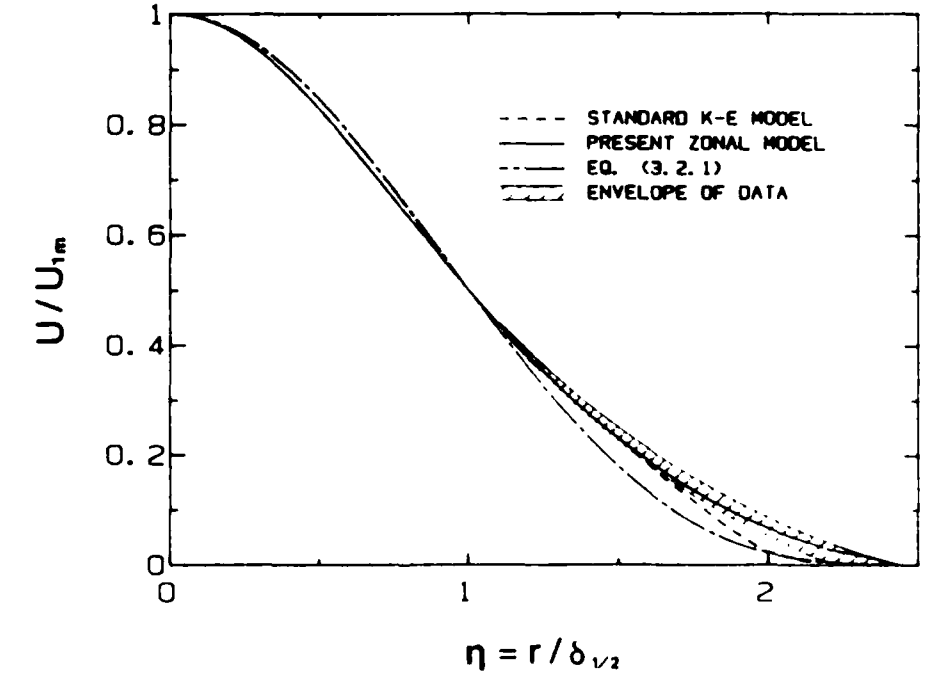

Fig. 6.1. Prediction of mean velocity for axisymmetric pure jet.

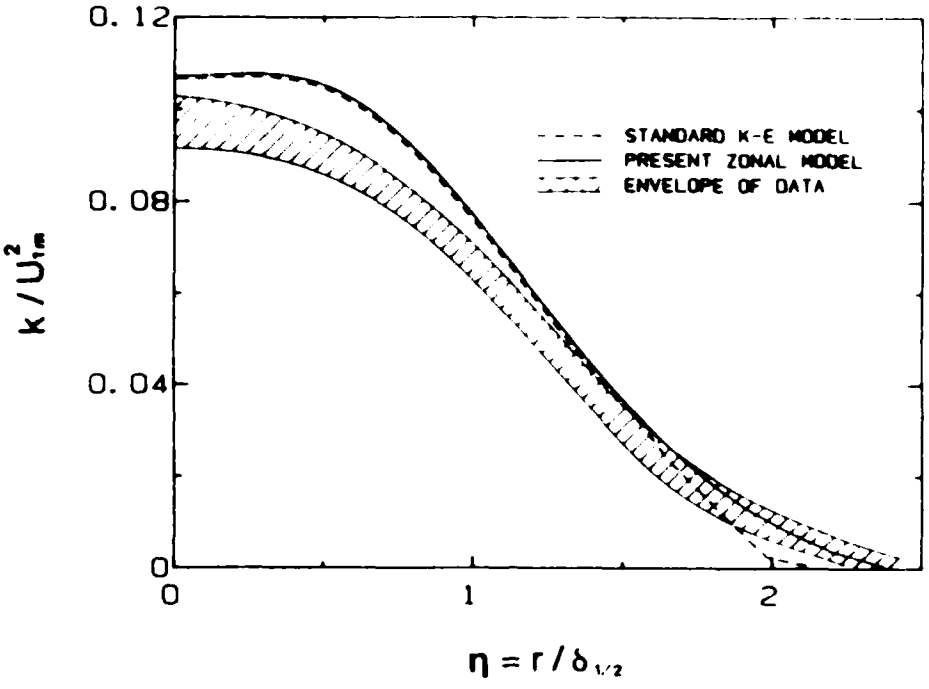

Fig. 6.2. Prediction of turbulent kinetic energy for axisymmetric pure jet.

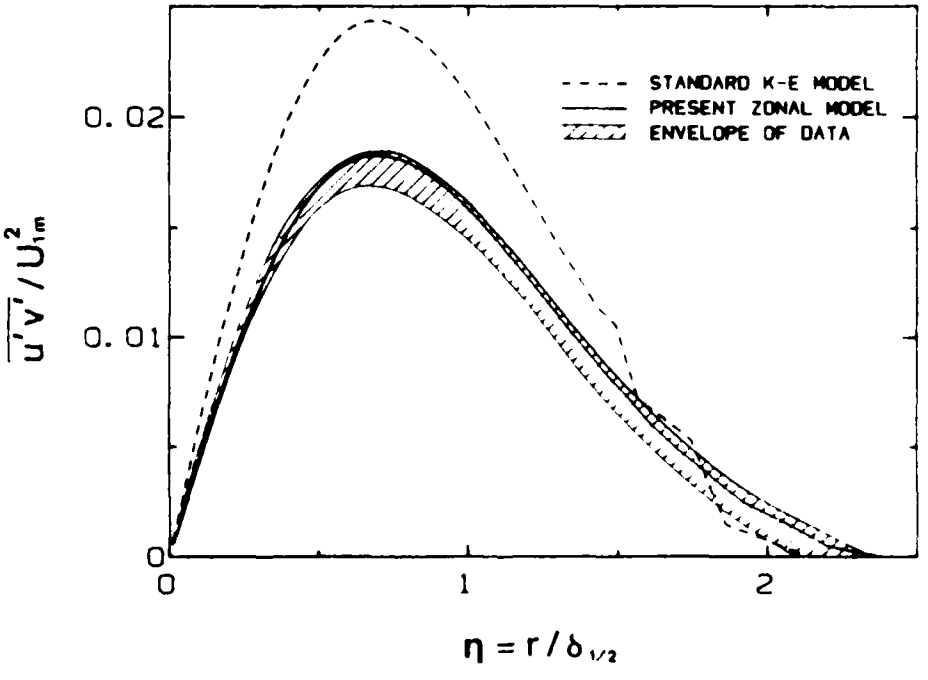

Fig. 6.3. Prediction of shear stress for axisymmetric pure jet.

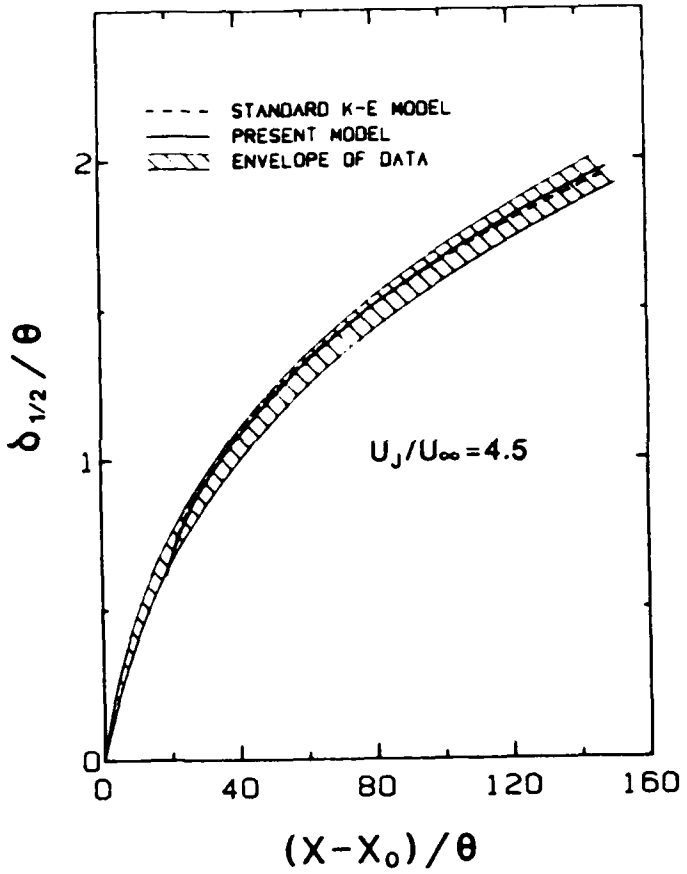

Fig. 6.4. Prediction of spreading rate for axisymmetric co-flowing jet.

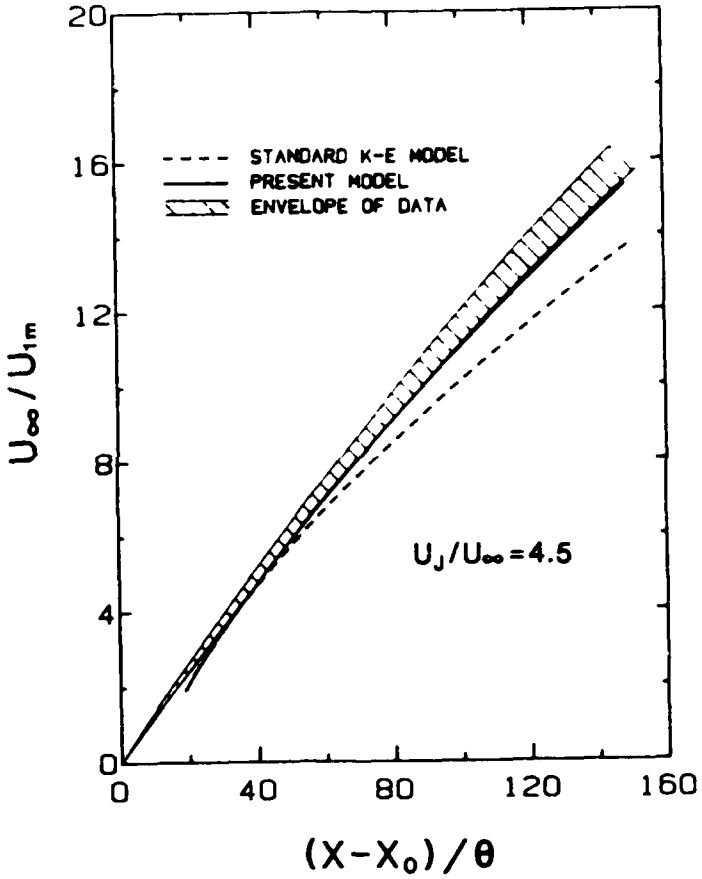

Fig. 6.5. Prediction of centerline-velocity decay for axisymmetric co-flowing jet.

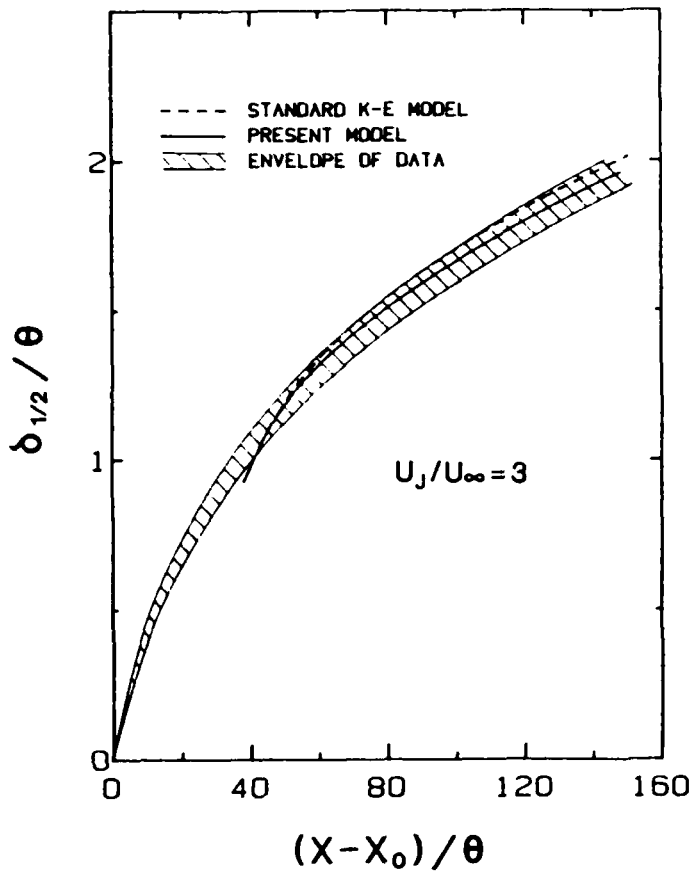

Fig. 6.6. Prediction of spreading rate for axisymmetric co-flowing jet.

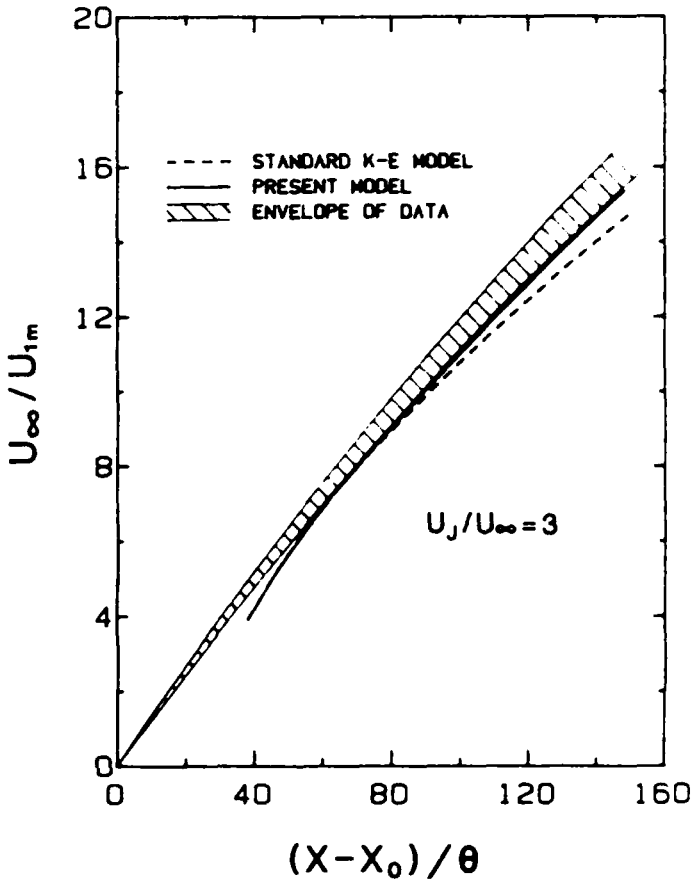

Fig. 6.7. Prediction of centerline-velocity decay for axisymmetric co-flowing jet.

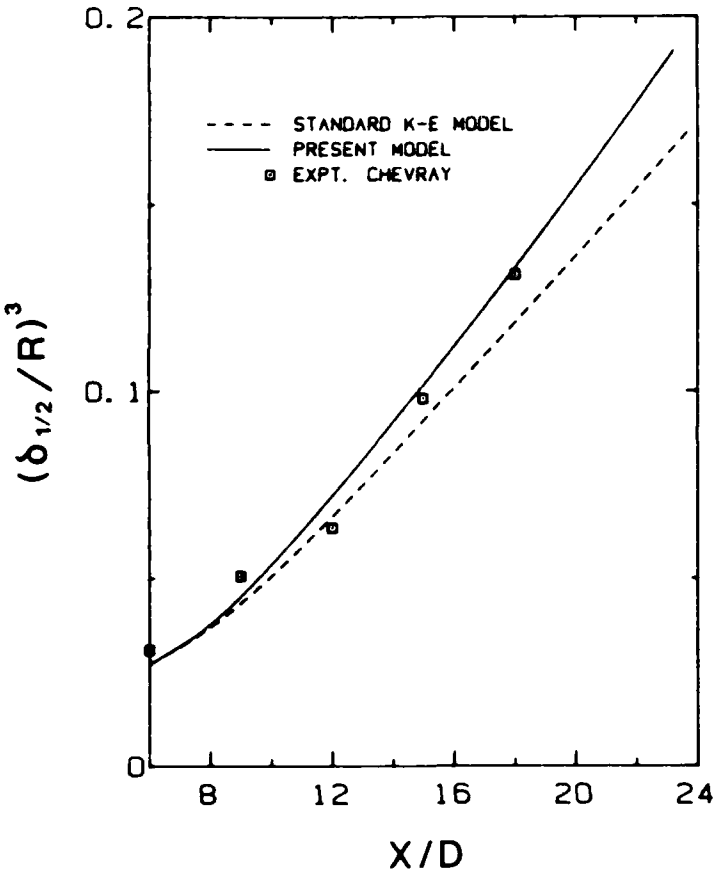

Fig. 6.8. Prediction of spreading rate for axisymmetric wake.

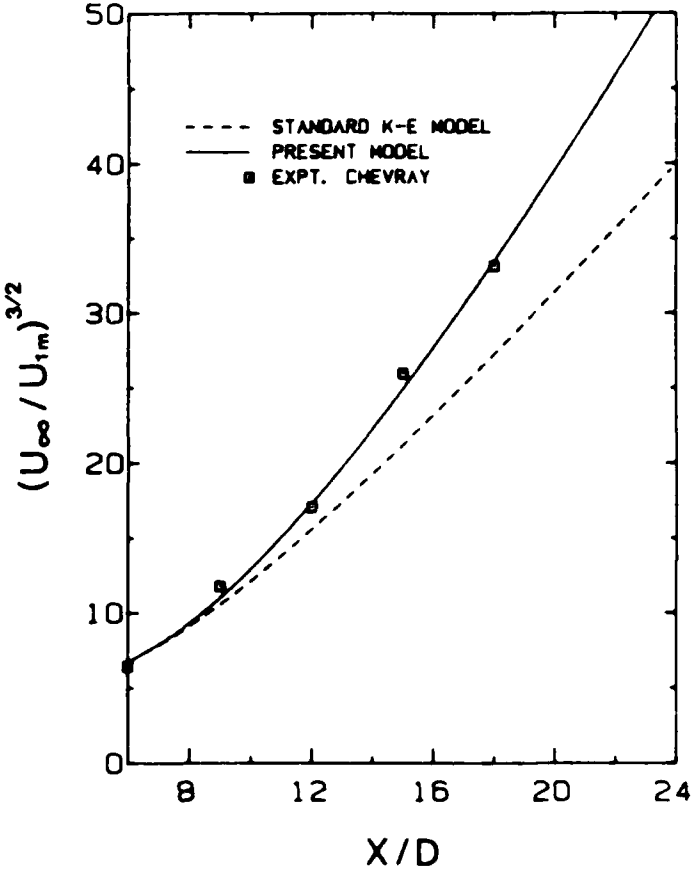

Fig. 6.9. Prediction of centerline-velocity-deficit decay for axisymmetric wake.

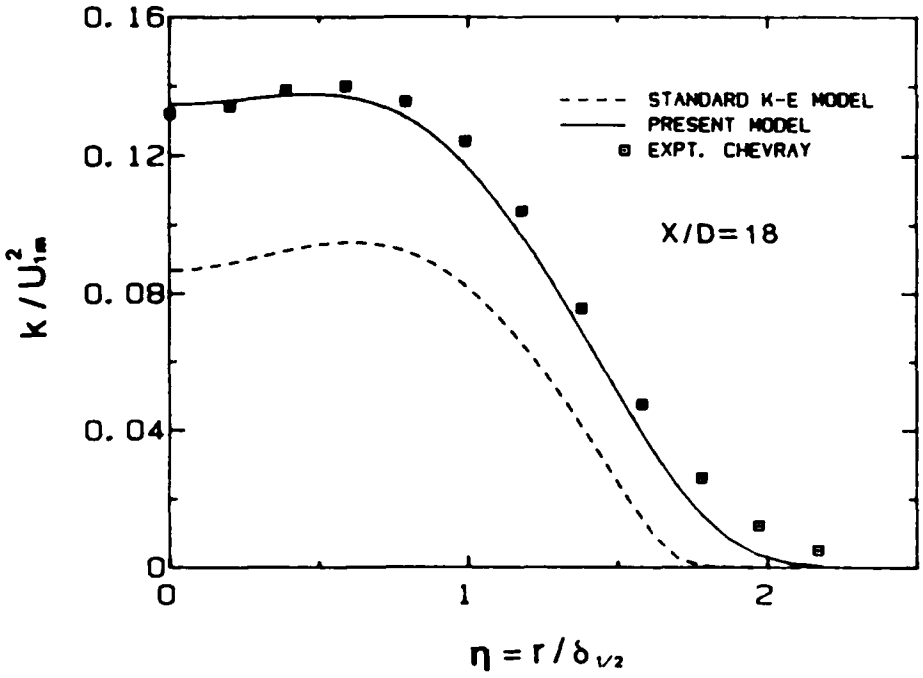

Fig. 6.10. Prediction of turbulent kinetic energy for axisymmetric wake.

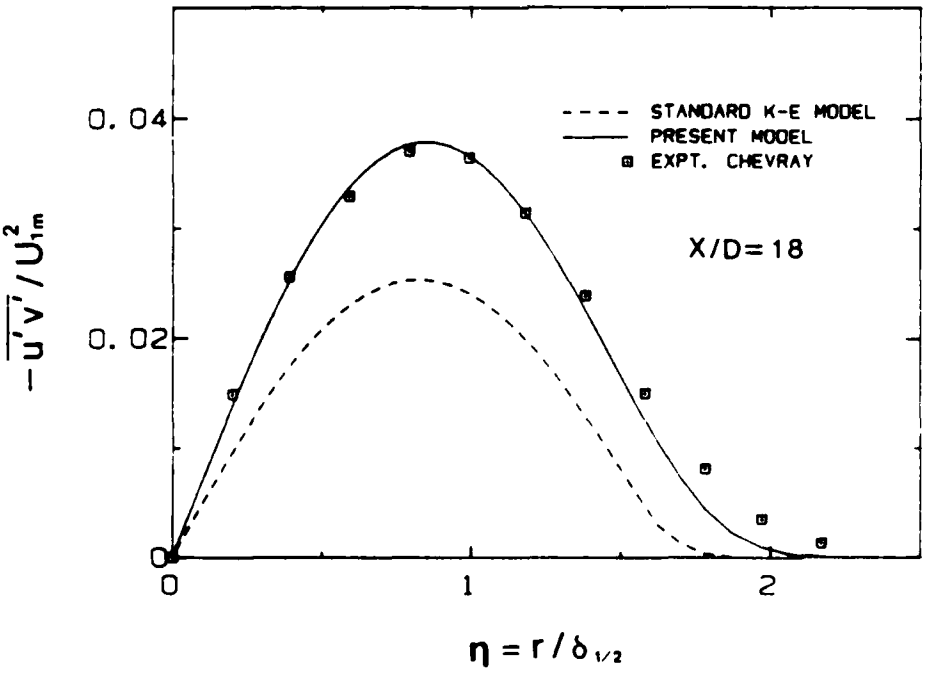

Fig. 6.11. Prediction of shear stress for axisymmetric wake.

Appendix A

FORMULATION OF FINITE DIFFERENCE EQUATIONS

In this appendix, the finite difference equations for the governing equations, Eqs. (4.2.3) to (4.2.6) are formulated. We first write the governing equations in terms of a first-order system of PDEs. For this purpose we introduce three new dependent variables, $T(\xi,\eta)$, $Q(\xi,\eta)$, and $W(\xi,\eta)$, so that Eqs. (4.2.3) to (4.2.6) can be written as:

$$\frac{\partial U}{\partial \xi} - \frac{\eta}{E}\frac{dE}{dx}T + \frac{1}{E\eta^i}\frac{\partial}{\partial \eta}\left(\eta^i V\right) = 0 \tag{A.1}$$

$$U\frac{\partial U}{\partial \xi} - U\frac{\eta}{E}\frac{dE}{dx}T + \frac{V}{E}T = \frac{1}{E^2\eta^i}\left\{T\left[\eta^i\frac{\partial \nu_t}{\partial \eta} + i\left(\nu+\nu_t\right)\right] + \eta^i\left(\nu+\nu_t\right)\frac{\partial T}{\partial \eta}\right\} \tag{A.2}$$

$$U\frac{\partial K}{\partial \xi} - U\frac{\eta}{E}\frac{dE}{dx}Q + \frac{V}{E}Q = \nu_t\frac{T^2}{E^2} - \varepsilon + \frac{1}{E^2\eta^i\sigma_k}\left[Q\left(\eta^i\frac{\partial \nu_t}{\partial \eta} + i\nu_t\right) + \eta^i\nu_t\frac{\partial Q}{\partial \eta}\right] \tag{A.3}$$

$$U\frac{\partial \varepsilon}{\partial \xi} - U\frac{\eta}{E}\frac{dE}{dx}W + \frac{V}{E}W = C_{\varepsilon_1}\frac{\varepsilon}{K}\nu_t\frac{T^2}{E^2} - C_{\varepsilon_2}\frac{\varepsilon^2}{K} + \frac{1}{E^2\eta^i\sigma_\varepsilon}\left[W\left(\eta^i\frac{\partial \nu_t}{\partial \eta} + i\nu_t\right) + \eta^i\nu_t\frac{\partial W}{\partial \eta}\right] \tag{A.4}$$

$$T = \frac{\partial U}{\partial \eta} \tag{A.5}$$

$$Q = \frac{\partial K}{\partial \eta} \tag{A.6}$$

$$W = \frac{\partial \varepsilon}{\partial \eta} \tag{A.7}$$

Recall from Chapter IV that $i = 0$ for plane flows and $i = 1$ for axisymmetric flows.

We now consider the grid box shown in Fig. 4.1(b). We denote grid points and spacings by

$$\xi^0 = \text{starting x-location}, \quad \xi^{n+1} = \xi^n + \Delta\xi_n, \quad n = 0, 1, 2, \ldots \tag{A.8}$$

$$\eta_o = 0; \quad \eta_{j+1} = \eta_j + \Delta\eta_j; \quad j = 0, 1, \ldots, J; \quad \eta_J \equiv \eta_\infty \tag{A.9}$$

and approximate the quantities $(U,V,K,\varepsilon,T,Q,W)$ at point (ξ^n,η_j) by $(U_j^n, V_j^n, K_j^n, \varepsilon_j^n, T_j^n, Q_j^n, W_j^n)$. We also define the following midway quantities:

$$\xi^{n+1/2} \equiv \frac{1}{2}\left(\xi^n + \xi^{n+1}\right), \qquad \eta_{j+1/2} \equiv \left(\eta_j + \eta_{j+1}\right) \tag{A.10}$$

We approximate Eqs. (A.1) to (A.4) at the center of each grid box and Eqs. (A.5) to (A.7) at midpoint $(\xi^{n+1},\eta_{j+1/2})$. Keeping all the known quantities (solutions at $\xi = \xi_n$) on the right-hand sides, we have

$$2E_{n+1/2}\Delta\eta_j\left(\eta_{j+1/2}\right)^i U_{j+1/2}^{n+1} - \Delta\xi_n\Delta\eta_j\left(\eta_{j+1/2}\right)^i \eta_{j+1/2} \left.\frac{dE}{dx}\right|_{n+1/2} T_{j+1/2}^{n+1}$$
$$+ 2\Delta\xi_n\left[\left(\eta_{j+1}\right)^i V_{j+1}^{n+1/2} - \left(\eta_j\right)^i V_j^{n+1/2}\right] = Rl_{j+1/2}^n \tag{A.11}$$

$$- \Delta\xi_n E_{n+1/2}(\eta_{j+1/2})^i \; \eta_{j+1/2} \left.\frac{dE}{dx}\right|_{n+1/2} \Big[T^{n+1}_{j+1/2} \; (U^n_{j+1/2} + U^{n+1}_{j+1/2})$$

$$+ T^n_{j+1/2} U^{n+1}_{j+1/2} \Big] + \Delta\xi_n E_{n+1/2}(\eta_{j+1/2})^i \; (V^{n+1/2}_j + V^{n+1/2}_{j+1})(T^n_{j+1/2} + T^{n+1}_{j+1/2})$$

$$- \Delta\xi_n \Bigg\{ T^{n+1}_{j+1/2} \Big[(\eta_{j+1/2})^i \left(\left.\frac{\partial \nu_t}{\partial \eta}\right|^{n+1}_{j+1/2} + \left.\frac{\partial \nu_t}{\partial \eta}\right|^{n}_{j+1/2} \right)$$

$$+ i(2\nu + \nu^n_{t_{j+1/2}} + \nu^{n+1}_{t_{j+1/2}}) \Big] + T^n_{j+1/2} \Big[(\eta_{j+1/2})^i \left.\frac{\partial \nu_t}{\partial \eta}\right|^{n+1}_{j+1/2} + i\nu^{n+1}_{t_{j+1/2}} \Big] \Bigg\}$$

$$+ 2(E_{n+1/2})^2 \; (\eta_{j+1/2})^i \; (U^{n+1}_{j+1/2})^2 - 2\Delta\xi_n (\eta_{j+1/2})^i \; M_{j+1/2} \Big[\nu^{n+1}_{t_{j+1/2}} \cdot$$

$$\cdot \; (T^{n+1}_{j+1} - T^{n+1}_j + T^n_{j+1} - T^n_j) + (2\nu + \nu^n_{t_{j+1/2}}) \; (T^{n+1}_{j+1} - T^{n+1}_j) \Big] = R2^n_{j+1/2} \qquad \text{(A.12)}$$

$$4(E_{n+1/2})^2(\eta_{j+1/2})^i\left[K^{n+1}_{j+1/2}(U^{n+1}_{j+1/2}+U^n_{j+1/2})-K^n_{j+1/2}U^{n+1}_{j+1/2}\right]$$

$$-2\Delta\xi_n E_{n+1/2}(\eta_{j+1/2})^i\,\eta_{j+1/2}\left.\frac{dE}{dx}\right|_{n+1/2}\left[Q^{n+1}_{j+1/2}(U^n_{j+1/2}+U^{n+1}_{j+1/2})\right.$$

$$\left.+Q^n_{j+1/2}U^{n+1}_{j+1/2}\right]+2\Delta\xi_n E_{n+1/2}(\eta_{j+1/2})^i\,(V^{n+1/2}_j+V^{n+1/2}_{j+1})(Q^n_{j+1/2}+Q^{n+1}_{j+1/2})$$

$$-\Delta\xi_n(\eta_{j+1/2})^i\left[\nu^{n+1}_{t_{j+1/2}}(T^n_{j+1/2}+T^{n+1}_{j+1/2})^2+\nu^n_{t_{j+1/2}}(T^{n+1}_{j+1/2})^2\right.$$

$$\left.+2\nu^n_{t_{j+1/2}}T^{n+1}_{j+1/2}T^n_{j+1/2}\right]+4\Delta\xi_n(E_{n+1/2})^2(\eta_{j+1/2})^i\,\varepsilon^{n+1}_{j+1/2}$$

$$-2(\Delta\xi_n/\sigma_k)\left\{(Q^n_{j+1/2}+Q^{n+1}_{j+1/2})\left[(\eta_{j+1/2})^i\left.\frac{\partial\nu_t}{\partial\eta}\right|^{n+1}_{j+1/2}+i\nu^{n+1}_{t_{j+1/2}}\right]\right.$$

$$\left.+Q^{n+1}_{j+1/2}\left[(\eta_{j+1/2})^i\left.\frac{\Delta\nu_t}{\partial\eta}\right|^{n}_{j+1/2}+i\nu^{n}_{t_{j+1/2}}\right]\right\}-4(\Delta\xi_n/\sigma_k)(\eta_{j+1/2})^i\,M_{j+1/2}\cdot$$

$$\cdot\left[\nu^{n+1}_{t_{j+1/2}}(Q^{n+1}_{j+1}-Q^{n+1}_j+Q^n_{j+1}-Q^n_j)+\nu^n_{t_{j+1/2}}(Q^{n+1}_{j+1}-Q^{n+1}_j)\right]=R3^n_{j+1/2}$$

(A.13)

$$8(E_{n+1/2})^2(\eta_{j+1/2})^i\left[\varepsilon^{n+1}_{j+1/2}(U^{n+1}_{j+1/2}+U^{n}_{j+1/2})-\varepsilon^{n}_{j+1/2}U^{n+1}_{j+1/2}\right]$$

$$-4\Delta\xi_n E_{n+1/2}(\eta_{j+1/2})^i\,\eta_{j+1/2}\left.\frac{dE}{dx}\right|_{n+1/2}\left[W^{n+1}_{j+1/2}(U^{n}_{j+1/2}+U^{n+1}_{j+1/2})\right.$$

$$\left.+W^{n}_{j+1/2}U^{n+1}_{j+1/2}\right]+4\Delta\xi_n E_{n+1/2}(\eta_{j+1/2})^i(V^{n+1/2}_{j}+V^{n+1/2}_{j+1})(W^{n}_{j+1/2}+W^{n+1}_{j+1/2})$$

$$-\Delta\xi_n(\eta_{j+1/2})^i\,C_{\varepsilon_1}\left[Z^{n}_{j+1/2}\nu^{n}_{t_{j+1/2}}(T^{n+1}_{j+1/2})^2+2Z^{n}_{j+1/2}\nu^{n}_{t_{j+1/2}}T^{n}_{j+1/2}T^{n+1}_{j+1/2}\right.$$

$$\left.+(Z^{n+1}_{j+1/2}\nu^{n+1}_{t_{j+1/2}}+Z^{n}_{j+1/2}\nu^{n+1}_{t_{j+1/2}}+Z^{n+1}_{j+1/2}\nu^{n}_{t_{j+1/2}})(T^{n}_{j+1/2}+T^{n+1}_{j+1/2})^2\right]$$

$$+4\Delta\xi_n(E_{n+1/2})^2(\eta_{j+1/2})^i\,C_{\varepsilon_2}\left[Z^{n+1}_{j+1/2}(\varepsilon^{n+1}_{j+1/2}+\varepsilon^{n}_{j+1/2})+Z^{n}_{j+1/2}\varepsilon^{n+1}_{j+1/2}\right]$$

$$-4(\Delta\xi_n/\sigma_\varepsilon)\left\{(W^{n}_{j+1/2}+W^{n+1}_{j+1/2})\left[(\eta_{j+1/2})^i\left.\frac{\partial\nu_t}{\partial\eta}\right|^{n+1}_{j+1/2}+i\nu^{n+1}_{t_{j+1/2}}\right]\right.$$

$$\left.+W^{n+1}_{j+1/2}\left[(\eta_{j+1/2})^i\left.\frac{\partial\nu_t}{\partial\eta}\right|^{n}_{j+1/2}+i\nu^{n}_{t_{j+1/2}}\right]\right\}$$

$$-8(\Delta\xi_n/\sigma_\varepsilon)(\eta_{j+1/2})^i\,M_{j+1/2}\left[\nu^{n+1}_{t_{j+1/2}}(W^{n+1}_{j+1}-W^{n+1}_{j}+W^{n}_{j+1}-W^{n}_{j})\right.$$

$$\left.+\nu^{n}_{t_{j+1/2}}(W^{n+1}_{j+1}-W^{n+1}_{j})\right]=R4^{n}_{j+1/2}\qquad\text{(A.14)}$$

$$(\Delta\eta_{j-1}+\Delta\eta_j)\,T^{n+1}_{j}-2(U^{n+1}_{j+1/2}-U^{n+1}_{j-1/2})=0\qquad\text{(A.15)}$$

$$(\Delta\eta_{j-1}+\Delta\eta_j)\,Q^{n+1}_{j}-2(K^{n+1}_{j+1/2}-K^{n+1}_{j-1/2})=0\qquad\text{(A.16)}$$

$$(\Delta\eta_{j-1} + \Delta\eta_j)\, W_j^{n+1} - 2(\varepsilon_{j+1/2}^{n+1} - \varepsilon_{j-1/2}^{n+1}) = 0 \qquad \text{(A.17)}$$

where

$$R1_{j+1/2}^n = 2E_{n+1/2}\Delta\eta_j(\eta_{j+1/2})^i\, U_{j+1/2}^n$$

$$+ \Delta\xi_n\Delta\eta_j(\eta_{j+1/2})^i\, \eta_{j+1/2} \left.\frac{dE}{dx}\right|_{n+1/2} T_{j+1/2}^n \qquad \text{(A.18)}$$

$$R2_{j+1/2}^n = 2\Delta\xi_n(\eta_{j+1/2})^i\, M_{j+1/2}\, (2\nu + \nu_{t_{j+1/2}}^n)(T_{j+1}^n - T_j^n)$$

$$+ 2(E_{n+1/2})^2(\eta_{j+1/2})^i\, (U_{j+1/2}^n)^2 + \Delta\xi_n E_{n+1/2}(\eta_{j+1/2})^i\, \eta_{j+1/2} \left.\frac{dE}{dx}\right|_{n+1/2} \cdot$$

$$\cdot\, U_{j+1/2}^n T_{j+1/2} + \Delta\xi_n T_{j+1/2}^n \left[(\eta_{j+1/2})^i \left.\frac{\partial\nu_t}{\partial\eta}\right|_{j+1/2}^n + i(2\nu + \nu_{t_{j+1/2}}^n) \right] \qquad \text{(A.19)}$$

$$R3_{j+1/2}^n = 2\Delta\xi_n E_{n+1/2}(\eta_{j+1/2})^i\, \eta_{j+1/2} \left.\frac{dE}{dx}\right|_{n+1/2} U_{j+1/2}^n Q_{j+1/2}^n$$

$$+ 4(E_{n+1/2})^2\, (\eta_{j+1/2})^i\, U_{j+1/2}^n K_{j+1/2}^n + \Delta\xi_n(\eta_{j+1/2})^i\, \nu_{t_{j+1/2}}^n (T_{j+1/2}^n)^2$$

$$- 4\Delta\xi_n(E_{n+1/2})^2(\eta_{j+1/2}^i)\, \varepsilon_{j+1/2}^n + 2(\Delta\xi_n/\sigma_k)\, Q_{j+1/2}^n \left[(\eta_{j+1/2})^i \left.\frac{\partial\nu_t}{\partial\eta}\right|_{j+1/2}^n + i\nu_{t_{j+1/2}}^n \right]$$

$$+ 4(\Delta\xi_n/\sigma_k)\, (\eta_{j+1/2})^i\, M_{j+1/2}\, \nu_{t_{j+1/2}}^n (Q_{j+1}^n - Q_j^n) \qquad \text{(A.20)}$$

and

$$R4^n_{j+1/2} = 4(\Delta\xi_n/\sigma_\varepsilon)\, W^n_{j+1/2}\left[(\eta_{j+1/2})^i \left.\frac{\partial \nu_t}{\partial \eta}\right|^n_{j+1/2} + i\nu^n_{t_{j+1/2}}\right]$$

$$+ 8(E_{n+1/2})^2\,(\eta_{j+1/2})^i\, U^n_{j+1/2}\varepsilon^n_{j+1/2} + 8(\Delta\xi_n/\sigma_\varepsilon)(\eta_{j+1/2})^i \cdot$$

$$\cdot M_{j+1/2}\nu^n_{t_{j+1/2}}(W^n_{j+1} - W^n_j) + \Delta\xi_n(\eta_{j+1/2})^i\, C_{\varepsilon_1} Z^n_{j+1/2}\nu^n_{t_{j+1/2}}(T^n_{j+1/2})^2$$

$$- 4\Delta\xi_n\,(E_{n+1/2})^2\,(\eta_{j+1/2})^i\, C_{\varepsilon_2}\, Z^n_{j+1/2}\varepsilon^n_{j+1/2}$$

$$+ 4\Delta\xi_n E_{n+1/2}(\eta_{j+1/2})^i\, \eta_{j+1/2} \left.\frac{dE}{dx}\right|_{n+1/2} U^n_{j+1/2}W^n_{j+1/2} \qquad \text{(A.21)}$$

In the above equations,

$$M_{j+1/2} = \frac{1}{\eta_{j+1+1/2} - \eta_{j-1/2}}\,, \qquad j = 1, 2, \ldots, J-1$$

(A.22)

$$M_{1/2} = \frac{1}{\eta_{1+1/2} + \eta_{1/2}}$$

$$Z = \frac{\varepsilon}{K} \qquad \text{(A.23)}$$

and

$$T^n_{j+1/2} = T^n_j + I_{j+1/2}(T^n_{j+1} - T^n_j) \qquad \text{(A.24)}$$

where

$$I_{j+1/2} = \frac{\eta_{j+1/2} - \eta_{j-1/2}}{\eta_{j+1+1/2} - \eta_{j-1/2}}\,, \qquad j = 1, 2, \ldots, J-1$$

(A.25)

and

$$I_{1/2} = \frac{2\eta_{1/2}}{\eta_{1/2} + \eta_{1+1/2}}$$

Expressions similar to Eq. (A.24) apply to $Q^n_{j+1/2}$, $W^n_{j+1/2}$, $Q^{n+1}_{j+1/2}$, and $W^{n+1}_{j+1/2}$. However, those T, Q, and W associated with V (in Eqs. (A.12) to (A.14) have an upwind differencing switch in them and are expressed as follows:

$$T^n_{j+1/2} = D_{j+1/2}\left[T^n_j + L_{j+1/2}(T^n_{j+1} - T^n_j)\right]$$

$$+ (1 - D_{j+1/2})\left[T^n_{j+1} - L_{j+1/2}(T^n_{j+2} - T^n_{j+1})\right] \qquad \text{(A.26)}$$

where $D_{j+1/2}$ is a switching parameter ($D_{j+1/2} = 1$ is for central differencing and $D_{j+1/2} = 0$ is for upwind differencing), and

$$L_{j+1/2} = \frac{\eta_{j+1+1/2} - \eta_{j+1/2}}{\eta_{j+2+1/2} - \eta_{j+1/2}} \quad , \quad j = 0, 1, \ldots, J-2$$

and $\qquad \text{(A.27)}$

$$L_{J-1/2} = 0$$

Again, expressions similar to Eq. (A.26) apply to $Q^n_{j+1/2}$, $W^n_{j+1/2}$, $T^{n+1}_{j+1/2}$, $Q^{n+1}_{j+1/2}$, and $W^{n+1}_{j+1/2}$ in those convection terms. The boundary conditions are:

$$U^{n+1}_{J+1/2} = U_\infty \quad , \quad V^{n+1/2}_o = 0 \quad , \quad T^{n+1}_o = 0$$

$\qquad \text{(A.28)}$

$$K^{n+1}_{J+1/2} \to 0 \quad , \quad \varepsilon^{n+1}_{J+1/2} \to 0 \quad , \quad Q^{n+1}_o = 0 \quad , \quad W^{n+1}_o = 0$$

END

7-87

DTIC